Max-Planck-Institut für Polymerforschung
Max Planck Institute for Polymer Research

Protein Nanocapsules for the Delivery of Active Biomacromolecules

Dissertation

zur Erlangung des Grades
„Doktor der Naturwissenschaften"
im Promotionsfach Chemie

am Fachbereich Chemie, Pharmazie,
Geographie und Geowissenschaften
der Johannes Gutenberg-Universität Mainz

vorgelegt von Marina Machtakova
geboren in: Sosnovyj Bor, Russland

Mainz, 2021

JG|U

JOHANNES GUTENBERG
UNIVERSITÄT MAINZ

This thesis was carried out from April 2018 until July 2021 in the Department of Physical Chemistry of Polymers, led by Prof. Dr. Katharina Landfester, in the group of Dr. Héloïse Thérien-Aubin at the Max-Planck-Institute for Polymer Research, Mainz.

1. Berichterstatter: Prof. Dr. Katharina Landfester

2. Berichterstatter: Prof. Dr. Stephan Gehring

Tag der mündlichen Prüfung:

Declaration

I hereby declare that I wrote the dissertation submitted without any unauthorized external assistance and used only sources acknowledged in the work. All textual passages, which are appropriated verbatim or paraphrased from published and unpublished texts, as well as all information obtained from oral sources are duly indicated and listed in accordance with bibliographical rules. In carrying out this research, I complied with the rules of standard scientific practice as formulated in the statutes of Johannes Gutenberg-University Mainz to insure standard scientific practice.

Mainz, 2021 Marina Machtakova

Abstract

The design of nanocarriers for the delivery of active biomacromolecules requires special considerations to accomplish both a successful delivery process and the preservation of the biological function of the biomacromolecule. In addition to the common challenges faced in the *in vivo* delivery of small molecules, the delivery of biomacromolecular payload is significantly impeded by the sensitive structure of those payloads. In such cases, the delivery system should not only be biocompatible, biodegradable, and stable under *in vivo* conditions. Moreover, it should also be able to release the biomacromolecular payloads with a high degree of control, and the formulation process should not hamper the structure of the active macromolecule. Consequently, the ideal delivery system should be highly tunable and adaptable to be potentially used in combination with any molecule from the large pool of functional biomacromolecular therapeutic agents. The main aim of this thesis was to develop nanocapsules composed of functional proteins so that they can be delivered to cells while preserving their native biological function and activity, simultaneously providing the possibility to encapsulate and release other active biomacromolecular payload.

Biomacromolecules, especially proteins, can not only be used as the payload for delivery but also as the main constituting units of the delivery carrier, thus improving the biodegradability and biocompatibility of the resulting delivery system. In this thesis, such protein nanocapsules are used as the main delivery system and as the functional payload. First, a nanocapsule synthesis method enabling the preservation of the intrinsic function of the protein was developed (section 4.1). The formation of protein nanocapsules was achieved by the interfacial crosslinking of miniemulsion droplets containing the active biomacromolecules. Such an approach increased the efficient mass fraction of active biomacromolecules delivered by 50-1000 folds compared to conventional delivery systems. Furthermore, the inner aqueous core of the nanocapsule acted as a reservoir for other reagents. To establish the methodology, nanocapsules formed only with catalytic proteins, e.g. enzymes, were designed, and the results show that the synthesis process preserved a high degree of the enzyme structure and enzymatic activity. The resulting nanocapsules were also taken up by cells and were able to perform enzymatic catalysis within the cellular environment, which is of great potential for the *in situ* generation of toxic compounds and drugs.

An important challenge in the delivery of any type of therapeutic agent, but especially critical in the case of biomacromolecular therapeutic agents, is their efficient release from the nanocarrier. In the case of biomacromolecular therapeutic agents, this step is more complex due to the size of the molecules to be released. Given that the protein/enzyme nanocapsules design here is highly degradable, it enables the controlled release of model encapsulated macromolecules.

In this case, protein nanocapsules made with ovalbumin were used as a model system (section 4.2), and the control over the permeability of the nanocapsule shell and the release of the encapsulated payload was tuned by the degree of crosslinking. The crosslinking of the shell influences the mesh size of the shell network and hence the release of encapsulated macromolecules. The presence of biological proteases influences the degradation of the resulting nanocapsule, and model payload of molecular weight from 5 000 − 600 000 g mol^{-1} can be released under artificial conditions but also *in vitro* after the uptake of the nanocapsules by dendritic cells. This approach is generally applicable to the delivery of any biomacromolecular therapeutic agent.

Consequently, protein nanocapsules are both, highly biodegradable in the intracellular environment and highly functional if the intrinsic activity of the protein building blocks can be preserved. Those properties enable the application of protein nanocapsules as nanotherapeutics for intracellular therapy and offer novel possibilities for the formulation of antigen proteins as nanovaccines against cancer. In this case, protein nanocapsules can be synthesized exclusively from antigen proteins. This method provides several advantages: the use of foreign carrier materials is prevented, reducing the risk of emerging side effects and the generation of immunity against body-foreign carrier compounds; the amount of delivered antigen can be significantly increased because of the high loading capacity of the nanosystem; and the nanocapsules are a great platform to co-deliver multiple active agents. Hence, nanocapsules composed of the antigen protein Aspartyl (asparaginyl)-β-hydroxylase (ASPH) were synthesized in section 4.3. This antigen is often overexpressed in hepatocellular carcinoma (HCC), making it a potential target for the development of vaccines against HCC. In this proof-of-concept study, the nanocapsules synthesis process was down-scaled so that only 2-5 mg of protein were used per batch. The ASPH NCs were functionalized with an immunostimulatory adjuvant and a high cellular uptake and low toxicity of the nanocapsules was demonstrated. Further, the NCs showed a high capability to activate the targeted antigen-presenting cells and prove the applicability of the concept for the delivery of many potential antigens.

Zusammenfassung

Die Entwicklung von Nanoträgern für den gezielten Transport von medizinischen Wirkstoffen ist eine der zukunftsträchtigsten Anwendungen der Nanotechnologie. Dadurch lassen sich Medikamente selektiv zu verschiedenen, von einer Krankheit betroffenen, Zellen bringen und die Nebenwirkungen einer systemischen Verabreichung können vermieden werden. Dabei stellt der Transport von biologischen makromolekularen Wirkstoffen, so wie z.B. einer RNA, eines Proteins oder eines Enzyms, eine besondere Herausforderung dar, da während des Formulierungs- und des Transport-Prozesses die sensible Struktur des Wirkstoffes geschützt werden muss. In diesem Fall muss der Nanoträger nun nicht nur bioabbaubar und gleichzeitig während des Transportes stabil sein, sondern auch kontrollierte Freisetzungsmechanismen aufweisen, die die Abgabe des makromolekularen Wirkstoffes ermöglichen. Dementsprechend muss der ideale Nanoträger möglichst flexibel und anpassbar sein, sodass die Vielzahl von komplexen biologischen Makromolekülen transportiert werden kann. Daher war das Hauptziel dieser Arbeit, Methoden einer Nano-Formulierung zu entwickeln, mit denen Proteine unter Erhaltung ihrer nativen Struktur und Funktion zu bestimmten Zellen transportiert werden können, wobei gleichzeitig die kontrollierte Freisetzung ermöglicht werden sollte. Die Einkapselung von funktionellen Proteinen in Nanoträgern ist ein weit verbreiteter Ansatz. Doch diese höchst biokompatiblen und natürliche Polymere eignen sich auch als Bausteine für die Nanoträger selbst, wodurch stark bioabbaubare Systeme hergestellt werden können. Daher zielt diese Arbeit darauf ab, funktionelle Proteine als Nanoträger zu verwenden, wobei das Protein gleichzeitig als Träger und als Wirkstoff dienen kann.

Im ersten Abschnitt der Arbeit wurde eine Methode entwickelt, mit der Protein-Nanokapseln hergestellt werden können und die native Struktur und Funktion des Proteins erhalten wird. Dazu wurden Enzyme mit spezifischen biologischen Eigenschaften verwendet, aus denen mittels einer grenzflächenkontrollierten Vernetzung Enzymkapseln hergestellt wurden. Dadurch wurde in der Herstellung eines Transportsystems für Enzyme vollständig auf zusätzliche Materialien verzichtet und stattdessen eine Nanokapsel aus dem Enzym selbst hergestellt. Dadurch konnte die effektive Menge an transportierten Enzym im Vergleich zu konventionellen Trägern, die Enzyme lediglich einkapseln, um das 50-1000-fache erhöht werden. Außerdem dient das Innere der Enzymkapsel als ein Reservoir für weitere Reagenzien, die zusammen mit dem Enzym transportiert werden können. Während der Synthese der Enzymkapsel konnte die intrinsische Aktivität des Enzyms zu einem hohen Grad bewahrt werden, sodass enzymatisch aktive Nanokapseln hergestellt wurden. Diese konnten nach der Aufnahme durch Makrophagen enzymatische Reaktionen in der Zelle durchführen und bieten ein hohes Potential für die *in situ* Herstellung von toxischen Wirkstoffen in Zellen.

Eine große Herausforderung für den effektiven Transport von allen Wirkstoffen, aber insbesondere von makromolekularen Wirkstoffen liegt in der kontrollierten Freisetzung. Dieser Prozess ist bei Makromolekülen besonders komplex, da ihr hohes Molekulargewicht einen großen hydrodynamischen Radius bewirkt und dadurch die Diffusion der Makromoleküle hindert. Falls Proteinkapseln zum Transport solcher Wirkstoffe eingesetzt werden, kann die Freisetzung über den Abbau der Proteinkapsel selektiv gesteuert werden. Daher wurde im zweiten Abschnitt dieser Arbeit die Abbaubarkeit von Ovalbumin-Nanokapseln in Abhängigkeit der Vernetzungsdichte untersucht. Dabei beeinflusst die Vernetzung der Hülle den Abbau der Protein Nanokapsel und damit die Freisetzung von eingekapselten Makromolekülen. Der Abbau findet dabei durch natürliche Enzyme wie die Proteinase statt. Makromoleküle mit dem Molekulargewicht von 5 000 g mol^{-1} bis 600 000 g mol^{-1} konnten somit unter künstlichen Bedingungen, aber auch nach der Aufnahme durch dendritische Zellen freigesetzt werden. Dieser Ansatz zeigt die breite Anwendbarkeit der Proteinkapseln für den Transport und die Freisetzung von Makromolekülen.

Folglich haben Protein Nanokapseln nicht nur ein hohes Maß an Bioabbaubarkeit, sondern weisen auch eine hohe Funktionalität auf, wenn die intrinsische Bioaktivität des Proteins bewahrt werden kann. Diese Eigenschaften ermöglichen den Einsatz von Protein-Nanokapseln als Nanotherapeutika und erleichtern insbesondere die Formulierung von Antigen-Proteinen als Nanovakzine im Kampf gegen Krebs. Denn hierbei kann die Protein-Nanokapsel ausschließlich aus dem Antigen-Protein hergestellt werden, wodurch die Verwendung von weiteren Transport-Materialien vermieden wird. Das ist besonders wichtig, da das Risiko von potenziellen Immunantworten gegen solche Materialien minimiert wird und mögliche Nebenwirkungen verringert werden. Des Weiteren erhöht sich dadurch effektiv die Menge an transportiertem Antigen und durch die Kapsel-Plattform können mehrere zusätzliche Therapeutika mittransportiert werden. In Abschnitt 4.3 wurden daher Nanokapseln vollständig aus dem Antigen-Protein Aspartyl (asparaginyl)-β-hydroxylase (ASPH) hergestellt. In den Zellen des hepatozellulären Karzinoms (HCC), eines malignes Tumors, der von den Leberzellen ausgeht, wird ASPH oftmals überexpremiert und eignet sich daher für die Entwicklung eines potentiellen Vakzins gegen HCC. Die hier durchgeführte Studie zeigt die Herstellung von ASPH-Nanokapseln, in der lediglich 2-5 mg des Antigen Proteins notwendig sind. Nach der Synthese der ASPH Nanokapseln wurden diese anschließend mit Immunostimulatoren funktionalisiert und die Nanovakzine anschließend von dendritischen Zellen aufgenommen. Dabei wiesen sie keinerlei Toxizität auf und waren in der Lage, die dendritischen Zellen zu stimulieren und zu aktivieren. Diese Ergebnisse belegen die Anwendbarkeit der Protein Nanokapseln als Nanovakzine und ermöglichen die Nachahmung mit anderen potentiellen Antigenen.

Acknowledgments

x

Table of Contents

1. Motivation

At the time of writing this thesis, the COVID-19 pandemic has put the world on hold for over a whole year. Every aspect of human life, from politics, economy, education to communication, is influenced by the virus, which has witnessed the death of over 3 million people. In the midst of this global health crisis, which is of unprecedented dimension in our history, there is one big hope: the fast vaccine development and authorization of mRNA-based vaccines from Pfizer/BioNTech and Moderna. Remarkably, the design, approval, and distribution of those vaccines were achieved in less than a year and represent a landmark in modern medicine.[1] This new class of mRNA-based vaccines delivers the genetic sequence of viral proteins to the host cell, inducing the expression of the virus protein and leading to the immunity against the original virus. This approach is considered safe, not infectious, and scalable.[2] However, there is one major prerequisite for the application of mRNA vaccines: the design of an appropriate delivery system.[3] Using mRNA alone would lead to low efficacy, as mRNA is easily degraded by RNAses during circulation in the blood and cannot efficiently cross the cellular membrane due to its large size.[4] It is only in concert with a lipid nanoparticle, a feat of nanotechnological engineering, used as a delivery system for the mRNA, that the impactful mRNA vaccine formulation was able to be so successful. It is clear that this scientific success providing a way out of the global crisis is the result of the underlying collaboration in bio- and nanotechnology. This success also raises the general awareness of all the potential and benefits of nanomedicines and biomacromolecular therapeutics.

The ideas behind the mRNA vaccine concept combine both the benefits of biomacromolecular therapeutic agents and the principles of nanotechnological drug delivery. On the one hand, mRNA is a highly specific and powerful biomacromolecular therapeutic agent. On the other hand, the liposomal nanoparticles fulfill the fundamental purpose of a delivery system, which is that precisely engineered nanomaterials are able to protect their drug cargo from degradation, control their biodistribution and intracellular uptake, and release it at the intended site.[5] Only in combination, those two components can achieve excellent therapeutic outcomes and contribute to solving severe medical challenges.

However, mRNA is only one example of biomacromolecular therapeutic agents. Apart from mRNA, several other biomacromolecular therapeutic agents, including proteins, peptides, or other genetic material, display high potential in the design of new treatments against a large variety of diseases, disorders, and conditions. Unfortunately, the development of new therapies based on the use of active biomacromolecules is impeded by their challenging vectorization.

The sensitive structure of those biomacromolecules is detrimental for preserving their biological function during vectorization, and caution must be taken to preserve this structure during the formulation and the delivery process. Furthermore, once successfully encapsulated, the release of those biomacromolecular therapeutic agents is difficult to control due to their high molecular weight and hydrodynamic radius. To simultaneously protect, deliver and release this new class of therapeutic agents, new delivery systems must be designed. Amongst the potential candidates, polymer delivery systems provide a high degree of functionality and versatility and are thus ideal candidates for the delivery of those biomacromolecules. They can be adapted to the specific cargo according to their size, shape, composition, and functionalization to ensure an optimized delivery process. Using biocompatible and natural polymers, e.g. proteins, highly potent and biodegradable nanocarrier can be designed. They are easily degradable by naturally occurring enzymes, which can be exploited for the controlled release of encapsulated biomacromolecules. Further, the versatility of proteins is of great potential, since almost any protein can be selected as the nanocarrier material. In this way, functional biomacromolecules can be formulated as hollow nanocarriers themselves and simultaneously be delivered to cells on the one hand, while allowing the encapsulation of other cargo for the co-delivery of other functional payloads on the other hand.

Overall, the fundamental goal in designing successful delivery methods for biological macromolecules was targeted in this thesis. On the one hand, protein nanocarriers were optimized for the encapsulation and release of a variety of macromolecules, while on the other hand, proteins with specific functions were formulated without additional carrier material as nanocapsules themselves. Both of those options were optimized in their process, in order to maintain the biological function of the biomacromolecule involved, which is a prerequisite for the successful application of efficient biomacromolecular therapeutic agent.

2. State of the art

2.1. Active biomacromolecular therapeutic agents

The use of biomacromolecular therapeutic agents, which are biological macromolecules, such as peptides, proteins, and oligo(nucleic acid)s is emerging as a powerful option for the treatment of conditions like cancer, immunological and infectious diseases or metabolic disorders. One of the cornerstones of the efficacy of this new class of drugs relies on their high specificity leading to significantly decreased off-target effects.[6] New treatments based on those biological macromolecules have benefited from extensive advances in molecular biology, which are enabling the large-scale production of such delicate biomolecules. This increased availability now offers an alternative to traditional treatments based on small synthetic molecules, which often display both a low specificity and toxic side-effects in healthy tissues.[7]

2.1.1. The potential of biomacromolecular therapeutic agents

Given the unique advantages of biomacromolecular drugs over small molecule therapeutic agents, their implementation in new treatment strategies represents one of the most promising fields in several pharmaceutical and medical areas.

In oncology, several biomacromolecular therapeutic agents have been identified as the potential basis for new treatments. For instance, cytokines are proteins with the ability to attack foreign, infected, or damaged cells found in cancerous tissues.[8] Monoclonal antibodies can "mark" cancer cells to make them more visible to the immune system or can block their growth-factor receptors and thus inhibit the growth of new cancer cells.[8] Enzymes can be used for the *in situ* generation of toxic anti-cancer agents in diseased cells.[9] Growth factors, which are also proteins, can be used to promote the proliferation of rapidly dividing cells such as hair follicle cells and bone marrow cells after the damage due to cytotoxic chemotherapy or a bone marrow transplant.[10] Oligonucleotides such as mRNA, DNA or siRNa can be delivered to the cancer cells to induce the production of the therapeutic protein like those mentioned above directly in the specific cell or to knock down specific genes in the cancer cells leading to their apoptosis.[11]

In gene therapy, which has the ambitious goal to exploit the cellular machinery to trigger the production of the required therapeutic agents *in situ*, biomacromolecules are also highly potent. This medical area has a high potential to fight an array of diseases like cancer, Alzheimer, HIV and AIDS, cystic fibrosis, heart disease, diabetes, or hemophilia.[12-14] It is based on harnessing the information encoded in nucleic acids to trigger gene inhibition of defective genes or express new molecules to correct an unbalanced system. For example, small interfering RNA (siRNA), microRNA (miRNA) and inhibitory antisense oligonucleotides (ASOs) can prevent the production of specific cellular products.

In contrast, plasmid DNA, messenger RNA (mRNA), small activating RNA (saRNA), CRISPR (clustered regularly interspaced short palindromic repeats)/Cas (CRISPR-associated protein) systems have been used to lead the cells treated to express new compounds.[15] Hence, gene therapy can be viewed as a more precise and personalized therapeutic method than conventional drug treatments.[16, 17]

Additionally, the next generation of highly specific vaccines is based on the concepts and techniques of molecular biology. Those vaccines are based on protein antigens incorporated in a recombinant eukaryotic expression vector (such as a plasmid DNA or mRNA) which are then introduced into the body. They are able to produce the foreign antigen in the specifically targeted cells leading to an antigen-specific immune response that controls the disease.[18]

In all of those areas, biomacromolecular therapeutic agents provide novel and unique opportunities. Although many achievements have been made in the preclinical evaluation of biomacromolecular therapeutic agents, to date, successful clinical outcomes are only seen in exceptional cases. One of the crucial challenges currently encountering many clinical trials is the inadequate and off-target delivery of these therapeutic agents.[19] In particular, several studies attributed the failure of the treatment with biomacromolecular therapeutic agents to the presumably poor delivery mechanism.[20 21 22] For example, one potential treatment in gene therapy against heart failure would require the delivery of a gene coding the enzyme calcium ATPase. The successful treatment would deliver the Calcium ATPase gene into the heart's muscle to increase the production of calcium handling proteins, which are essential to the myocardial contraction and relaxation and consequently rescue patients suffering from heart failure.[23] However, a large study on patients with heart failure showed no significant efficacy of such a treatment. This therapeutic failure was attributed to a lack of an appropriate delivery system for the gene.[24] Results from similar studies have displayed identical effects ranging from insignificant clinical benefits to emerging resistance mechanisms and, most dramatically, health risks due to the inappropriate delivery.[25] Thus, to fully exploit the therapeutic potential of biomacromolecules, efficient delivery systems are urgently required.

2.1.2. Challenges for the delivery of biomacromolecular therapeutic agents

In general, the delivery of biomacromolecular therapeutic agents involves a multistep process, and each of these steps presents specific challenges for an effective treatment outcome. Some of those challenges, like their transport to the right site of delivery, are shared with therapies based on small molecules. However, some challenges are unique to the delivery of biomacromolecular therapeutic agents.[6]

One of the key challenges in the delivery of biomacromolecular therapeutic agents is to overcome the instability of the biomolecules. In general, biological macromolecules are vulnerable to the loss of their structure due to the effect of physico-chemical triggers such as temperature, pH and the ionic strength of the surrounding environment. Those conditions can disrupt the specific intra- and inter- molecular interactions based on labile forces responsible for the complex structures. These physico-chemical cues can cause aggregation, deamidation, isomerization, hydrolysis, oxidation and denaturation, resulting in the irreversible loss of biological activity. Moreover, not only does any alteration of their specific structure need to be prevented, but the primary structure also needs to be protected since it can be subjected to enzymatic degradation *in vivo*. Various proteases and nucleases found in the biological media can degrade the molecules into smaller fragments.[26, 27] This is a critical factor that leads to short *in vivo* half-life times, ranging from a few minutes to a few hours, exhibited by some biomacromolecular therapeutic agents.[28] This is a reason why their use as medications, like in the case of insulin to treat diabetes, often requires frequent and constant dosing to maintain an appropriate *in vivo* concentration when the biomacromolecular therapeutic agent is administered systemically.[29]

Another challenge to the successful utilization of biomacromolecular therapeutic agents is the lack of drug availability at the desired disease site.[30] Designed to act at a highly specific site or tissue, the biomacromolecular therapeutic agent can only do so if it accumulates at the target site at an efficient concentration. Even when the degradation of a fraction of the administered medication can be prevented, the remaining intact biomolecules lack intrinsic navigation, targeting, and the ability to penetrate the right tissues in *in vivo* systems.[31, 32]

Another key challenge is the delivery of the large biomacromolecules used as therapeutic agents across the cellular membrane and in the cytoplasm. After billions of years of evolution, the cell membrane has evolved to precisely regulate the transport of molecules in and out of the cytosol, to protect the intracellular environment from extracellular interference.[33] The high molecular weight and the intrinsic hydrophilicity of many biomacromolecular therapeutic agents are associated with a general reduction in their permeability across biological barriers such as cell membranes.[34] Cellular membranes can selectively and actively allow the entry of small molecules and ions, while the lipid

bilayer is impermeable to high-molecular-weight substances.[35] The intrinsic lipophilic nature of biological membranes is another major obstacle in the permeation of hydrophilic biomacromolecules to the targeted intracellular site.[36] Furthermore, in the case of nucleic acid-based drugs, the active molecule bears the same surface charge as the negatively charged cellular surface, which makes their transport across the membrane nearly impossible without the aid of external forces.[37] As a result, only a marginal fraction of biomacromolecular therapeutic agents can successfully reach their intracellular target, which leads to an insufficient therapeutic efficacy.

In summary, only the design of an appropriate drug delivery system would be able to overcome the aforementioned limitations. This illustrates the need and the significance of the development of innovative drug delivery systems for active biomacromolecular therapeutic agents and their use in medical and pharmaceutical technologies.

2.2. Delivery of active biomacromolecular therapeutic agents in polymer nanosystems

To date, the challenges faced in the delivery of biomacromolecular therapeutic agents have been tackled using a variety of nanosystems, which resulted from tremendous efforts in the interdisciplinary field of nanotechnology. A strategy developed to protect biomacromolecular therapeutic agents from degradation is their encapsulation in a controlled environment such as liposomes or silica nanocapsules.[38] [9] For a targeted delivery, different nanosystems have been functionalized with targeting ligands, such as folic acid (FA, vitamin B9), and biotin (vitamin B7)[39] or antibodies.[40] For an improved cellular uptake of the macromolecules, they were conjugated to cell-penetrating peptides.[41] Those strategies are now paving the way for the more efficient and safe delivery of biomacromolecular therapeutic agents. However, maybe the most challenging task still faced by the field is to find a way to combine all the upsides (and none of the downsides) of those strategies in one optimal delivery system. Recent advances in the synthesis of polymer nanocarriers indicate that this technology is the most likely platform to be able to do so. Polymer nanotechnology allows to build delivery vehicles of greater sophistication in architecture and function with a true precision in the generation of the synthetic architecture, placement of functionality, and ease of conjugation or complexation.[42]

In many aspects, polymer drug delivery systems can enhance the *in vivo* efficacy of biomacromolecular therapeutic agents (Figure 2.1). For this purpose, an ideal drug delivery system (DDS) should combine the following functions: good cargo protection during the delivery, high colloidal stability in biological media, functionalization with shielding moieties, the inclusion of active targeting ligands, a high cellular uptake efficiency, and a controlled release.[43]
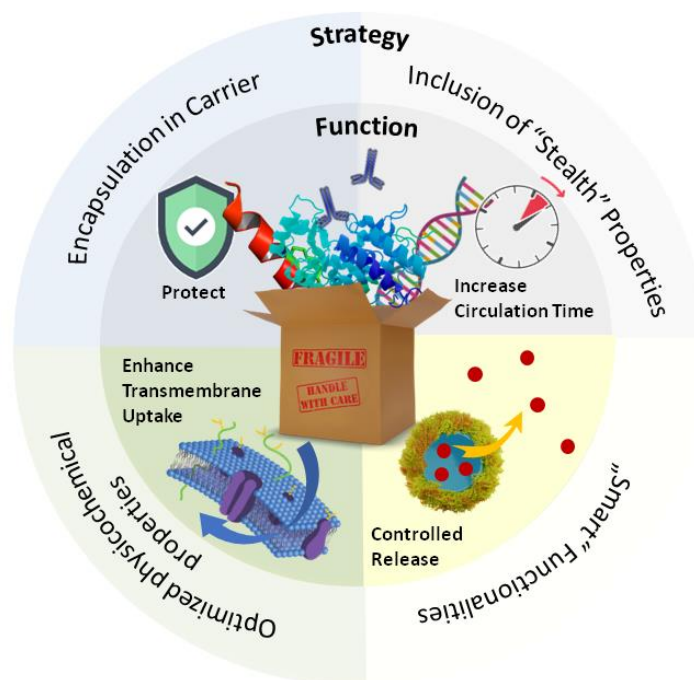
Figure 2.1: Pathways towards the enhancement of the *in vivo* efficacy of biological macromolecules by the rational design of polymer drug delivery systems.

2.2.1 Mechanisms to improve the efficacy of polymer nanosystems as drug delivery systems

First, to protect the valuable biomacromolecular cargo from the harsh environmental conditions or enzymatic degradation, the payload can be entrapped in a carrier. Here, the loading of the drug can be achieved either by the physical entrapment of the biomacromolecule in a carrier matrix or by its covalent conjugation to the carrier material.[44] One critical factor to be considered is the drug loading efficiency, which tends to vary with the drug type, the type of carrier, the solvents used, the temperature, and the mixing time of the different precursors.[45] In general, the covalent conjugation between drug and carrier can increase the encapsulation efficiency but is accompanied by other limitations. For instance, the direct chemical modification of the sensitive biomacromolecular therapeutic agents can alter their delicate structure, and covalently linked cargo can display limited release and a loss of efficacy due to the formation of irreversible linkages.[46]

Then, once the DDSs are introduced into the body, the drug carriers are surrounded by a large amount of proteins and other biomolecules, which adsorb onto the surface of the DDS to form the protein corona.[47] This interaction can induce the dissociation or aggregation of the DDS, influence its distribution throughout the body, and reduce the efficiency of any targeting functionality of the carrier.[47, 48] Hence, high stability and minimal non-specific interactions with biomolecules are prerequisites in the design of efficient DDS. The main strategy to reduce the aggregation and clearance

induced by the interactions with serum components consists in the functionalization of the carrier with hydrophilic shielding moieties such as poly(ethylene glycol)s, poly(phosphoester)s, or proteins. The attachment of these polymers decreases the unspecific adsorption and forms "stealthy" systems with prolonged blood circulation times and decreased clearance by the immune system.[49]

Once the DDS is stable *in vivo*, the next challenge consists in achieving an efficient accumulation of the therapeutic agent at the intended site of action. To do so, passive and active targeting strategies have been developed. Passive targeting consists in the transport of nanocarriers to the disease tissues and cells by convection or passive diffusion.[50] This accumulation can be facilitated by inherent biophysicochemical properties of the nanosystem such as size, shape, charge and flexibility.[51] In the case of cancerous tissues, passive targeting is closely related to the enhanced permeability and retention effect, which arises from the unique anatomical and pathophysiological properties of the tumors.[52] Most solid tumors exhibit enhanced vascular permeability, which ensures a sufficient supply of nutrients and oxygen to the tumor tissues to fuel their rapid growth. This effect facilitates the transport of DDSs into tumor tissues by diffusion and retention.[53] On the other hand, active targeting relies on the affinity of ligands attached to the DDSs to bind to specific proteins, antigens, or receptors that are overexpressed on the surface of the targeted cells or tissue.[54] Those specific ligands enhance the binding of the DDS to targeted receptors expressed on the surface of specific cells only present at the intended site of action.[51] Various molecules have been employed as targeting ligands such as antibodies, nucleic acid strands, peptides, and other small molecules for the improvement of the retention and cellular uptake of DDS. Compared to an un-targeted system, this technique further enhances the therapeutic efficacy and minimizes side-effects arising from the accumulation of drugs in healthy tissue.[53]

Then, once the DDS accumulated at the desired site of action, the delivery system has to overcome the plasma membrane of the targeted cell. Classically, the uptake mechanisms can either be endocytic or non-endocytic.[55] During endocytosis, the DDS is surrounded by an area of the cell membrane, which then cleaves off from the cell to form a vesicle containing the ingested DDS (endosome).[56] In contrast, during a non-endocytic uptake, the material can fuse or simply penetrate the cellular membrane without being trapped in an additional vesicle.[57] The rate and efficiency of cellular uptake for DDSs is significantly influenced by the physicochemical properties of the delivery vehicle. These include the size, the geometry/shape, the surface charge, the surface chemistry, the hydrophobicity, the roughness, the rigidity, and the composition of the DDS and have to be optimized through the design of the system.[58] In general, the uptake can be enhanced by the functionalization of the carrier with positively charged cell-penetrating peptides. Those substances are known to improve the delivery capacity through the cellular membrane.[59] For the enhancement of endocytosis, receptor-mediated uptake can be used. Several ligands on the surface of the delivery vehicle can increase the

interaction with the receptors of the cell membrane and facilitate the uptake.[57] However, the mechanism of cellular internalization is the result of a strong interplay between each of the mentioned properties, and there is not one optimal combination ideal for all applications.[58]

Finally, if a DDS can successfully overcome the cellular barrier, it should release the therapeutic with the right dosage and with a predetermined release profile.[60] Such a controlled release maintains the drug concentration within the therapeutic window and decreases the number of required doses. Furthermore, it can reduce the total amount of drug needed for a specific therapeutic effect, which increases the efficacy of the treatment.[43] For polymer DDSs, the release of a drug include both the transport of the molecules within the polymer system and through the interface DDS/environment. In general, the release can be caused by different mechanisms, which can be either diffusion- or degradation- controlled or a combination of both.[61]

One of the most common release mechanisms is the passive diffusion of the payload through the DDS matrix. It describes the process of a random movement of a molecule, which is driven by the gradient of chemical potential, which can be approximated by the concentration gradient, between an area of high concentration (inside the DDS) to an area of low concentration (outside the DDS). If the release of cargo is driven by diffusion, it is dependent on several parameters, such as the mesh size of the polymer matrix, the chemical structure of the building blocks and the degradability of the material.[62] In turn, it is also affected by the physico-chemical properties of the payload, which include the molecular weight, the hydrodynamic radius, the hydrophilicity and the interactions with the nanocarrier.[63]

Degradation-controlled release occurs due to the hydrolysis or enzymatic degradation of the polymer nanocarrier. In hydrolytic degradation, water penetrates into the matrix and breaks hydrolytically labile bonds, like ester bonds, which are included within the polymer backbone. This leads to a swelling of the matrix and an increase of the mesh size and an increased diffusivity of the payload.[64] In enzymatic degradation, enzymes degrade specific linkages present in the nanocarrier, for example, protease will degrade amide linkages, and the overall result is a dynamic increase of the drug diffusivity through the matrix.[64] Many disease tissues also show a significantly over- or under expression of certain enzymes. For instance, the enzymatic degradation of polymer nanosystems can be exploited for a controlled release of drugs at cancerous sites. The concentration of enzymes such as esterases or proteases, is 2- to 4-fold higher in malignant tumors than in normal tissues.[11] Consequently, those enzymes can degrade polymer nanosystems incorporating the appropriate enzyme-labile bonds and a controlled release can be achieved.[65] [66]

In recent years, another important release mechanism has emerged to control the release from nanocarriers. Smart DDSs are designed to respond to environmental triggers, which leads to a change of the nanocarrier properties. A wide range of internal stimuli, such as changes in the pH value, the redox state, the temperature and the concentration of metabolites, can be utilized for the development of a triggered drug release from the polymer DDSs. For example, many disease tissues and inflammation sites display a higher local temperature in comparison to healthy tissues.[67] Thermoresponsive DDSs rely on a prompt change of the polymer solubility in water at a specific temperature.[68] During this process, the nanosystems undergo shrinking or swelling, which leads to changes in the mesh size of the polymer network and leads to the release of the payload. On the other hand, solid tumors may show an acidic pH environment (pH 6–7) that can be used to trigger chemical changes in polymers.[61] In this case, the incorporation of pH-labile groups such as acetal functionalities in the polymer backbone or in the crosslinker of the polymer system can result in the degradation of the polymer system in acidic environments.[69] Another physiological condition that can be exploited for the triggered release of payload from polymer DDSs is the redox potential. Reduction-responsive linkages like disulfide or diselenide bonds can be incorporated in the nanosystems and later they can be cleaved by reactive oxygen species (ROS) in the cell. This leads to the dissociation of the DDS and the release of the encapsulated therapeutic agent.[70, 71]

2.2.2 Structures of polymer drug delivery systems

Depending on the drug to encapsulate, the administration route, or the targeted application, polymer DDSs can be designed with different architectures such as polymer-conjugates, polyplexes, layer-by-layer assemblies, nanogels, nanocapsules and polymersomes (Figure 2.2).
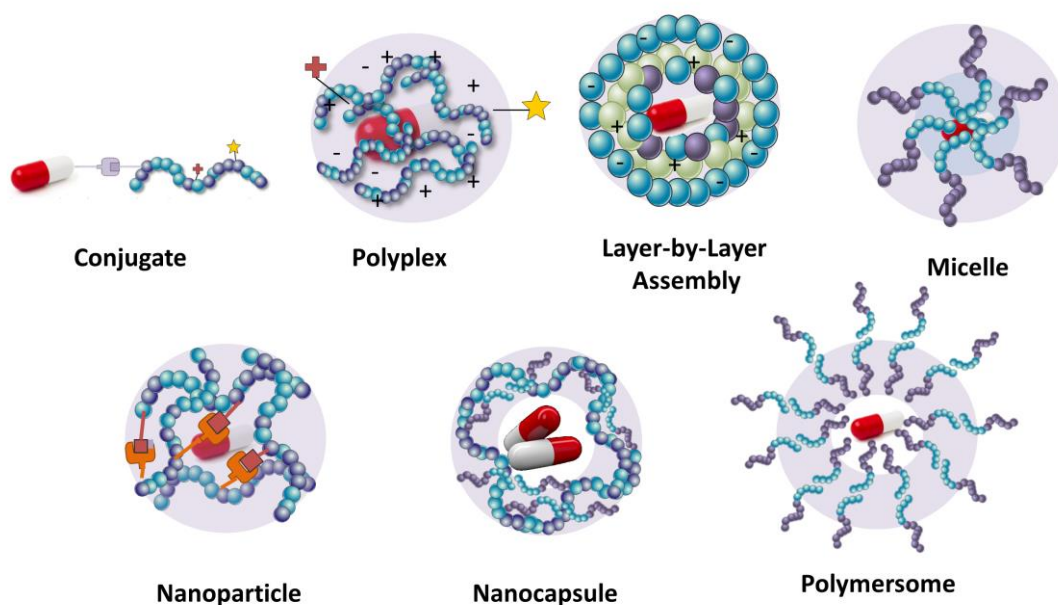

Figure 2.2: Types of polymer DDSs for biomacromolecular therapeutic agents.

Polymer-drug conjugates

The conjugation of synthetic polymers with various biomacromolecular therapeutic agents is the simplest polymer DSS possible. Such polymer–drug conjugates are pharmacologically active constructs comprising one or more therapeutic agents covalently bound to a polymer chain.[72] Since the first polyethylene glycol (PEG)–protein conjugate, Adagen® (bovine pegademase), was approved by the FDA in 1990[73], functional polymer bioconjugates have been widely explored and are continuously evolving.[74] A commonly used model of a polymer–drug conjugate consists of a biocompatible water-soluble polymer backbone as the main delivery vehicle tethered to the biomacromolecular agent (Figure 2.3 a). The polymer chain is employed to deliver the drugs, while increasing their aqueous solubility and protecting the cargoes from a rapid exclusion from the body. With an increase of the molecular weight of the polymer segment, the conjugate tends to specifically accumulate in solid tumors due to their enhanced permeability and retention effect.[75] Several types of biomacromolecular therapeutic agents can be employed in the design of polymer conjugates, irrespective of their size, charge or chemical structure. Furthermore, one or several therapeutic molecules can be tethered to the same polymer backbone and complementary moieties can also be

11

attached to the polymer backbone, such as adjuvant drugs, fluorescent tags, PEG molecules, or targeting moieties.

Generally, there are two strategies to synthesize polymer conjugates. The "grafting to" method, where a preformed polymer is directly coupled to the target biomacromolecular therapeutic agent, represents the most common and straightforward methodology.[76] In this approach, amino and thiol groups present in the biomacromolecular therapeutic agent are frequently employed as conjugation sites. Alternatively, biomacromolecular therapeutic agents can be functionalized with non-endogenous amino acids or other appropriate external small molecules by using specific reactions. Those can be employed for the site-specific conjugation of polymers using bioorthogonal coupling chemistries. Many examples exploiting such a strategy exist. For instance, the unnatural amino acid *p*-azidophenylalanine was site-specifically incorporated into proteins,[77] and the azido end-group enabled a copper-medicated click-reaction with an alkyne functionalized PEG. In another example, a ketone-containing amino acid, *p*-acetylphenylalanine was attached to a human growth hormone and the conjugation of an aminooxy-functionalized PEG optimized the pharmacological properties of these therapeutic agents.[78] The "grafting to" approach has several advantages. Firstly, the polymer component can be synthesized in a non-aqueous solution prior to the final conjugation step. Secondly, this separate synthesis process enables the design of well-defined polymer building blocks for preparing advanced materials with controlled structures, often including several reaction steps. Thirdly, a wide variety of (bioorthogonal) reactions is available to efficiently preserve the sensitive structures of the biomacromolecular therapeutic agent during the conjugation process. However, this approach also suffers from shortcomings, such as a potential low yield of the reaction between the polymer and the biomacromolecule. Here, two large molecules must react together and the reaction can be limited due to steric hindrance leading to insufficient functionalization yields.[79] Moreover, the resulting product can be challenging to purify from unreacteacted starting material and by-products.[80]

Consequently, the "grafting from" method has emerged for the synthesis of polymer-drug conjugates. The development of "grafting from" methodologies have benefited from advances in controlled and living polymerization techniques, such as reversible addition–fragmentation transfer (RAFT) and atom transfer radical polymerization (ATRP).[81] Typically, in the "grafting from" approach, the initiator is first linked to a biomacromolecular therapeutic agent, forming a macroinitiator from where the polymerization is initiated to achieve the controlled growth of the polymer chain. The overall process results in high reaction yield since only small molecules, first the initiator and then the monomers one at a time, are coupled to the reactive site.[82] Still, cautions must be taken when this method is used with biological substrates. For example, the polymerization method used to graft a polymer from a protein should not have reactive moieties undergoing side reactions with the functional groups present on amino acid residues.

Additionally, the polymerization technique should not denature the macromolecular therapeutic agent, either through chemical modification or by inducing irreversible solubility changes.[79]

The versatility of such an approach enables the design of a highly multifunctional system with increased complexity tailored to the specific delivery challenge.[83] In general, polymer-drug conjugates display high drug loading, sustained drug release and enhanced stability without undesirable drug leaking. Because only a single polymer chain is attached to the drug and the ratio of drug to polymer is high, the potential *in vivo* toxicity and immuno-stimulatory effect that can arise from the administration of material foreign to the body is limited in comparison to other delivery vehicles.[84] Furthermore, considering especially biomacromolecular therapeutic agents, one of the most promising benefits of polymer conjugation is the opportunity to improve the operational and storage stability of the drug. The stability of the biomacromolecular therapeutic agent under diverse or extreme temperatures and pH ranges can be enhanced due to the sterical shielding of the therapeutic agent by the polymer.[85] This can also modulate the pharmacokinetic properties and increase the circulation time and cellular uptake of the drug.[72] All of these benefits lead to an increased therapeutic effect observed for multiple drugs after their conjugation.[75] However, during the conjugation process, the choice of chemistry is crucial in preserving the activity of the biomacromolecular therapeutic agent. The direct covalent modification can alter the sensitive 3D structure of the biomacromolecular agent, even when extensive care is taken to preserve the specific folding of the drug during the conjugation process. Hence, this method always comes with a risk of denaturation and loss of functionality of the drug.[86, 87] Additionally, while biomacromolecular therapeutic agents encapsulated inside particles can be fully protected from degradation in blood, polymer-conjugates are still vulnerable to some degradation processes and generally show limited protection of the biomacromolecular therapeutic agents in comparison to other polymer delivery systems.[72]
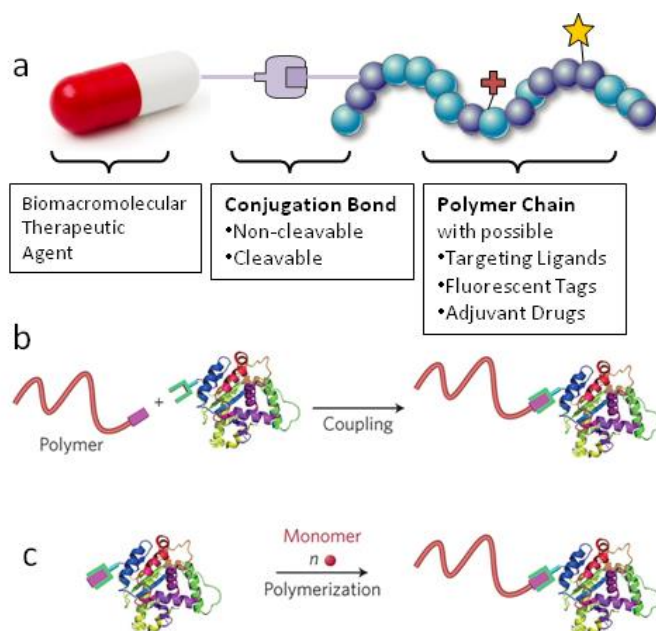
Figure 2.3: a) Schematic representation of a polymer-biomacromolecular therapeutic agent conjugate, b) general methods to prepare polymer conjugates: b) Grafting-to approach[88], c) Grafting-from approach[88]. B and C reproduced with the permission of the American Chemical Society.

Coacervates and electrostatic polyplexes

The formation of supramolecular structures between two polymers based on specific interactions such as electrostatic, hydrogen bonding and hydrophobic forces can produce coacervates.[89] From the molecular point of view, coacervates can also be formed by the interaction between biomacromolecular therapeutic agents and other polymers.[90] Polyelectrolyte complexes, coacervates formed by the combination of oppositely charged polymers are of particular interest in the development of polymer DDSs for biomacromolecular therapeutic agents since nucleic acids and proteins often carry negative charges.[91][196] The morphologies of the resulting complexes display a large diversity depending on the balance of water, polymer and salt ions within the complex.[92] In general, they can range from loosely associated colloids with more liquid-like properties in the case of coacervates, to more dense precipitates in the case of polyplexes.[93] In solution, charged polymers are attracted to oppositely charged materials and interfaces and exhibit a transition to an adsorbed state, resulting in nanospheres with physical crosslinking. Such complexes can be formed between polymers and biomacromolecular therapeutic agents (Figure 2.4 a).[94]

Coacervates and polyplexes are usually prepared by mixing two polymer solutions through pipetting followed by maturation during a short incubation time (Figure 2.4 b).[95] Because of the labile nature of the resulting interactions, the complex formation is dynamic and can be reversed in response to small changes in local conditions.[91]

In such case, many factors such as the ionic strength (salt concentration), the polyacid/polybase ratio, the total polymer concentration, the pH, the molecular weight of the polyelectrolytes, and the temperature play major roles.[96] For example, it was found that high ionic strengths could dissolve the polyplexes due to the Debye screening effect of the added salt (Figure 2.4 c). At high salt concentration, the local concentration of ions close to the polymers is high and can shield the effective charge of the polymer. Consequently, fewer charges are available for the formation of the complex, which can lead to the dissociation of the polyplex.[97, 98] Furthermore, the ratio of the polyacid/polybase is another important parameter. Many studies have investigated the influence of the polyanion/polycation ratio. For example, polyplexes prepared from DNA and poly-l-lysine showed that the highest DNA loading occur at a DNA/poly-l-lysine mass concentration ratios between two to three.[99] Other studies using PDMAEA or chitosan for the complexation of DNA showed similar results, suggesting that increasing the DNA/polymer ratio leads to the formation of durable complexes and provides a better coverage as well as a better release of DNA.[100, 101]

Another key parameter in the formation of the polyplexes is the molecular mass of the polymer employed. The ideal molecular weight for the complexation of one specific biomacromolecular therapeutic agent can be different from payload to payload. For example, the complexation and delivery of plasmid DNA, messenger RNA, and replicon RNA with a library of poly(2-ethyl-2-oxazoline)/poly(ethylene imine) copolymers with varying molar mass and charge densities,[102] showed that the optimal polymer design for each nucleic acid species was different and could significantly influenced the transfection efficiency of the delivered nucleotide. Those biomacromolecular therapeutic agents differ greatly in their structural composition and charge density and it was found that the polymer molecular weight forming the most efficient polyplexes decreased from 83, 72 and 45 kDa for DNA, RepRNA and mRNA complexation (Figure 2.4 d). However, the formation, dissociation and behavior of polyplexes with biomacromolecular therapeutic agents is influenced by an array of factors and the polyplexes also have a dynamic nature which contributes to the formation of poorly uniform particles.[103]

The main advantage of the complexation of biomacromolecular therapeutic agents with polymers is the absence of a chemical modification of the drug.[104] Hence, the sensitive intermolecular interactions in the molecule can be more easily preserved and are not hampered by external chemical modifications. This leads to an improved preservation of the intrinsic bioactivity of the drug after the complexation in comparison to polymer functionalization. The complex formation process is able to bind, protect and facilitate the cellular uptake of the cargo. Moreover, especially charged polyplexes with positive surface potential can efficiently improve the internalization of their payloads by the cells because they interact electrostatically with the negatively charged cell membranes and mediate the endosomal membrane destabilization required for the cytosolic release and delivery at the intended

site of action.[105] The excellent delivery of the molecules to the cytosplasm is often ascribed to the so-called proton sponge effect of cationic material where the endosomal membrane destabilization is caused by the inflow of anionic molecules for charge compensation.[106] [107] This results in a swelling and generation of osmotic pressure in the endosomal compartment and leads to the disruption of the membrane. This process strongly improves the polyplex delivery efficiency and is another major advantage of such DDS. However, this approach is also constrained by some factors. While gene materials are usually strongly charged and thus very suitable for the formation of polyplexes, the formation of polyplexes with certain proteins and polypeptides, which can be moderately charged or even neutral at physiological conditions depending on their isoelectric point, can be challenging.[108] Additionally, the number of charged residues in a protein is limited and strongly varies from one protein to another, hampering further the formation of protein-based polyplexes.[109] More generally, the systemic delivery of polyplexes can be hindered by their instability under physiological conditions. Indeed, various physiological salt and proteins found in blood can readily bind to the polyplexes and increase the risk for the premature release of the payload or even for the complete dissociation of the polyplex.[110]
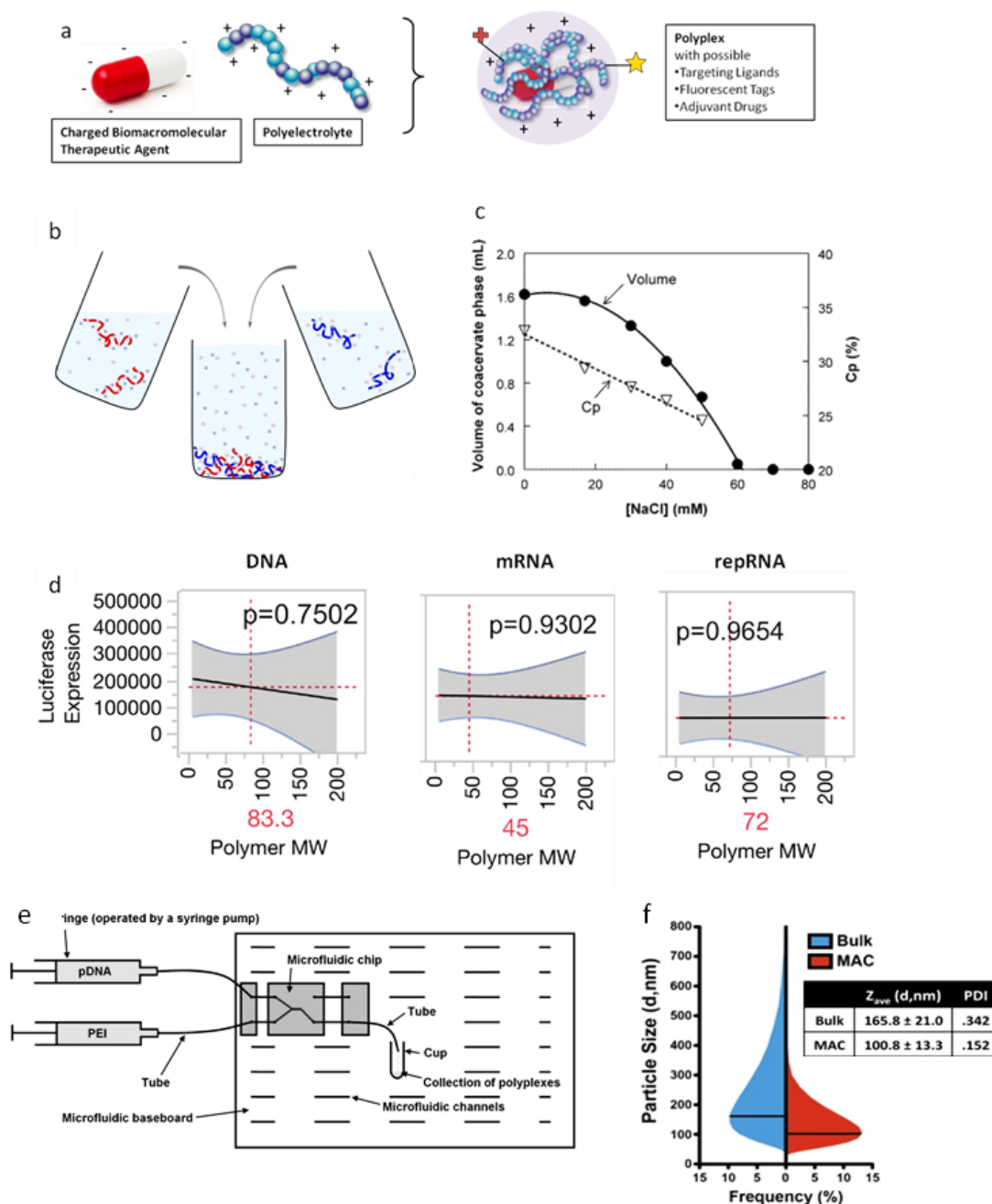
Figure 2.4: a) Schematic representation of the formation of polyplexes, b) Mixing solutions of polycations and polyanions leads the formation of a polyelectrolyte complex phase[95], c) Composition of Whey Protein/Gum Arabic coacervate phase as a function of the ionic strength after 48 h of phase separation, total biopolymer concentration (Cp) in the coacervate phase[98], d) Prediction profiles for the optimal polymer molecular weight for each nucleic acid with luciferase expression as the output. Gray shading indicates 95% confidence interval, and the p value in bold font indicates significance[102], e) Schematic illustration of polyplex preparation by the microfluidic lab-on-a-chip assembly[111], f) Size frequency distributions by intensity of polyplexes measured by dynamic light scattering immediately following preparation, with Z-average diameters indicated with black lines. Z-average diameter ± SEM and polydispersity indices are reported below for bulk and MAC preparations of pDNA polyplexes[112]. B reproduced with the permission of Elsevier; C,D and E reproduced with the permission of the American Chemical Society, F reproduced with the permission of Nature.

Layer-by-layer assemblies

Another class of drug delivery platforms based on electrostatic complexation is the layer-by-layer (LbL) assembly of polyelectrolytes. This simple method expands the simple electrostatic complexation by the design of multilayer architectures with layers of, usually, alternating charges with a nanometer-scale precision. The technique is based on the alternating adsorption of complementary layers of building blocks which can be synthetic or natural polyelectrolytes or other components, such charged as biomacromolecular therapeutic agents (Figure 2.5 a).[113] [114]For the application in drug delivery, colloidal LbL particles and capsules are of particular interest. In these cases, the single layers can be assembled either on a core template which can be a drug reservoir or a solid nanoparticle.[115]

To assemble a LbL particle system, a colloidal substrate bearing a defined charge or a polyelectrolyte in solution is mixed with a complementary polyelectrolytes followed by washing, usually through centrifugation (Figure 2.5 b).[116] This steps can be repeated several times, each time using an oppositely charged macromolecule to the charge of the previous step to achieve the desired loading of the biomacromolecular therapeutic agent. However, the formation of LbL assemblies on a nanoscale colloidal particle is not always easy. The procedure involves many centrifugation and filtration cycles to remove the excess of unbound polymers.[117] To improve the throughput of the formation of LbL assemblies, "wash-less" procedures have been developed and rely on preventing the excess addition of polymers by closely monitoring the properties of the system.[118]

Similarly to the formation of electrostatic polyplexes, the LbL deposition has the advantage of using mild conditions (aqueous solutions, absence of chemical modifications) that are more favorable for the preservation of the fragile structure and activity of the biomacromolecular therapeutic agents. Once covered by multiple layers of polyelectrolytes, the cargo is protected and the risk of degradation during transport decreases. The LbL system can be built by integrating a variety of functions and molecules in the different layers. For example, the functionalization of the surface can be readily realized by using multifunctional compounds, and has been use for the PEGylation or the introduction targeting moieties on the LbL DDS, and this functional layer will be immobilized via electrostatic interactions at the surface of the DDS. The control of the outer layer of the LbL DDS is crucial in determining the activity of the DDS, a systematic screening of 10 different polymers as outer layers used for the formation of LbL assemblies showed that the surface chemistry of those systems significantly influenced the specificity for targeting ovarian cancer (Figure 2.5 c,d).[119] The results clearly indicated that LbL-NPs with carboxylated surface chemistries produced by the coating of the DDS with poly-l-aspartate (PLD) or poly-l-glutamate (PLE)) possessed a striking affinity to ovarian cancer cells in comparison to sulfonated surfaces. The surface chemistry of the LbL DDSs can also be control by the formation of a stealth layer or a layer containing targeting ligands can cover the LbL system by the simple mixing of a charged polymer bearing the appropriate side-chains.

Moreover, additional drugs and adjuvants can be easily incorporated in LbL systems, one therapeutic agent can be deposited in the core of the assembly and another one in the surrounding layers, thus creating an independently tunable device for the co-delivery of multiple therapeutic agents.[120] This co-localization of drugs enables the construction of defined signal pathways and artificial architectures that can mimic biological functions found in natural organisms.[121] For example, polystyrene (PS) carriers were used as the substrate for the assembly of glucose oxidase (GOX) and horseradish peroxidase (HRP) in conjunction PEI and polystyrene sulfonate.[122] Because both enzymes preserved their enzymatic activity during the formation of the LbL nanosystems, coupled enzymatic reaction between the GOX and the HRP could still be performed after the assembly and the LbL nanoparticles were able to mimic the sequential cascade reactions observed inside cellular compartments. The breath of materials compatible with this approach is another of the most notable advantages of this method. Conventional polyelectrolytes such as poly(allylamine hydrochloride) (PAH), poly(diallyld-imethylammonium chloride) (PDDA), and poly(ethylene-imine) (PEI), poly(sodium styrenesulfonate) (PSS), poly(sodium vinylsulfonate) (PVS), and poly(acrylic acid) (PAA) have been widely used for the synthesis of LbL assemblies. Moreover, since many biomacromolecular therapeutic agents are bearing charges on their surface, they are also optimal candidate for the assembly by electrostatic LbL. Unfortunately, the LbL systems, just like the polyplexes, can suffer from an inherent limited stability *in vivo* due to the potential perturbation in the electrostatically assembled systems.[123]
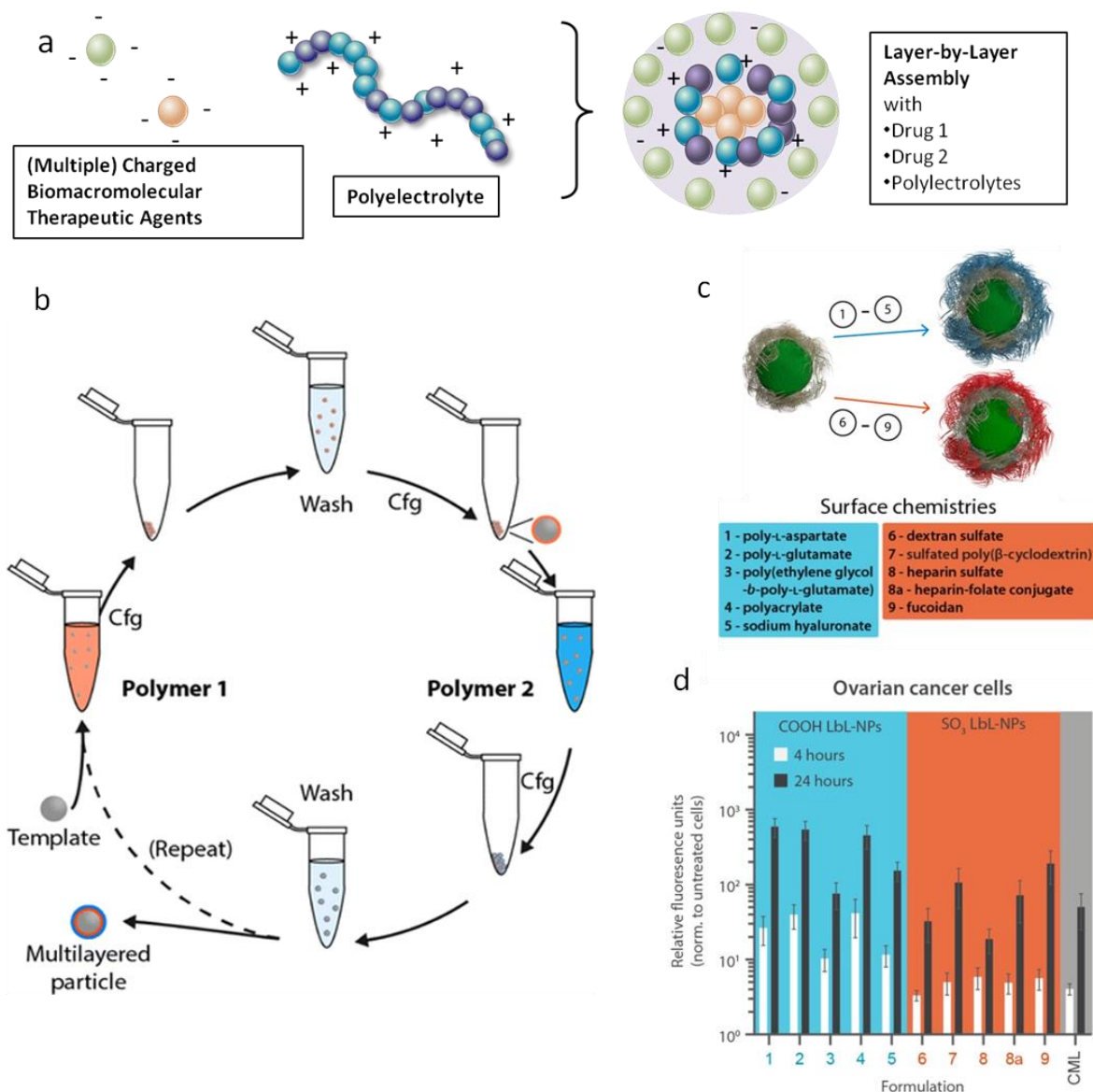
Figure 2.5: a) Schematic representation of LbL assemblies, b) Schematic illustration of immersive assembly on particulate substrates using centrifugation in between washing steps[116], c) Scheme of LbL functionalization with 10 different anionic polymers[119], d) Pooled median nanoparticle fluorescence intensity for 10 ovarian cancer cell lines incubated with carboxylated LbL-NPs, sulfated LbL-NPs and carboxylated non-LbL NPs[119]. B, C and D reproduced with the permission of The American Chemical Society.

Polymer micelles

Polymer micelles are supramolecular nanostructures that are usually formed by the self-assembly of amphiphilic block copolymers.[124] Classically, they are formed from block copolymers containing both hydrophilic and hydrophobic segments. In aqueous environments, the block copolymers assemble to spherical nanostructures where the hydrophobic part of the block copolymer is excluded from the aqueous surrounding forming the micelle core. The hydrophilic part builds the nanoparticle shell with a brush-like architecture (Figure 2.6 a). To date, polymer micelles have been used in many clinical studies for the delivery of low-molecular weight, hydrophobic drugs such as paclitaxel, doxorubicin or cisplatin. The studies showed great success for the reduction of the toxic side effects of the loaded drugs as well as a high therapeutic efficacy of the delivery system.[125]

Novel approaches expand the delivery potential of polymer micelles to the delivery of biomacromolecular therapeutic agents. Micelles containing a hydrophilic core can be assembled through electrostatic interaction by pairing oppositely charged block ionomers. In such cases, the block copolymers used in the formation of the polymer micelles combine neutral and charged segments. The neutralization of the charge of the block copolymers by a charged payload induces the required amphiphilicity for the micelles assembly.[126, 127] Such micelles exhibit extremely narrow size distributions and are used for the delivery of biomacromolecular therapeutic agents such as charged nucleic acids, proteins or enzymes.[128]

The formation of polymer micelles is mainly driven by non-covalent intermolecular interactions. In the case of traditional amphiphilic micelles, hydrophobic forces govern the self-assembly, whereas electrostatic forces induce the formation of PIC micelles.[129] In both cases, the process is driven by a gain in entropy. If amphiphilic polymers assemble, solvent molecules are released because the hydrophobic components are withdrawn from the aqueous media. If charged polymer segments combine, the release of counter ions complexing the charges leads to an increase of entropy. An important parameter for the construction of self-assembled polymer micelles is their stability against dissociation, especially under the highly diluted conditions that can be observed after a systemic injection. This parameter is described by the critical micelle concentration (CMC).[130] Below the CMC, the polymers only exist as single chains. As the polymer concentration increases and reaches the CMC, the polymer chains start to associate and form micelles. In comparison to low-molecular weight surfactants, block copolymers generally exhibit a lower CMC and thus higher stability. This property is attributed to the larger polymer segments resulting in stronger interactions. For instance, the CMC of stable polymer micelles are between 0.0005–0.002%.[130] Amphiphiles with higher CMC values may not be suitable as DDS, since they are unstable in an aqueous environment and easily dissociate upon dilution.

21

Polymer micelles can be synthesized by using both synthetic polymers and natural macromolecules.[127] The different segments incorporated control the assembly process, the encapsulation of the cargo and the stability in biological environments. In order to form the micelle shell, highly hydrophilic and flexible polymers are often exploited. Among them, PEG remains one of the most popular choice due to its desired properties such as high hydrophilicity, linearity, chain flexibility, lack of charge, and availability in a wide range of MWs with narrow MW distribution.[127] Micelle shells composed of PEG or PEG-derivatives usually show a very low aggregation both *in vivo* and during the storage time due to the steric repulsive effect between the PEG layers. Moreover, they have a reduced charge-related interaction with cells which limits the cellular uptake by non-targeted cells.[131] Alternative shell forming segments can be composed of other hydrophilic polymers such as poly(glycerol) (PG), poly(*N*-vinyl-2-pyrrolidone) (PVP), poly(vinyl alcohol) (PVA), poly(oxazolines) (POxs), poly(acrylic acid), poly(malic acid), polysaccharides, and poly(amino acids). All of those polymers are non-toxic, biodegradable and most of them already clinically approved.[127] For the formation of the micelle core, either hydrophobic or ionic polymers can be uzed. Micelle cores containing hydrophobic drugs are mostly constructed of hydrophobic polyethers, polyesters, and polyamino acids. For the delivery of charged biomacromolecules, several polycations have been considered as core-forming segments. Those include poly(ethylenimine), polylysine, cationic polyaspartamides, polyamidoamine dendrimers and poly(2-(*N,N*-dimethylamino)ethyl methacrylate). To provide an efficient delivery of the sensitive biomacromolecules, considerations that are similar to the ones for polyplexes or LbL formation have to be taken into account. These include polymer features and functionalities such as a high complexation ratio, strong cargo binding, high stability and the controlled release of the cargo.

The flexibility to combine several polymer segments in one polymer chain allows for the development of multifunctional micellar delivery systems and custom-made architectures. One interesting approach includes the synthesis of micelles composed of triblock copolymers forming tree-layered polymer micelles. Those can include hydrophilic, ionic and hydrophobic segments (Figure 2.6b). Hence, it is possible to stabilize the micellar core through hydrophobic interactions, incorporate hydrophobic drugs, encapsulate charged biomacromolecular agents and provide a shielding PEG-layer around the micelle with one well designed polymer.[132, 133] For example, copolymers with nonionic and hydrophilic poly(ethylene glycol) (PEG) segments, cationic poly(l-lysine) (PLys) segments, and a segment of poly[PAsp(DET)] bearing a hydrophobic dimethoxy nitrobenzyl ester (DN) moiety in the side chain [PEG-PLys-PAsp(DET-DN)] were used to spontaneously formed sub-100 nm-sized polymer micelles with a hydrophobic PAsp(DET-DN) core as well as PEG shell.[132] This micelle was able to encapsulate siRNA into the intermediate PLys layer. Each of the layers was essential for the delivery of the siRNA: the hydrophobic block largely increased the stability of the micelle core and thus the loading

efficiency of siRNA in the PLys layer, whereas the PEG outer layer efficiently inhibited the aggregation of the nanosystems (Figure 2.6 b). Such a design enabled the delivery of siRNA to HeLa cells and led to the controlled release of the payload. The efficiency of the release was shown by the encapsulation of Alexa488-labeled siRNA and Alexa546-labeled siRNA (1:1 in molar ratio), generating a FRET signal of the two dyes associated with the micelle formation. While control micelles without a shielding PEG-layer (DCM) maintained a high FRET efficiency for at least 12 h after the cellular internalization, the micelles composed of three layers (TCM) showed significantly low FRET levels associated to the successful release and spread of the siRNA payloads (Figure 2.6 c).
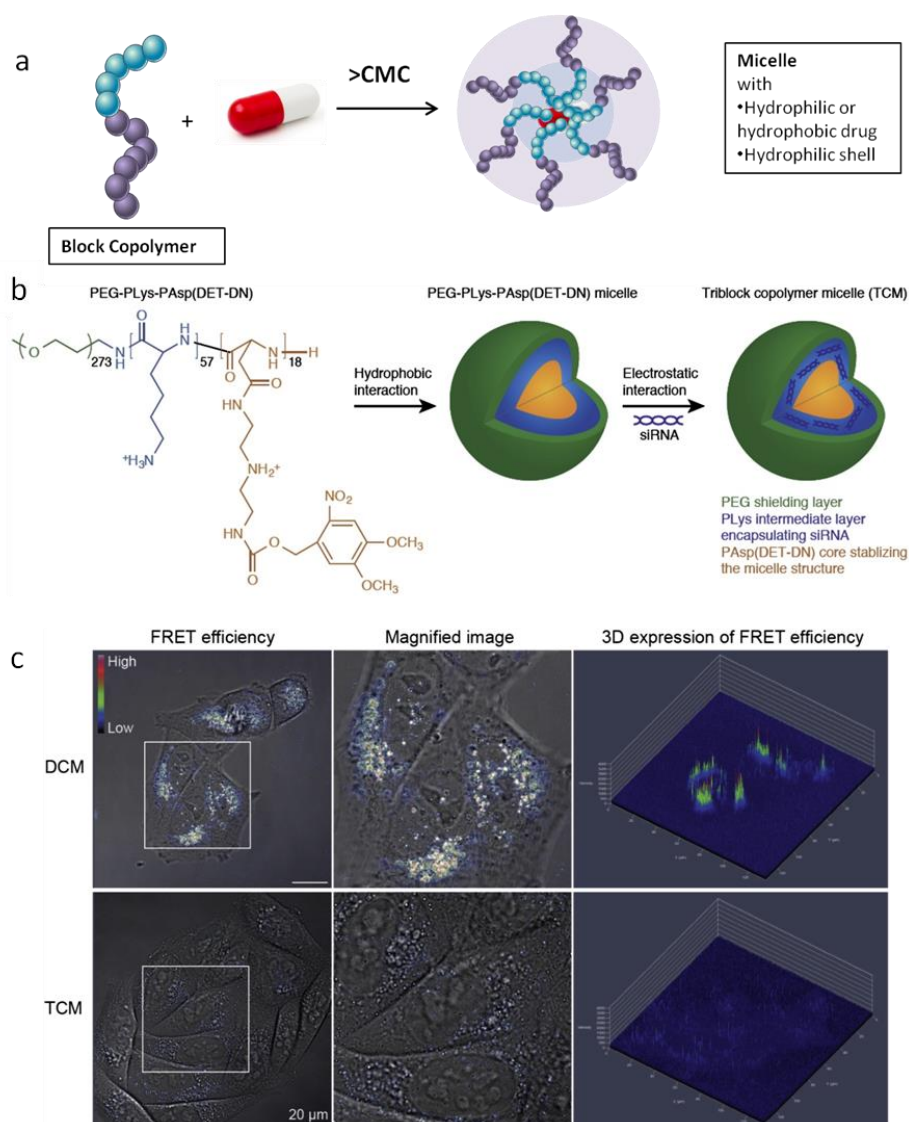

Figure 2.6: a) Schematic representation of a polymer micelle, b) Schematic illustrations of hydrophobic triblock copolymer micelle having hydrophilic PEG, siRNA-loading cationic poly(l-lysine) (PLys), and hydrophobic core-forming polyaspartamide derivative[132], c) Release of two different dye-labeled siRNA payloads from polymeric micelles: FRET images of the micelles within cultured HeLa cells 12 h after the start of image acquisition. FRET ratio (Alexa546 intensity/Alexa488 intensity × 500) expressed in a rainbow scale: red, green, and blue signals mean high, moderate, and low FRET efficiency[132]. B and C reproduced with the permission of Elsevier.

The delivery of biomacromolecular therapeutic agents using polymer micelles provides a highly controlled platform for a broad range of therapeutic agents or a combination of therapeutic agents. Modern processes to synthesize well-controlled and well-defined block copolymers allow the design of complex micelle structures with varying morphologies and compositions. Furthermore, the encapsulation of the macromolecular therapeutic agents does not require the use of harsh chemical modifications and the dense polymer shell protects the therapeutic agents from denaturation. Unfortunately, similar to other self-assembled systems, micelles can suffer from an inherent limited stability *in vivo* due to the potential perturbation in the non-covalent interactions governing the assembly. [134]

Polymersomes

Polymersomes are reservoir-like nanosystems that can be used for the encapsulation of macromolecular therapeutic agents. They differ from nanocapsules in the nature of their polymer shell, and from micellar system in the mechanism of formation.[39] Polymersome are usually built with copolymer block bearing one hydrophilic and one hydrophobic block., which self-assemble in a bilayer polymer membrane,[135] reminiscent of the phospholipidic double layer of the liposome, and the block copolymers used can be considered as synthetic mimics of phospholipid to some extent.[136] The polymersomes, like the liposomes, have an aqueous core separated from the surrounding environment by a semi-permeable hydrophobic membrane (Figure 2.7 a). However, polymersome, while allowing for similar encapsulation and release of payloads as the liposomes, also offers more versatility in terms of composition and potential stimuli.[137] The polymersomes also usually display a larger stability in dilute environment in comparison to liposomes.[138]

Several approaches can be employed to synthesize polymersomes.[136] For example, the block copolymers can be dissolved in a good solvent for both blocks, and this polymer solution used to cast a thin polymer film. The addition of water onto the polymer film leads to the swelling of the polymers film and during the rehydration process, polymersomes are budding from the hydrated film (Figure 2.7 b).[139] However, this method usually generates polymersomes with broad size distributions. Alternatively, the block copolymers can be dissolved in an organic solvent, which is then injected in an aqueous solution under vigorous stirring. This procedure induces the insolubility of the hydrophobic blocks, triggering the copolymer self-assembly into polymersomes as a result of increasing interfacial tension between the hydrophobic blocks and water (Figure 2.7 c).[140] In such case, the size and size distribution of the vesicles can be varied by selecting different organic solvents,[141] or tuned with the polymer concentration. Increasing the polymer concentration usually results in an increase of the polymersome size due to the increased number of polymer chains in the same volume of solution resulting in the emergence of polymersomes of larger surface area and diameter.[142]

Moreover, the polymersome size can be influenced by the mixing speed. During the mixing of the water and organic solvent containing the polymer, polymer molecules diffuse into the water phase. If the mixing rate is high, the polymers diffuse into the water phase quickly and self-assemble into small polymersomes. However, when the mixing rate decreases, the polymer molecules can diffuse more freely into the water phase and will self-assemble more slowly, which leads to larger polymersomes.[143] This method to produce polymersome facilitates the encapsulation of water-soluble cargo molecules, since the polymersomes form after the addition of the polymers to water, but it is difficult to completely remove the organic solvent trapped in the membrane bilayer. This fact can hamper the encapsulation of sensitive macromolecular biologics, which can be denatured and inactivated by the residue of organic solvents. Moreover, if applied in biological systems, this fact can even cause toxic side effects and damage the living cells.[144] Alternatively, polymersomes can be prepared by the direct dissolution of block copolymers in aqueous media. Critical parameters influencing the morphology of the resulting nanosystems are the mass or volume fraction of the hydrophilic block and the interaction parameter of the hydrophobic block with water.[145]

The flexibility and dynamics of the polymersome membrane is one great advantage of those nanosystems. Polymersomes can simultaneously encapsulate hydrophilic therapeutic agents of high and low molecular in their inner core, and they can integrate hydrophobic agents in their double layered membrane. This leads to the possibility to efficiently co-deliver multiple substances in one nanosystem.[135] The release of the encapsulated molecules can be controlled by the functionalization of the membrane of polymersomes with molecules tuning the permeability of the membrane and increasing the mass transport of the active molecules. Several approaches have been developed to do so such as the functionalization of the polymersome membrane with channel-forming transmembrane proteins[146], DNA nano-pores[147], or smart gates.[148] However, the elaborate engineering of the polymersome membranes successfully leads to the controlled release of small molecules and drugs, but the release of biomacromolecules through polymersome pores is current challenge. The design of smart membranes can provide one solution to this, as it can incorporate heterogeneous membrane sections with finely controllable and responsive behavior.[148] By the incorporation of responsive polymers in the membrane, the permeability of the membrane can be controlled. The employed polymers adjust their properties in response to external stimuli, leading to the swelling of the membrane and the controlled release of payload. One example of this type of system where smart gates are formed in polymersome membranes exploits the responsive polymers polyNIPAM and poly(diethylamino)ethyl methacrylate (polyDEA).[148] Upon self-assembly at 40 °C in the mixture of neutral water and tetrahydrofuran (THF), the thermoresponsive polyNIPAM moiety is dehydrated and the pH-responsive polyDEA segment is deprotonated. This results in polymersomes with closed gates in the membrane. The polyNIPAM-based segment enables the design of a "boarding gate" in the

membrane, opening up below the LCST of PNIPAM (e.g., 20–30 °C). Under these conditions, biomacromolecules can be loaded and the gate can be closed at physiological temperature (e.g., 37 °C) to lock the payload (Figure 2.7 d). The pH-sensitive polyDEA segments in the polymersome membrane were designed to serve as the "release gate", allowing the release of the encapsulated plasmid DNA in acid environment (such as in endosomes) upon the protonation of the polyDEA. The protonation leads to a swelling of the polymersomes from around 450 nm at pH 6.8 to 610 nm at pH 5.4 and allows for the transfection of cells with GFP-encoding plasmid DNA due to the successful release of the payload *in vitro* and *in vivo* (Figure 2.7 e).

The key factor making polymersomes such an appealing delivery vehicle is the ease to include multiple functionalities in the polymer design. The polymersomes can be designed with high selectivity, controlled permeability and versatile surface functionalities. They can exhibit long blood circulation times when their surface is functionalized with polymer segments like PEG.[149] In addition, sensitive and fragile cargos like biomacromolecular therapeutic agents are efficiently protected from the surrounding environment by the robust nature of the polymersome bilayer, which increases the life-time of encapsulated cargo over a long period.[150]
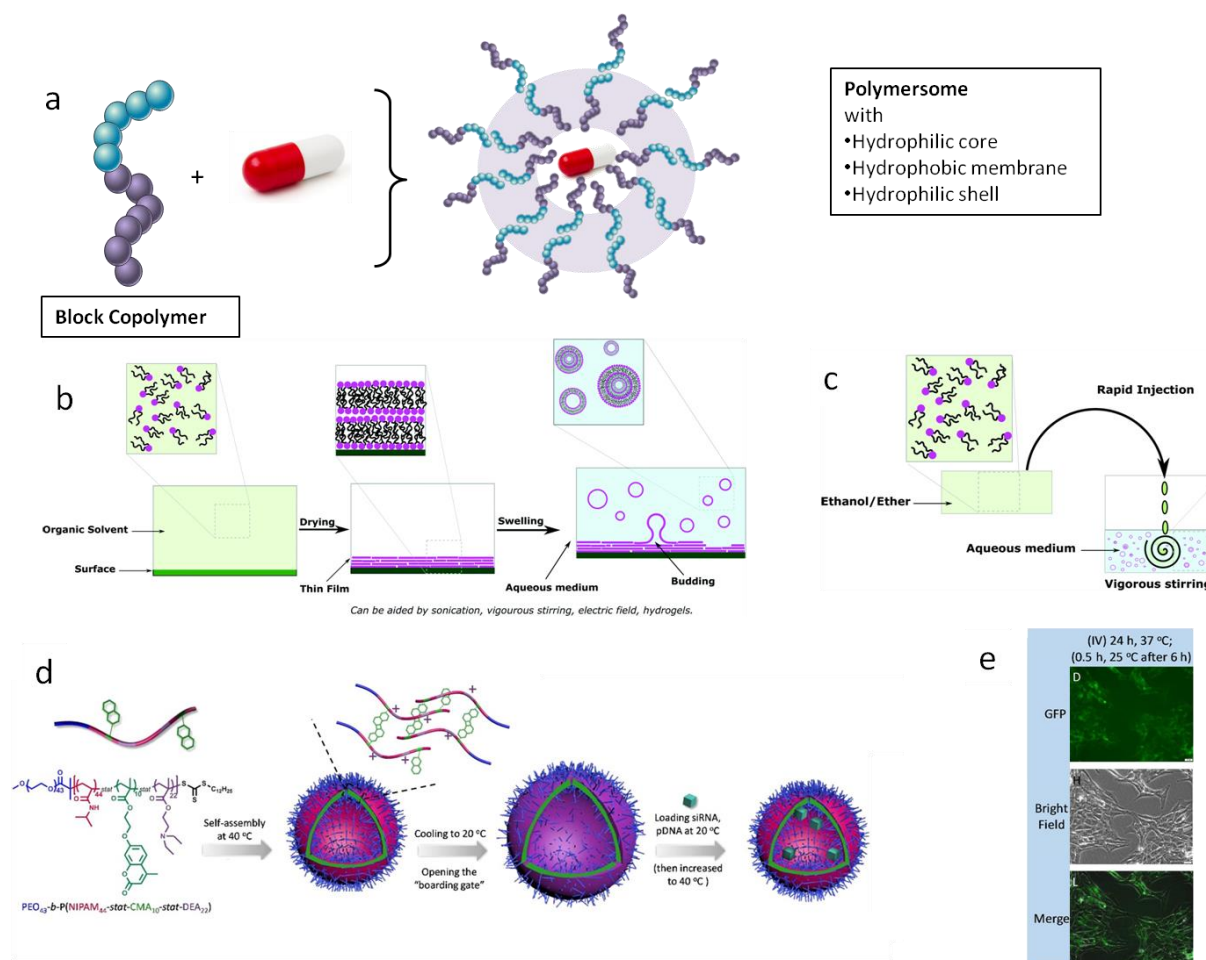
Figure 2.7: a) Schematic representation of polymersomes, b) General method to prepare polymersomes by the rehydration method[139], c) General method to prepare polymersomes by the mixing of organic and aqueous solvents[139], d) Self-assembly of polyNIPAM-polyDEA block copolymers into a polymersome with a "boarding gate" and a "release gate" [148], e) Cellular delivery and release of GFP-encoding plasmid DNA by polymersomes with smart gates visualized by the expression of GFP in the cells[148]. B and C reproduced with the permission of the Royal Chemical Society, D and E reproduced with the permission of The American Chemical Society.

Nanoparticles, nanogels and nanocapsules

Over the past decade, covalently crosslinked polymer nanocarriers have attracted growing interest for their use in the delivery biomacromolecular therapeutic agents due to their flexibility and adaptability in terms of hydrophilicity, stability, size, charge. [151, 152] Crosslinked polymer nanocarriers are nanosized networks composed of polymer chains linked together through chemical or physical crosslinking points (Figure 2.8 a). In a polymer nanoparticle or polymer nanogel, the polymer matrix is uniformly distributed in the entire nanocarriers, while in a nanocapsule, the polymer network is segregated at the carrier surface, creating a shell that can engulf either an aqueous or organic core. The main distinction between nanoparticles and nanogels is the swelling of the polymer network, in a

nanoparticle, the defined three-dimensional polymer network is mostly desolvated, while in the case of nanogels the network holds a large quantity of solvent.[153]

The crosslinked polymer nanocarriers used in the design of DDS can be made from virtually any polymer, of natural or synthetic origin, or a combination of thereof, encompassing a wide range of chemical compositions and bulk physical properties.[154] They can be produced by direct polymerization methods or it is also possible to use preformed polymers in the preparation of the nanocarriers.[155] They can be obtained from the crosslinking of self-assembled structures, solvent evaporation, polymerization in heterogeneous media like miniemulsion, precipitation polymerization, or many other techniques.[156] Almost any polymerization reaction and any preformed polymer are suitable to be used in this vast range of processes. For example, radical, anionic, cationic, oxidative or polyaddition polymerization reactions can be performed with many different monomers (e.g. styrene, acrylates, methacrylates, fluoroacrylates, acrylamides, aniline, pyrrole) to obtain solid polymer nanocarriers.[157] [158, 159] [157] Furthermore, many preformed synthetic and natural polymers such as *N*,*N*-bis(acryloyl)cysteamine[160], poly(lactide-*co*-glycolide)[161], poly(ethylene glycol)- poly(l-lysine)[162], lignin[163], hydroxyethyl starch[164], hyaluronic acid[165], or heparin[166] were used to synthesize such DDSs.

For example, the self-assembly of polymers has been used to produce nanogels.[167-170] [171] This method usually involves the controlled self-assembly of the hydrophilic nanogel precursors followed by a chemical crosslinking under mild conditions and in aqueous media.[172] The crosslinking of the polymers in a self-assembled system is a powerful strategy to overcome the inherent risk of a disassembly of self-assembled system, which is often accompanied by the premature release of encapsulated payloads. Furthermore, if polymers are first self-assembled into vesicles with a hollow aqueous core based on hydrophobic or electrostatic interactions and further crosslinked, nanocapsules can be obtained. The self-assembly of the polymers employed as precursors can usually be achieved by the incorporation of complementary functional groups, which form physical crosslinks with each other. For this purpose, chemical crosslinking of functional groups such as amines, hydroxides, aldehydes, thiols, or acrylates have been used and provide nanoparticles with a high stability and enables the controlled entrapment of various cargo molecules.[173] The crosslinking of self-assembled systems to produce nanocarriers often does not require the use of organic solvents or additional harsh reagents, which is advantageous for the encapsulation of highly sensitive biomacromolecular therapeutic agents. However, the prerequisite for this method is the use of polymers with both the ability to form polymer self-assemblies and the ability to be chemically crosslinked under mild conditions, which limits the number of suitable materials.[174]

Another technique for the preparation of nanoparticles is the polymerization in heterogeneous media, like a miniemulsion.[172] In this method, an aqueous solution of monomers, or already preformed polymers and crosslinkers is emulsified in a hydrophobic solvent, resulting in a surfactant-stabilized emulsion of water droplets in an oil phase.[173] The monomer-containing droplets are then polymerized or the preformed polymers are crosslinked to obtain solid polymer nanoparticles, nanogels or nanocapsules. Miniemulsion polymerization is compatible with a wide variety of polymerization and crosslinking techniques.[155] Examples of commonly used monomers include acrylamide (AAm), pH-sensitive acrylic acids (AA) and thermoresponsive N-isopropylacrylamide (NIPAM).[175] Furthermore, various natural polysaccharides such as starch, cellulose, chitosan, dextran or hyaluronic acid can be crosslinked in emulsions to yield biocompatible nanoparticles and nanogels.[153] Various drugs can be loaded within the aqueous droplets, which usually results in very high encapsulation efficiencies.[157, 176] However, the generation of the initial heterogeneous media requires the use of organic solvents and the addition of surfactants, which could possibly interfere with the sensitive structure of the encapsulated biomacromolecular therapeutic agents. Another technique yielding nanoparticles and nanogels without the aid of surfactants and organic solvents is precipitation polymerization. This process requires the use of a solvent, which can dissolve both the monomer and initiator or already preformed polymers and their crosslinker. Upon the initiation of the polymerization or crosslinking reaction, the polymer network becomes insoluble and precipitates as solid particle.[173]

The distinct structures produced by the different methods display different properties. Polymer nanocapsules are hollow containers in which a large variety of substances can be placed within the core reservoir. The resulting hosting capacity enables the delivery and the controlled release of various drugs from such DDSs.[155] In comparison to solid nanoparticles, nanocapsules with a liquid core allow for the encapsulation of a much larger amount of payloads.[177] Furthermore, the polymer content in a nanocapsule is lower compared to solid polymer nanoparticles of the same size, endowing the nanocapsules with lower risks of immune responses against the body-foreign polymers.[178] Nanogels, usually made of hydrogel, are polymer matrices with the ability to absorb a high amount of water in their network. Such a dynamic network of swollen hydrophilic polymers can contain ions, salts, polysaccharides or other stabilizing molecules co-dissolved with the drug and provides an optimal environment during the delivery process. Conversely, nanoparticles are built with an unswollen network of rigid crosslinked polymers and usually display a very high stability during the delivery process. In all cases, the release of biological agents incorporated in those polymer systems can occur by diffusion and mass transport through the polymer network. However, the release process can also be triggered by either the degradation of the nanoparticle or by a change in the structure of the polymer nanosystems, which occurs as a consequence of environmental signals present at the intended release site.[172] In either cases, the crosslinking density of the polymer network decreases

while the mesh size is increased. The mesh size controls steric interactions between the drugs and the polymer network. When the mesh is larger than the drug, the drug release process is dominated by diffusion. By controlling the mesh size, molecules of different size can be released with great control. For example, the release of model macromolecules from ketone-functionalized dextran-based nanocapsules was controlled by a reversible crosslinking of the shell.[69] The hydrazone network density resulting from the reaction with a poly(styrene-*co*-methacryloyl hydrazide) crosslinker was tuned by the pH-responsive equilibrium between hydrazide and hydrazone groups. Such dynamic covalent bonds undergo a reversible disassembly under an acidic pH value and the prepared NCs are suitable for a controlled release of macromolecules (Figure 2.8 d).

The encapsulation of biomacromolecular therapeutic agents in nanoparticles, nanogels or nanocapsules offers many advantages. The polymer network can be finely tuned to interrupt biomacromolecular drugs without their chemical modifications and thus preserve a high degree of their specific three-dimensional structures. The crosslinking points in the polymer nanosystems endow those DDSs with great stability and allow for further surface functionalizations without the risk of premature drug release or the loss of physical integrity of the DDS.[179] The release of encapsulated biomacromolecular therapeutic agents can be controlled either by the degradation of the polymer itself or the swelling/deswelling of the polymer matrix. Moreover, the versatility of the preparation techniques provides the opportunity to incorporate an array of responsive units and smart properties either within the polymers or in the crosslinking points.
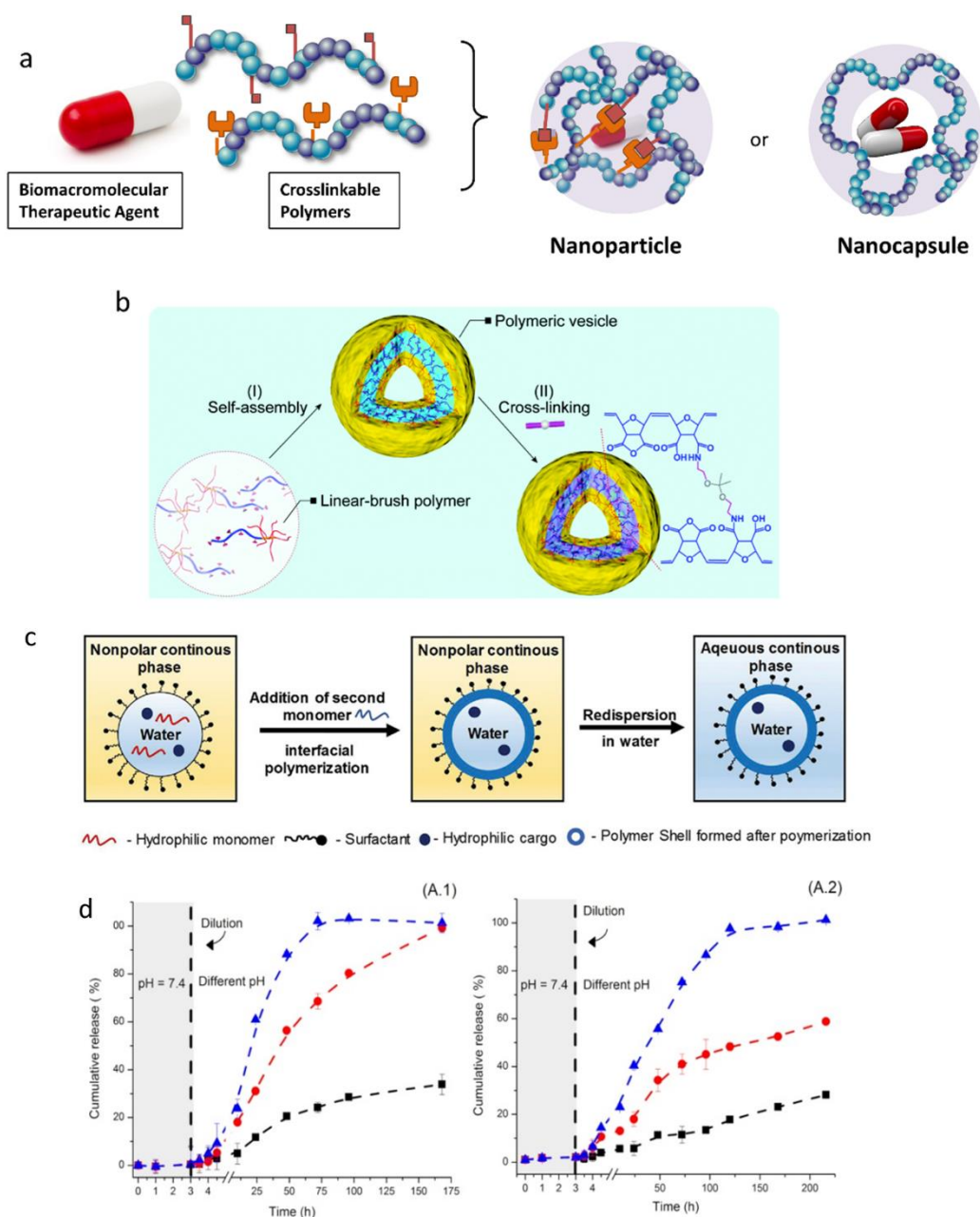
Figure 2.8: a) Schematic representation of nanogels, b) Scheme of the crosslinking of self-assembled polymersomes by the reaction between the cross-linker 2,2'-(propane-2,2-diyl bis(oxy))diethanamine and the anhydride units in the bilayer membrane[180], c) Scheme of the nanocapsule formation through interfacial polymerization on miniemulsion droplets[155], d) pH-responsive release of rhodamine-functionalized dextran as the payload with a molecular weight (1) M_n = 150 kDa and (2) M_n = 500 kDa from hydrazone-crosslinked dextran nanocapsules (pH value of 7.4 (■), 6.0 (●), and 5.2 (▲))[69]. B reproduced with the permission of The Royal Chemical Society; C reproduced with the permission of Wiley Online Library, D reproduced with the permission of The American Chemical Society.

2.3 Protein nanocarrier

Among the polymer materials employed for the design of drug delivery systems, proteins have emerged as alternative precursors to common synthetic polymers. Proteins are particularly interesting as they show excellent biocompatibility and have a low toxicity. They can be easily degraded by natural enzymes commonly found in the human body. The degradation rate can vary with the availability and concentration of the enzymes, which can be exploited to control the release of the delivered cargo from the protein nanocarrier. Such enzyme-degradable systems do not require an external trigger to promote the release since the overexpression of enzymes at the site of a disease can control their decomposition in a predefine type of cell.[181]

Among many available proteins, proteins from the albumin family have been widely explored for the design of nanocarriers since they are readily available, remain stable over a wide range of pH values, and are the most abundant plasma proteins. One major innovation in the last years was the development of paclitaxel-albumin nanoparticles (Abraxane), the first FDA-approved DDS where a drug is encapsulated in a shell of protein. The delivery of paclitaxel, a chemotherapeutic agent, by the albumin nanoparticle increased the efficacy of the drug and lowered the side effects.

Among protein nanocarriers, proteins formulated as hollow nanocapsules show great benefits as DDS since they provide a high encapsulation efficiency and have a high loading capacity for both small molecule drugs and therapeutic macromolecules. The crosslinked protein shell provides a diffusion barrier for the encapsulated payload, and the crosslinking density can be adjusted to control the release of the payload.

2.3.1 Preparation of protein nanocapsules by miniemulsion

Protein nanocapsules can be efficiently prepared by interfacial crosslinking of the proteins in miniemulsions. Miniemulsions are two-phase systems, which contain nanodroplets in the size range of 50-200 nm.[182] If an oil-phase is dispersed in aqueous media, a direct miniemulsion is obtained, whereas aqueous droplets in an organic media build an inverse miniemulsion.[155]

The preparation of miniemulsions typically involves several steps: the formation of a macroemulsion by stirring of the two immiscible phases, followed by applying high-energy forces to break the spontaneously formed droplets into homogeneous nanometer-size droplets with a low polydispersity. The first homogenization step involves the stirring of the two phases or mixing the biphasic system with a homogenizer. The shear obtained by these techniques results in the formation of a macroemulsion but is not efficient enough to generate homogeneous nanodroplets. High-energy methods like ultrasonication or high-pressure homogenization can yield the nanodroplets. Following this step, the newly formed droplets with an increased surface area have to be stabilized efficiently (Figure 2.9 a).

Power ultrasound is one possible system applied for the generation of miniemulsions. In this case, the ultrasound waves propagate through the pre-formed macroemulsion and produce acoustic cavitation, which is the formation and the collapse of air bubbles in the system.[183] The collapse of the air bubbles is caused by their implosion and causes intensive and powerful shock waves in the surrounding area. The force generated by the cavitation events leads to the disruption of the droplets of the emulsion and the reduction of the droplet size. Typically, the ultrasonication is performed until the size of the droplets becomes constant, which can take several minutes. However, the high energy of the ultrasound waves and the long duration of their application are often detrimental to sensitive biological molecules. This procedure may disrupt their complex three-dimensional structure and result in a loss of biological activity.[184]

Hence, a milder and more controlled preparation method for the formation of the miniemulsion is required when biomolecules are involved. In this case, high-pressure microfluidization can be used. This technique allows for the preparation of the miniemulsion in a continuous manner, where the macroemulsion is first divided into two microstreams.[185] The two streams are then recombined at a high speed and pressure in a Y-type interaction chamber, and the resulting collision of the droplets in the two microstreams leads to the disruption of the droplets and the formation of smaller droplets (Figure 2.9 b). Such a process induces high mechanical stress on the droplets of the macroemulsion in a localized area for a very short time.[186] This leads to the preservation of sensitive structures in biomacromolecules and is a great possibility to maintain the activity of the involved molecules.[184]

After the formation of a homogeneous miniemulsion, the newly formed interface needs to be stabilized. There are two major destabilization processes in miniemulsions, which are the growth of droplets due to coalescence and the Ostwald ripening mechanism. Coalescence results from the collision of droplets caused by their Brownian motion or their flow occurring in the system. It leads to the fusion of the droplets and an increase of polydispersity of the emulsion. In order to prevent coalescence, appropriate surfactants are added. Those surface-active agents stabilize the formed interface and prevent the effective collision of droplets by creating either electrostatic repulsion, steric repulsion or a combination of both between the droplets.[182] The concentration of surfactant used during the formation of the miniemulsion influences the size of the nanodroplets and the size of the resulting particles. Furthermore, surfactant choice influences the surface characteristics of the resulting nanoparticles, such as their surface charge and their colloidal stability.[187] In addition, the surfactant used also plays a major role in the biological fate of the resulting particles since the interaction of nanoparticles with cellular membranes is highly dependent on their surface properties. For instance, the composition, concentration, and charge of surfactants adsorbed on nanocapsules

significantly influenced the composition of the protein corona after incubation with plasma,[188, 189] and the cellular uptake of the particles.[190]

Another phenomenon disturbing the stability of the miniemulsion is Ostwald ripening. Ostwald ripening also results in the unwanted growth of the droplets.[191] The Laplace pressure p_{Laplace} exerted on the droplet decreases as the droplet radius R increases:

$$p_{\text{Laplace}} = \frac{2\gamma}{R} \qquad \text{(Equation 2.1)}$$

where γ is the interfacial energy between the droplet and the continuous phase.[192] Consequently, the formation of larger droplets is favored to minimize the Laplace pressure in the system. Hence, in emulsions with a relatively broad droplet size distribution, Ostwald ripening induces the growth of larger droplets with lower Laplace pressure at the expense of smaller ones with higher Laplace pressure via the diffusion of encapsulated material from smaller droplets to larger ones.[193] This leads to the minimization of pressure difference and the size distribution reaches a steady state when the Laplace pressure and Osmotic pressure are equilibrated. If the small droplets in the miniemulsion are not stabilized against the Ostwald ripening process, they will disappear, and the emulsion will separate in the two immiscible phases. To prevent this, the miniemulsion can be stabilized against the Ostwald ripening effect by the addition of osmotic pressure agents to the dispersed phase.[194]

The osmotic pressure inside the droplet Π_{osm} can be generated by the addition of a molecule of molecular weight M dissolve in the dispersed phase at a concentration c:

$$\Pi_{\text{osm}} = \frac{RTc}{M} \qquad \text{(Equation 2.2)}$$

The osmotic pressure agent is used to generate a osmotic pressure within the droplets and partially counteract the effects of the Laplace pressure.[195] The ideal osmotic pressure agent displays extremely low solubility in the continuous phase and provides additional osmotic pressure inside the droplets. Although the osmotic pressure generated inside the droplets does not entirely counteract the Laplace pressure, a reduction in the size of the droplet would result in an increase in the osmotic pressure, counter-balancing the variation in the Laplace pressure. With the addition of the osmotic pressure agent, the system can reach a steady-state where the droplets are no longer evolving (Figure 2.9 c). For direct miniemulsions, often hexadecane or silanes are employed as osmotic pressure agents, whereas salts can be used in inverse miniemulsions.
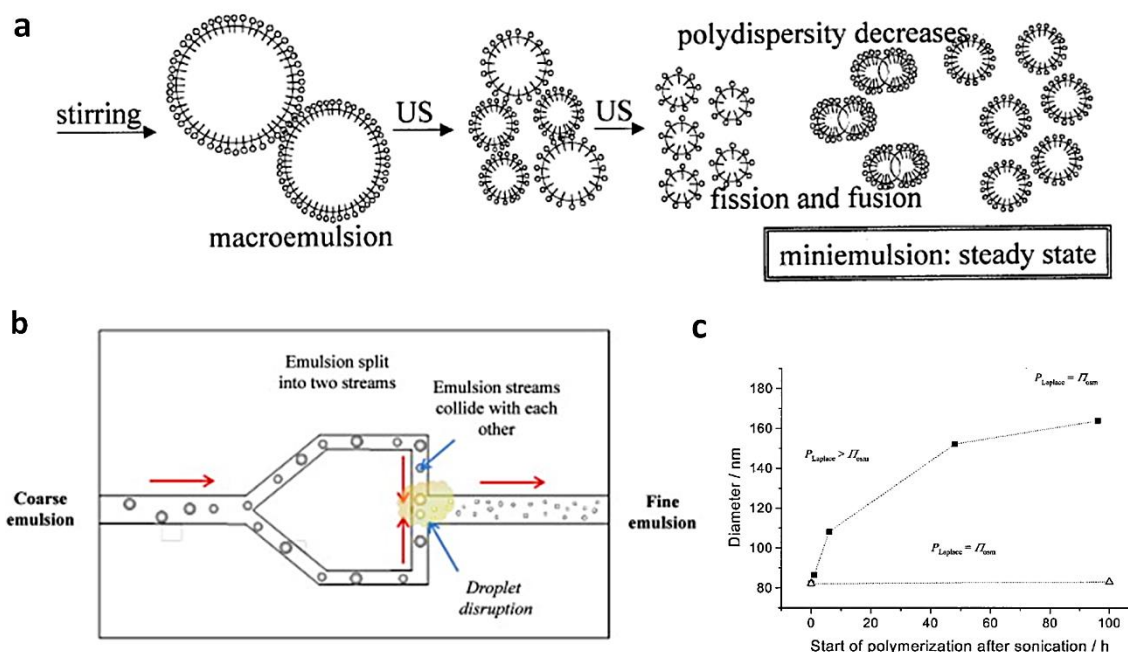
Figure 2.9: a) Formation of the miniemulsion by ultrasound[192], b) Formation of the miniemulsion by microfluidization[186], c) Growth of miniemulsion droplets after the emulsification with and without an osmotic pressure agent[192]. A and C reproduced with the permission of John Wiley & Sons, Ltd and B reproduced with the permission of Elsevier.

The synthesis of protein nanocapsules is performed in an inverse miniemulsion with a buffered aqueous solution of the protein dispersed in an organic solvent like cyclohexane or toluene (Figure 2.10).[196] After the formation of the miniemulsion, a reactive crosslinking agent is added to the continuous phase, and the reaction between the protein and crosslinker occurs at the interface of the two phases. When the reaction kinetic is fast enough, and the surface tension of the crosslinked polymer is controlled, a solid protein shell can be formed covering the precursor droplet.[164] Other materials can be encapsulated in the nanodroplet with high efficiency if they are co-dissolved with the protein in the dispersed phase.[197] Furthermore, the amount of crosslinker added to the system can be used to control the thickness and permeability of the nanocapsules, as well as the resulting release properties of the system. Once the crosslinking reaction occurred, the nanocapsules can be purified by centrifugation and redispersion in a fresh organic solvent and transferred to water. Many chemical reactions can occur at the droplet interface resulting in crosslinked protein core/shell structures.[198] For instance, the step-growth formation of polyurethane and polyurea networks using a di-functional isocyanate crosslinker results in the reliable crosslinking of the protein and leads to high encapsulation efficiencies. However, there may be competitive reactions with nucleophilic amino- and hydroxyl-groups of the encapsulated cargo.

For this reason, biorthogonal crosslinking reactions such as the interfacial polyaddition with azide-alkyne or the trazole-ene 1,3 dipolar cycloaddition can be employed. In this case, the protein precursor has to be modified with one or both of the functionalities and then "clicked" together under mild conditions.
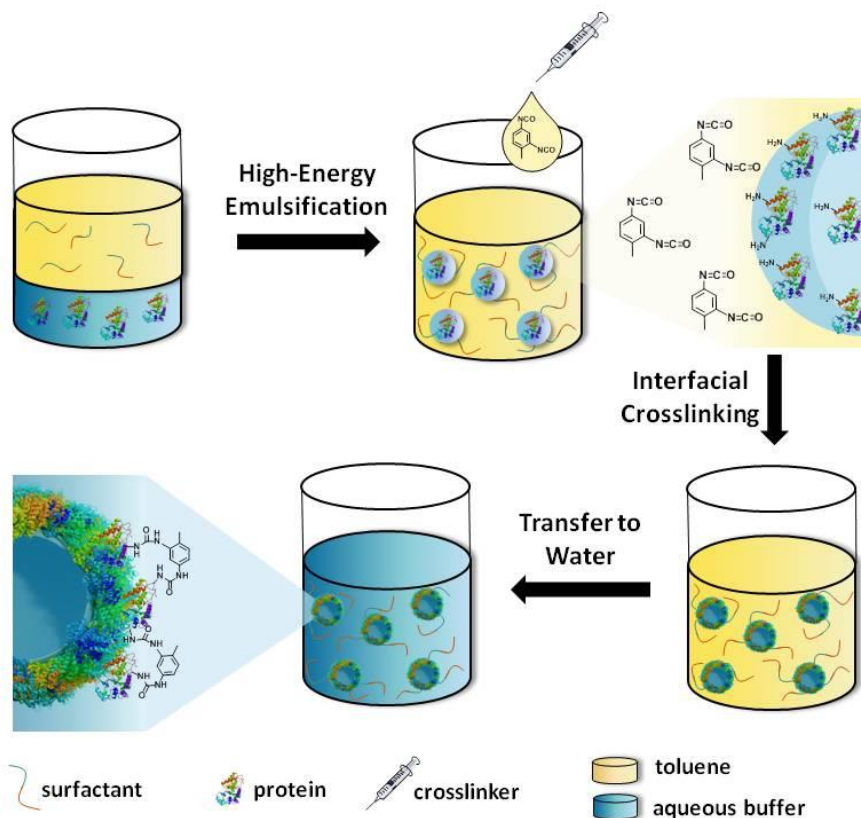

Figure 2.10: Synthesis of protein nanocapsules via inverse miniemulsion.

2.3.2 Nanocapsules made with proteins and their application

A very efficient strategy for the design of protein nanocarriers is the synthesis of the nanocapsules using proteins displaying a specific function. The proteins can preserve their native function after their processing into nanocarriers leading to the generation of nanosystems where the excipient has a function.

For example, nanocapsules synthesized from antigen proteins have a great potential for the development of novel nanovaccines. One major risk emerging from the use of polymer nanocarriers in vaccination is the severe side effects that can occur *in vivo*, which often include the generation of immunity against the polymer carrier compounds.[199] Hence, an interesting solution would be to formulate the nanocarrier exclusively out of the specific antigen. This approach prevents possible side effects and further increases the dose of antigen delivered.[200]

For this reason, the synthesis of nanocapsules composed solely of an antigen protein offers an elegant approach to prevent immune responses not associated to the antigen itself. For instance, the hepatitis C virus non-structural protein 5A (NS5A) was used to synthesize full protein nanocapsules, which induced an antigen-specific immunity in mice.[200]

Ovalbumin is another model antigen protein and acts as an immunostimulating adjuvant if employed in nanovaccines. Nanocapsules composed of ovalbumin and loaded with two small molecule adjuvants, resiquimod (R848) and muramyl dipeptide (MDP), showed a superadditive immune stimulation when delivered to dendritic cells. Furthermore, the nanocapsule formulation activated the immune cells with a higher efficiency than when the same adjuvants were administered in solution.[201]

Aspartyl (asparaginyl)-β-hydroxylase (ASPH) another interesting antigen candidate for the formulation of nanovaccines.[202] It is overexpressed in a variety of malignant tumors[203] and in the case of hepatocellular carcinoma (HCC) it produces a malignant phenotype with increased cell motility and metastases growth.[203] The expression of ASPH on the surface of the tumor cells suggests that ASPH could be used as an immunotherapeutic target in anti-cancer vaccines.[204] The design of a nanovaccine composed solely of ASPH nanocapsules offers a novel approach to target and eradicate ASPH expressing cancerous tumors with the goal to induce ASPH-specific immune responses. For this purpose, full-ASPH nanocapsules can be synthesized using the inverse miniemulsion technique. The nanocapsules can be further loaded with immune-activating adjuvants, such as monophosphoryl lipid A (MPLA) offering a new delivery concept to develop multi-functionalized nanovaccines for dendritic cell-focused cancer immunotherapy.

Another therapeutic application of protein nanocapsules, is the delivery of growth-factor proteins, which can be employed, for example, in the treatment of bone fractures. Growth factors are proteins, which play an important role in the stimulation of cell growth and differentiation and are known to promote the repair of poorly healed fractures.[205] However, their systemic administration results in a low therapeutic efficacy due to the poor *in vivo* half-life of the growth factors, their inefficient distribution at the fracture site, and an excessive inflammation induced by a potential overdose. The synthesis of protein nanocapsules composed of growth factor proteins increased the circulation time of the therapeutic proteins to over 48 h while maintaining the structure and function of the model growth factor bone morphogenetic protein-2 (BMP-2).[206] Such nanocapsules were passively targeted to the fracture site *in vivo* by exploiting malformed blood vessels, where they effectively realized the repair of a bone fracture while showing much lower inflammatory irritation than native BMP-2.

3. Experimentals

3.1 Materials

All chemicals were used as received unless otherwise mentioned. Polyglycerol polyricinoleate (PGPR) was provided from Danisco and was purified by dissolution in cyclohexane followed by centrifugation (4000 rpm, 5 min) to precipitate solid particles. The supernatant was recovered and the purified PGPR was dried by rotary evaporation.

3.2 Instrumentation

The pre-emulsions injected into the microfluidizer for emulsification were prepared by a T18 digital ULTRA-TURRAX operating at 20 000 rpm.

The miniemulsions were prepared by microfluidization (LV1 Microfluidics Corporation) using a Y-shape interaction chamber with 75 μm channels (700 bar, 2 cycles).

The size distribution of the nanocapsules was measured by dynamic light scattering (DLS) at 20 °C using a Malvern NanoS90 device at 90° angle.

Scanning electron microscopy (SEM) was performed by a 1530 Gemini LEO (Zeiss) microscope. For the sample preparation, 8.0 μL of the purified sample in toluene was dropped on a silica wafer and allowed to dry under ambient temperature.

Transmission electron microscopy (TEM) was performed by a Jeol 1400 transmission microscope with a voltage of 120 kV.

FT-IR measurements were performed with a Perkin Elmer Spectrum BX FT-IR spectrometer between 4000 and 600 cm^{-1}.

The CD measurements were carried out on a J-1500 JASCO circular dichroism spectrophotometer using a cuvette with a path length of 0.1 cm. The spectra were measured between 260 nm to 190 nm at a protein nanocapsule concentration of 0.02 mg mL^{-1}.

Zeta potential measurements were performed by diluting the nanocapsule dispersion in potassium chloride solution and measured with a Malvern Zeta Sizer (Malvern Instruments, UK).

Fluorescence intensity measurements were performed in 96-well plates on an Intinite M1000 plate reader from Tecan, Switzerland.

Nuclear magnetic resonance (NMR) analysis were performed on a Bruker Avance spectrometer operating at a frequency for 1H of 300 MHz.

Flow cytometry experiments were conducted on a BD LSR II. The data analysis was conducted with the FlowJo software 10.6.1.

3.3 Synthesis of nanocarriers

Synthesis of ovalbumin nanocapsules

The nanocapsules were prepared by a polyaddition reaction in an inverse miniemulsion, as described previously.[196] In a typical experiment, the aqueous phase was prepared by dissolving 20 mg of OVA in 0.2 mL PBS-buffer (pH 7.0). When the nanocapsules were used to encapsulate PEG, 4 mg of PEG was added to the aqueous solution. The organic continuous phase was prepared by dissolving 75 mg of PGPR in 3 mL toluene. The aqueous and organic phase were combined and pre-emulsified with an ultraturrax (20 000 rpm) and homogenized by one cycle through a microfluidizer (LV1, microfluidic corporation) at an operating pressure of 10.000 MPa in a 75 μm Y-shape emulsion chamber. A solution of 25 mg PGPR and 4 μL, 1 uL or 0.1 μL of crosslinking agent (TDI) in 0.5 mL of toluene was added dropwise to the miniemulsion over a period of 2 min. The reaction was stirred over 20 h at room temperature. The synthesized nanocapsules were purified by three cycles of centrifugation (30 min, 1200 RCF) followed by redispersion in fresh toluene for the removal of excess surfactant and unreacted crosslinker. To transfer the nanocapsules to an aqueous solution, 500 μL of the dispersion in toluene were added dropwise to a solution of Lutensol AT50 (0.1 wt %) in PBS buffer under sonication in an ultrasonic bath. The resulting dispersion was stirred in an open vial for 3 h to evaporate the toluene. The dispersion was purified using Amicon centrifugal filter (MWCO 300.000, two times, 30 min) and redispersed in fresh PBS-buffer to remove the unreacted protein, excess of surfactant, and unencapsulated payload.

Synthesis of enzyme nanoreactors

The enzyme nanoreactors were prepared similarly to the OVA NCs. The aqueous phase was prepared by dissolving 30 mg of enzyme (horseradish peroxidase, glucose oxidase and lysozyme) and 1 mg of NaCl in 0.3 mL PBS-buffer (pH 7.0). When the nanoreactors were used to encapsulate luminol, 0.7 mg of dextran-luminol was added to the aqueous solution. For the encapsulation of Cy5, 0.3 mg of the dye was added to the aqueous solution. The crosslinking reaction and the purification were identical to the OVA NCs.

Synthesis of enzyme nanoreactors by ultrasonication

The enzyme nanoreactors were prepared by a polyaddition reaction in an inverse miniemulsion. In a typical experiment, the aqueous phase was prepared by dissolving 30 mg of enzyme and 1 mg of NaCl in 0.3 mL PBS-buffer (pH 7.0). The organic continuous phase was prepared by dissolving 75 mg of polyglycerol polyricinoleate (PGPR) in 3 mL toluene. The aqueous and organic phases were combined and subjected to ultrasound (Branson sonifier 450 equipped with ½" tip) for 3 min (70% amplitude, 20 s pulse, 10 s pause). The emulsion was divided into three parts of 1 mL. A solution of 25 mg PGPR and 5 or 10 mg of crosslinking agent (TDI) in 0.5 mL of toluene was added

dropwise to 1 mL of the miniemulsion over a period of 2 min. The reaction was stirred over 20 h at room temperature.

Synthesis of ASPH-nanocapsules

The ASPH nanocapsules were prepared similarly to the OVA NCs. The aqueous phase was prepared by dissolving 5 mg of ASPH protein in 0.05 mL PBS-buffer (pH 7.0). When the nanoreactors were used to encapsulate Cy5, 10 µL of Cy5-Oligo was added to the aqueous solution. The crosslinking reaction and the purification were identical to the OVA NCs.

Determination of the protein concentration in nanocarriers

The concentration of proteins crosslinked as nanocarriers was quantified with a protein assay using bicinchoninic acid (BCA). Briefly, 100 mg of BCA, 200 mg of sodium carbonate, 16 mg of sodium tartrate and 95 mg of sodium hydrogen carbonate were dissolved in 10 mL of deionized water and the pH was adjusted to 11.3 by using 3.0 M NaOH. To this solution, 200 µL of 50 mg of $CuSO_4·5 H_2O$ in 1 mL of deionized water were added, and 200 µL of this solution were mixed with 10 µL of protein standard (OVA or horseradish peroxidase) or the protein nanocarrier dispersion of unknown concentration and incubated at 60°C for 30 min. The absorbance at 565 nm was recorded and the enzyme concentration was determined by comparison to the standard curve prepared with native protein.

3.4 Release profiles

After the transfer of the NCs to PBS-buffer, 10 mL of the suspension was filtered by centrifugal ultrafiltration for 30 min at 1770 RCF using Vivaspin 1000 K centrifugal concentrators. The NCs collected on the filter were redispersed in 10 mL of phosphate buffer pH = 7.4. The protein nanocapsule dispersion was diluted to a concentration of 1 mg mL^{-1}. The release of the macromolecular payload was measured by fluorescence spectroscopy after the incubation of the nanocapsules with proteinase K (1 u of proteinase K for 1 mg of protein NCs) for different periods of time in buffer solution. After appropriate time intervals (0.5 h, 1, 2 h, 3 h, 4 h and 24 h), 500 µL of the suspension was taken out and filtered by centrifugal ultrafiltration at 1770 RCF for 30 min using a spin filter (vivaspin 500 µL 1000 K), and the fluorescence of the filtrate was measured at λ_{ex} = 553 nm and λ_{em} = 576 nm.

Biodegradability of protein NCs

The biodegradability of the protein nanocapsules was conducted with Proteinase K. A concentration of 1 u proteinase K was added to 1 mg of nanocapsules dispersed in 1 mL of PBS buffer, pH 7.4.

Fluorescamine assay

The quantification of amine groups was determined by the fluorescamine assay. First, 0.5 mg of fluorescamine was dissolved in 1 mL of DMSO and 0.1 M borate buffer (pH 7.4) was prepared. Then, 363 μL of the borate buffer were mixed with 13 μL of nanocapsule dispersion or with hexylamine as standard and 125 μL of fluorescamine solution in DMSO were added. Immediately after vortexing the mixture, the fluorescence (λ_{exc}= 410 nm, λ_{em}= 470 nm) was recorded, and the amine content was determined by comparison to the standard curve prepared with hexylamine.

3.5 Enzymatic reactions

The activity of HRP and the HRP-nanoreactors was determined using 2,2'-azino-bis(3-ethylbenzothiazoline-6-sulphonic acid) (ABTS) as substrate. Briefly, the ABTS was first dissolved in 100 mM potassium phosphate buffer (pH 5.0) at a final concentration of 5 mg mL^{-1}. HRP or the HRP-nanoreactors were diluted to a protein concentration of 0.002 mg mL^{-1} in a solution of 40 mM PBS buffer (pH 6.8) containing 0.5% of Triton X-100. 0.190 mL of the ABTS solution were mixed with 3.3 μL of the enzyme solution in a 96-well plate. The reaction was started by the addition of 6.6 μL of 0.3% (w/w) hydrogen peroxide solution (H_2O_2) and the increase of absorbance was detected at 405 nm by UV/Vis spectrophotometry.

The activity of GOx was measured using o-anisidine as substrate. In a typical measurement, 24 mL of o-dianisidine (0.21 mM in 50 mM sodium acetate buffer, pH 5.1) were mixed with 5 mL of a 10% (w/v) β-D-(+) glucose solution in water. The pH of this reaction mixture was adjusted to 5.1 with 1 M HCl. Native horseradish peroxidase (5-150 U mL^{-1}) was dissolved in sodium acetate buffer (50 mM, pH 5.1) with a final concentration of 1.2 mg mL^{-1}. Native GOx or the GOx-nanoreactors were diluted to a concentration of 0.05 mg mL^{-1} in sodium acetate buffer (50 mM, pH 5.1). The enzymatic reaction was initiated by mixing 190 μL of the glucose/dianisidine mixture, 3.3 μL of the HRP-solution and 6.6 μL of GOx/ GOx-nanoreactors suspension in a 96-well plate. The increase of absorbance at 500 nm was detected for five min using a UV/Vis spectrophotometer.

The activity of lysozyme was measured by using a suspension of *Micrococcus lysodeikticus* as substrate. Briefly, *Micrococcus lysodeikticus* were suspended in 50 mM potassium phosphate buffer, pH 6.2 at a concentration of 0.5 mg mL^{-1}. A solution of native lysozyme or lysozyme-nanoreactors was prepared in 50 mM potassium phosphate buffer, pH 6.2 with a final concentration of 0.1 mg mL^{-1}. In order to initiate the enzymatic reaction, 150 μL of the *Micrococcus lysodeikticus* suspension were mixed with 6.0 μL of enzyme-solution and the increase in absorbance at 450 nm was detected for five min.

The HRP/GOx enzyme cascade reaction activity was quantified by using o-anisidine as substrate. 24 mL of o-dianisidine (0.21 mM in 50 mM sodium acetate buffer, pH 5.1) were mixed with 5 mL of a 10% (w/v) β-$_D$- glucose solution in water. The pH of this reaction mixture was adjusted to 5.1 with 1 M HCl. The HRP/GOx-nanoreactors were diluted to a protein concentration of 0.05 mg mL^{-1} in 50 mM sodium acetate buffer. The enzymatic reaction was initiated by mixing 190 µL of the reaction mixture and 6.6 µL of HRP/GOx-nanoreactors suspension in a 96-well plate. The time-dependent change of absorbance at 500 nm was detected for five min by using a UV/Vis spectrophotometer.

Enzymatic reaction was also analyzed using Michaelis-Menten kinetic model. For each nanocapsule the appropriate enzymatic assay was performed using different amount of substrate [S] and a constant concentration of enzyme [E]. The initial rate of product formation (v) obtained from the enzymatic assay was used to calculate the catalytic rate constant (k_{cat}) using the Michaelis-Menten equation:

$$v = \frac{V_{max}[S]}{K_M + [S]} \qquad \text{(Equation 3.1)}$$

where K_M is the Michaelis constant and V_{max} is the maximal conversion rate of the enzymatic system given by

$$V_{max} = k_{cat}[E] \qquad \text{(Equation 3.2)}$$

The ratio k_{cat}/K_M was used as an indicator of the catalytic efficiency.

Glucose determination in serum and plasma

For the determination of the glucose concentration in plasma and serum, 10 µL of the sample were diluted 100 times with PBS-buffer for serum and 1000 times for plasma. Furthermore, the samples were diluted 5 times with 0.1 M NaOH. For the chemoluminescence measurements, 100 µL of the diluted serum or plasma samples were loaded in a 96-well plate. A suspension of HRP/GOx-nanoreactors in 0.1 M NaOH (0.6 mg mL^{-1}, 100 µL) was injected directly in the well and the chemoluminescence emission was detected by the plate reader.

The results were compared to the glucose level measured using a commercial glucose HK assay (Sigma-Aldrich). Additionally, a glucometer (Adia Diabetes Set) based on the electrochemical enzymatic detection of glucose was used. The concentration of glucose in plasma and serum was determined using the HK assay and the glucometer through a series of standard addition experiments.

3.6 Cellular studies

Cellular uptake of the enzyme nanocapsules

For the cell culture and co-incubation, first, RAW 264.7 cells (Mouse macrophage cell line, CLS; Eppelheim; Deutschland) were seeded in μ-Dish 35 mm Imaging Chamber (ibidi, Germany) with the concentration of 20000 cells mL^{-1} overnight. Then, HRP nanoreactors (Cy5-loaded) were added to the cells with a concentration of 75 μg mL^{-1} for 1, 4 or 24 h and the cells were washed with fresh medium afterwards.

DAB Staining after the uptake of enzyme nanocapsules by macrophages

The cells were chemically fixed with 4% paraformaldehyde for 10 min and washed 3 times with PBS. Afterwards, the DAB/cobalt and urea hydrogen peroxide tablets (Sigma-Aldrich, Germany) were taken from the freezer and were allowed to reach room temperature. Then the tablets were dropped into an appropriate container. The container was filled with 5 mL ultrapure water and vortexed until the tablets dissolved. (The DAB staining solution was used within 15 min). The solution was added to the chemically fixed cells for 4 min. After staining the staining solution was removed and the cells were washed 2-3 times with PBS.

CLSM imaging after the uptake of enzyme nanocapsules by macrophages

The images for the intracellular localization of the particles were taken using a commercial setup (LSM SP5 STED Leica laser scanning confocal microscope, Leica, Olympus, Germany), consisting of an inverse fluorescence microscope (DMI 6000 CS) equipped with a multi-laser combination, in addition to five detectors operating in the range of 400–800 nm. An HCX PL APO CS 63×/1.4–0.6 oil-immersion objective was used in this study. HRP capsules were detected at 625-670 nm, which corresponds to red in color.

Intracellular uptake and toxicity evaluation of the ovalbumin nanocapsules

Dendritic cells (2 x 10^5 / well) were cultured at 37 °C and 5% CO_2 in 96-well U-bottom plates (Greiner Bio-One) in serum-free X-VIVO 15 medium (Lonza). Cells were incubated with different concentrations of Cy5-NCs for 20 h. After incubation, cell supernatant was removed and dendritic cells were detached by adding 200 μL of PBS buffer (containing 0.5% BSA and 2 mM EDTA) and incubating for 20 min on ice. Afterward, the cells were transferred to FACS round-bottom tubes, washed with 1 mL FACS buffer (PBS containing 2% of fetal calf serum) and centrifuged (400 g, 10 min, 4 °C). The supernatant was discarded, and cells were stained with 5 μl 7-AAD (BD Pharmingen) for 5 min. Afterward, the cells were characterized by flow cytometry (BD LSR II). Data analysis was conducted with the FlowJo software 10.6.1.

Cellular activation of dendritic cells by ovalbumin nanocapsules

For characterization of cellular activation, dendritic cells were incubated and stimulated as mentioned above. After transferring the cells to FACS round-bottom tubes and washing them, the cells were stained for 30 min at 4 °C with the following fluorochrome-conjugated antibodies: CD83 (FITC), CD123 (PE-Cy7) and HLA-DR (APC) all from BD Pharmingen, CD86 (V450) and CD80 (BV510) both from BD Horizon and CD1c (PerCP-eFluor 710) from eBioscience. After staining, the cells were washed and characterized by flow cytometry (BD LSR II). The data analysis was conducted with the FlowJo software 10.6.1.

Synthesis of recombinant ASPH protein

Full-length human ASPH (GenBank Accession No. S83325) was cloned into the gWIZ vector (Genlantis). Recombinant protein was then produced in the Expi293 expression system (Gibco) according to manufacturer's instructions. Recombinant ASPH was purified from cell culture supernatant using HisTrap HP columns (GE Healthcare) according to manufacturer's instructions.

Isolation of monocytes

Leukocytes were obtained from leukapheresis products collected from healthy donors after informed consent by the Blood Transfusion Center of the University Medical Center Mainz. Peripheral blood mononuclear cells (PBMCs) were isolated by density centrifugation at 1200 g for 20 min and 21°C using SepMate tubes (StemCell Technologies) and Histopaque-1077 (Sigma-Aldrich). Subsequently, the PBMC fraction was extracted and monocytes were isolated using the CD14 MicroBeads kit (Miltenyi Biotec), according to the manufacturer's instructions.

Maturation and activation of monocyte derived dendritic cells with ASPH nanocapsules

After purification, monocytes were cultured in 6 well suspension cell culture plates in 3 mL^{-1} X-VIVO 15 medium (Lonza) supplemented with 25 ng mL^{-1} IL-4 and 100 ng mL^{-1} GM-CSF (both from Immunotools) with 1 x 106 cells mL^{-1}. After three days in culture, half of the medium was replenished with fresh X-VIVO 15 supplemented with cytokines.

On day 5 soluble MPLA (1 µg mL^{-1}) or MPLA-ASPH NC in different concentrations were added to mature and activate the moDC. For negative controls, nothing was added to the cell culture. After another 48 h, the cells were harvested and transferred to FACS round-bottom tubes. After transferring the cells to FACS tubes and washing them, the cells were stained for 30 min at 4 °C with the following fluorochrome-conjugated antibodies: CD83 (FITC), CD80 (PE), CD40 (PE-Cy7), 7-AAD (PerCP) all from BD Pharmingen, CD86 (V450) and CD11c (BV510) both from BD Horizon. The uptake of nanocapsules was measured by encapsulating Cy-5 into the nanocapsules. After staining, the cells were washed and

characterized by flow cytometry (BD LSR II). Data analysis was conducted with the FlowJo software 10.6.1.

ASPH-specific T cell induction

ASPH-specific T cells were generated by co-culturing purified, autologous T cells with mature, protein-pulsed moDC. Monocytes were isolated and differentiated as mentioned above from a fraction of the extracted PBMC. The rest of the PBMC was frozen in Cryo-SFM medium (PromoCell) for later cell purification.

On day 5 ASPH (1 µg mL^{-1}) or MPLA-ASPH NC (25 µg mL^{-1}) were added to the culture. For ASPH-pulsed moDC soluble MPLA (1 µg mL^{-1}) was added after 4 h of incubation. After two days in culture, mature moDC were harvested, washed and seeded into 6 well suspension cell culture plates with 1.2 x 105 cells in 1,5 mL X-VIVO 15 medium. Autologous T cells were purified from thawed PBMC using the Pan T Cell Isolation Kit (Miltenyi Biotec) according to manufacturer's instructions. T cells were cocultured with moDC in a ratio of 60:1 (7.2 x 106) for 7 days.

After 7 days, T cells were rechallenged with freshly matured moDC for 7 h. Brefeldin A was added after 2 h of culture to stop the secretion of cytokines.

Activated T cells were permeabilized using the Cytofix/Cytoperm kit (BD Biosciences) according to manufacturer's instructions and stained with the following fluorochrome-conjugated antibodies: CD4 (FITC), CD154 (PE), IFNg (PE-Cy7), TNFa (APC) all from BD Pharmingen, CD137 (BV421) and CD8 (BV510) both from BD Horizon. After staining, the cells were washed and characterized by flow cytometry (BD LSR II). Data analysis was conducted with the FlowJo software 10.6.1.

3.7 Synthetic procedures

Conjugation of luminol to dextran

The synthesis was carried out according to the literature.[207] Briefly, dextran (MW 40 kDa, 30 g) was dissolved in water (400 mL) and potassium periodate (30 g) was added. The reaction mixture was stirred at room temperature overnight. Then, the reaction mixture was dialyzed against water for three days and freeze-dried.

The oxidized dextran (100 mg) was dissolved in dimethyl sulfoxide (DMSO) (10 mL) at 100 °C. The solution was cooled to 60 °C and glacial acetic acid (3.2 mL) and luminol (48 mg) were added to the solution subsequently. The reaction proceeded at 60 °C overnight. In order to precipitate the product, the reaction mixture was poured into methanol (100 mL) and filtered. Then, another 50 mL of methanol were added to the precipitate to remove unreacted luminol. After stirring for 30 min, the

product was collected by centrifugation. The modified dextran was dissolved in ethylene glycol (30 mL) and excess of sodium borohydride (400 mg) was added to the ice-cooled mixture. After reacting at room temperature for 4 h, the reaction was continued at 4 °C overnight without stirring. The obtained polymer was precipitated in acetone, washed three times with methanol and dissolved in water. The product was further purified by dialysis against water (pH 8). After freeze-drying a pale yellow powder was obtained (50 mg). The covalent immobilization of luminol on the dextran chains was confirmed by HPLC, and the purity was assessed by NMR.

Fluorescent labeling of ovalbumin

OVA (100 mg) was dissolved in 3 mL PBS buffer (pH 7.4) and 3 mg of Cy-5 NHS ester was added. The reaction was stirred overnight and then dialyzed against water for 3 days. The blue product was recover after lyophilization.

Synthesis of PEG-R848

PEG-NHS (160 mg) was dissolved in 4 mL of dry DCM and resquimod (R848) (10 mg) was added. Then, 6 µL trimethylamine was added, and the reaction was stirred overnight. The solvent was evaporated under reduced pressure and water was added to the remaining solid powder. The dissolved product was dialyzed against water for three days and freeze-dried.

Rhodamine labeling of PEG-R848

Polymer functionalized R848 (50 mg) was dissolved in 4 mL DMSO and Rhodamine B isothiocyanate (2 mg) was added. The reaction was stirred overnight and dialyzed against water for 5 days. The product was recovered after lyophilisation.

4. Results and discussion

This thesis focuses on developing protein nanocapsules as delivery carriers for biomacromolecular therapeutic agents, such as catalytic or therapeutic proteins and genetic material. To achieve the successful delivery of such payload, both, the intrinsic biological activity of the payload must be ensured and the release of the macromolecules from the carrier has to be controlled. To address those challenges, first, a versatile approach for the formulation of functional proteins as nanocapsules was developed, focusing on the preservation of the intrinsic activity of catalytic proteins, e.g. enzymes, during the synthesis process (section 4.1). Here, the versatility of the resulting full-enzyme nanocapsules was demonstrated by using different enzymes as nanocapsule building blocks and by the encapsulation of additional substances in the interior of the resulting enzyme nanoreactors.

Further, to gain insight over the release parameters of model macromolecules from protein-based nanocapsules, ovalbumin nanocapsules with a varying semi-permeability of the nanocapsule shell were developed (section 4.2). In general, the high biodegradability of the protein nanocapsules by natural proteases was confirmed and a low toxicity after the uptake by dendritic cells was demonstrated. Furthermore, by tuning the crosslinking density of the protein, the mesh size in the carrier shell was varied, which affected the release kinetics of encapsulated model macromolecules. Understanding the release profiles obtained from protein nanocapsules with varying mesh size under artificial conditions further allowed for the successful *in vitro* delivery and release of a macromolecular therapeutic adjuvant for the development of nanovaccines.

Then, the insights according to biodegradability and preservation of intrinsic biological function of proteins in the nanocarrier synthesis process gained in the previous sections were combined. For the development of a nanovaccine, the therapeutic antigen protein Aspartyl (asparaginyl)-β-hydroxylase (ASPH) was formulated as a hollow protein nanocapsule in order to reduce the risk of emerging immune effects against additional polymeric carrier material (section 4.3). In this study, the nanocapsule synthesis process was scaled down to use low amounts of the precious antigen protein and the full-antigen nanocapsules were functionalized with immune-stimulating adjuvants. After a successful intracellular uptake and antigen degradation, the adjuvant functionalized antigen-nanocapasules showed a high activation of the immune system cells.

4.1 Self-Sustaining enzyme nanocapsules perform on-site chemical reactions[*]

Natural proteins are appealing materials for the design of drug delivery carriers due to their high biocompatibility and biodegradability. However, they can provide more than just the building material for the delivery vehicle since many proteins also incorporate specific biological functions. When aiming at the delivery of those biologically active proteins, e.g. enzymes or antigens, those molecules can act both as biological payload and nanocapsule material. This approach has several advantages, since no additional carrier material is needed for the protein delivery, the effective amount of protein delivered is increased significantly and the protein nanocapsule also provides the possibility to co-deliver multiple additional substances together with the protein of choice. One important challenge when formulating protein nanocapsules with proteins holding an intrinsic function is to preserve the native activity of the protein during the nanocapsule synthesis process. Here, any environmental cues may hamper the sensitive structure of the protein leading to a loss of the biological activity. In this section, a mild technique to synthesize protein nanocapsules was developed, focusing on the preservation of the biological activity of the protein during the formulation. Enzymes were used as model protein systems because their function can be readily quantified by biological assays. To establish the methodology, nanocapsules formed only with enzymes were designed, and the results show that the synthesis process preserved a high degree of the enzyme structure and enzymatic activity. This concept was demonstrated by the preparation of enzyme nanoreactors with three different enzymes and also with a mixture of multiple enzymes in one nanocapsule. Loaded with sensing molecules, the enzyme nanocapsules allowed for the detection of glucose in biological media based on enzymatic catalysis confined on the nanoscale. More importantly, the system introduced here serves as an adaptable platform for biomedical applications since the nanocapsules also displayed good cellular uptake and high activity within cells. Consequently, they could act as nanofactories for the *in situ* generation of functional molecules.

4.1.1 Introduction

Enzyme-based nanoreactors act as small-scale mobile factories for the on-site production of new compounds and are increasingly finding applications for sensing, diagnostic and therapy.[208-211] However, the use of such nanosystems is often hampered not only by the loss of enzymatic activity but also by the limited access of reagents to the catalytic enzyme located in the inner cavity of the reactor. To address those limitations, highly efficient nanocapsules with a shell only composed of active enzymes able to encapsulate the required reactants in the core were prepared. This leads to the formation of self-sustaining nanoreactors.

The concept of nanoreactor is inspired by Nature, where enzymes perform multiple reactions in confined micro/nano-environments, such as subcellular organelles.[212, 213] In such systems, enzymes catalyze reactions with excellent specificity and with conversion rates that outperform chemical catalysts by several orders of magnitude.[214] Artificial nanoreactors mimic the cellular organization of enzymes and confine the biological catalysts in nanocompartents.[215]

The enzyme-based nanoreactors can perform a myriad of reactions and when designed with multiple complementary enzymes, even biomimetic cascade reactions can be implemented.[216, 217] Such nanosystems can find use in a wide range of applications where they are employed as artificial organelles,[218, 219] diagnostic devices[220] or therapeutic "drug nanofactories".[9, 221] The efficiency of this concept has been demonstrated in a variety of environment from free suspensions[222] to *in cellulo* after the uptake of the nanoreactors by cells.[223, 224]

One of the early examples of this concept is the use of enzymes encapsulated in liposomes to replicate natural cellular functions.[222] More recently, similar approaches showed the design of colloid- or polymersomes preserving the biological activity of enzymes that are encapsulated within the polymersome aqueous interior[216, 225] or bound to the membrane[226-228]. Other related studies showed the fabrication of enzyme–polymer nano-constructs (proteinosomes), comprising a shell of (multiple) polymer-enzyme conjugates for the performance of enzymatic cascades.[229]

However, the nanoreactors developed so far, the enzyme is encapsulated in or on a carrier, and the shell of the nanoreactor shell constitutes an additional diffusion barrier slowing down the influx rate of reactants.[230] In this case, complex membrane modifications are required to ensure the nanoreactor permeability.[225, 231] Furthermore, the use of any additional carrier material, such as lipids or polymers, limits the effective enzyme concentration in the system due to the volume occupied by the non-catalytic carrier. This leads to a decrease in the overall catalytic efficiency of those nanostructured enzyme systems.[232, 233] In addition, in multiple cases, the chemical reactant, which should be converted into the desired product, can only be difficultly included in such systems, and has to be provided externally. Furthermore, in complex environments such as *in vivo* conditions, the

49

availability of the reactant is limited by diffusion and the sufficient co-localization of enzyme and substrate can be hindered. Those drawbacks hamper the efficiency and the yield of the catalytic reactions and hence, the impact of the nanoreactors.

To overcome those limitations, a self-sustaining full-enzyme nanoreactor system was designed, which can carry the required reactants in the inner core. The only structural elements of the nanoreactor shell are crosslinked enzymes, and the inner aqueous core is a reservoir for the reagents needed for the catalytic reaction. Such nanoreactors were designed to increase the efficient mass fraction of active enzyme by 50-1000 folds in comparison to conventional nanoreactors,[234-236] to be almost entirely composed of biocompatible and biodegradable enzymes[237], and to not require for the diffusion of reagents through the nanoreactor shell (Figure 4.1.1). Alternatively, such nanoreactors would also be able to convert non-encapsulated substrates if necessary.
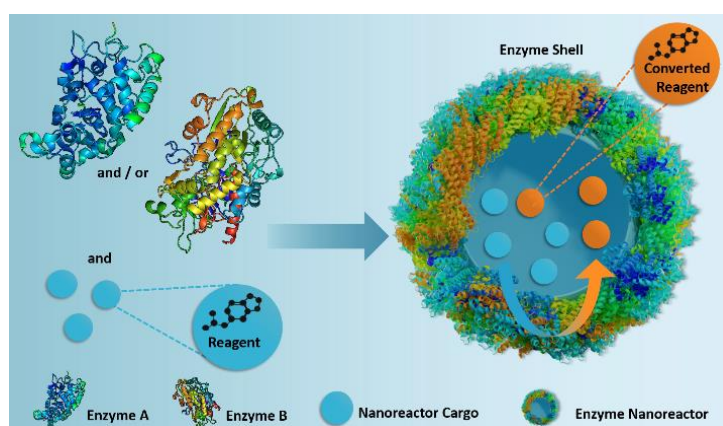
Figure 4.1.1: Fabrication of self-sustaining enzyme nanoreactors, which participate actively in both the transportation and the conversion of the reactants located in their inner core.

4.1.2 Results and discussion

Preparation of enzyme nanoreactors

The formation of the enzyme nanoreactors proceeded through a stepwise process. First, an aqueous solution of the enzyme was used to prepare an inverse (water-in-oil) miniemulsion by a high-energy emulsification process. The preparation of the miniemulsion is a critical parameter for the size and size distribution of the resulting NCs. Typically, miniemulsions can be prepared by ultrasonication as a result of cavitation-induced droplet disruption.[196, 238, 239] However, the high energy of the ultrasound waves and the long duration of their application are detrimental to sensitive biological molecules. The complex three-dimensional structure of the enzyme was disrupted by the use of ultrasound, resulting in a complete loss of enzymatic activity (Figure 4.1.2).
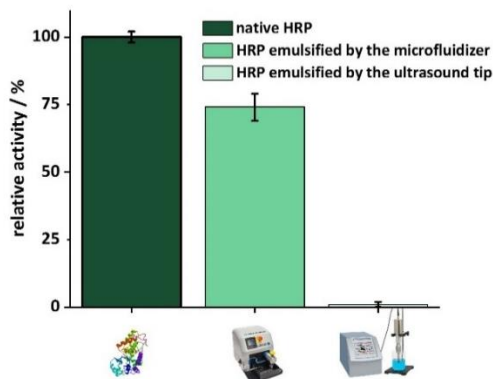
Figure 4.1.2: Influence of the emulsification process on the relative enzymatic activity of the HRP.

To circumvent this crucial drawback, a milder emulsification process, microfluidization, was used. Microfluidization induces high mechanical stress on the droplets of the emulsion in a localized area for a very short time.[164] The controlled collision of two microstreams in an interaction chamber produced a well-controlled emulsion and preserved a high degree of enzymatic activity (Figure 4.1.7).

After the emulsification, the crosslinking of the enzyme molecules present at the interface of the aqueous droplets was carried out by the addition of the crosslinker 2,4-toluene diisocyanate (TDI) to the organic phase. The polyaddition between the isocyanate groups of the TDI and the accessible nucleophilic groups of the enzyme (Figure 4.1.3) resulted in the formation of a nanoreactor shell composed of crosslinked enzymes. Such interfacial crosslinking reaction occurring on inverse-miniemulsion droplets is an ideal technique to control Furthermore, the shell of the resulting nanocapsules is semi-permeable, and while salts and small molecules can freely diffuse in and out of the inner core of the capsules,[240, 241] large macromolecules are trapped inside the core if added to the solution of capsule precursor before emulsification. The encapsulation of different payloads in such enzyme nanocapsules can potentially lead to the release of the degradation products of large macromolecular payloads such as polyprodrugs,[221] or to the release of large payloads through the enzymatic degradation of the nanoreactor itself, which could occur under specific conditions.[196]
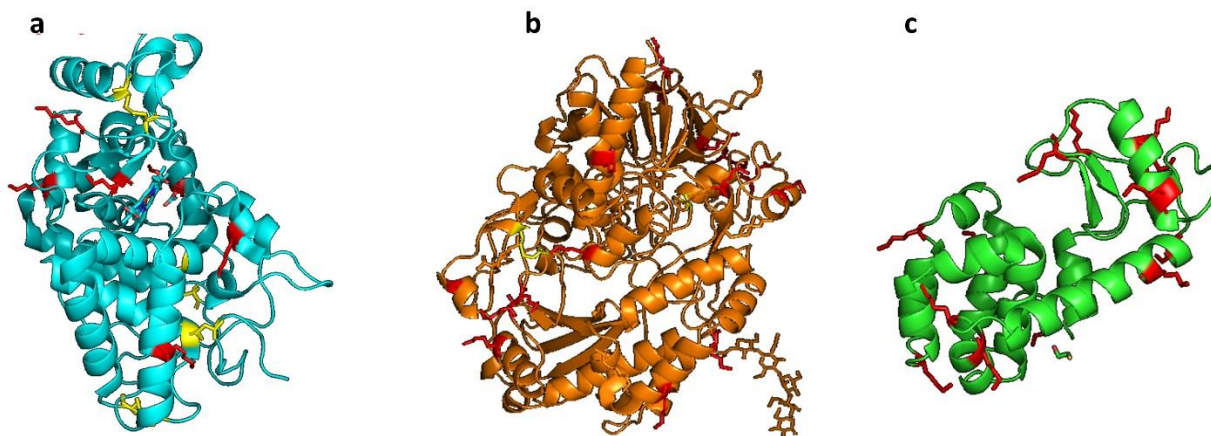
Figure 4.1.3: Enzyme folding with marked nucleophilic goups: lysine (red) and cysteine residues (yellow) for a) HRP, b) GOx, c) LYZ.

Finally, the nanoreactors were transferred to an aqueous buffer. Hollow enzyme NCs with mean diameters of 200-300 nm were obtained as confirmed by scanning electron microscopy (SEM) (Figure 4.1.7 a, 4.1.4 and 4.1.5) and dynamic light scattering (DLS) (Figure 4.1.6). The low values of polydispersity index measured by DLS (<0.2) were indicative of the presence of individual and homogenous nanocapsules with a limited size distribution. Furthermore, electron microscopy (TEM) showed that the crosslinked enzymes formed a shell surrounding an empty core, and the thickness of this shell varied between 10 and 15 nm (Figure 4.1.7 b).
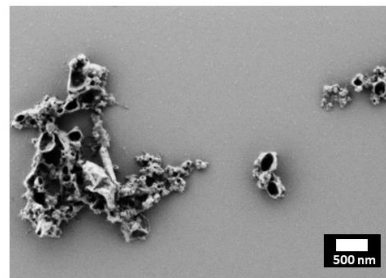
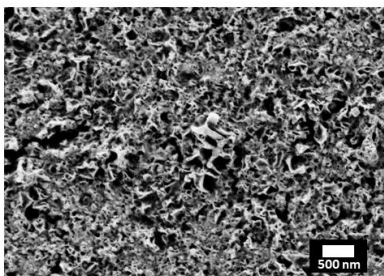**HRP NCs, low crosslinking**
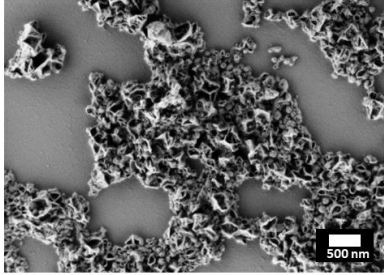
HRP NCs, high crosslinking
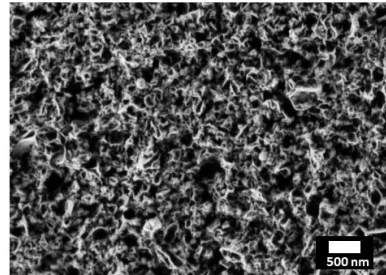
GOx NCs, low crosslinking
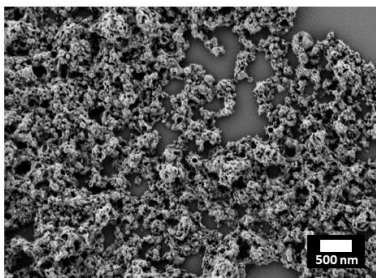
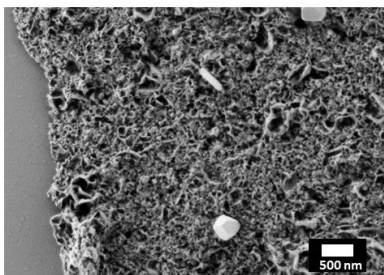**GOx NCs, high crosslinking**

LYZ NCs, low crosslinking

LYZ NCs, high crosslinking

HRP/GOx NCs, low crosslinking

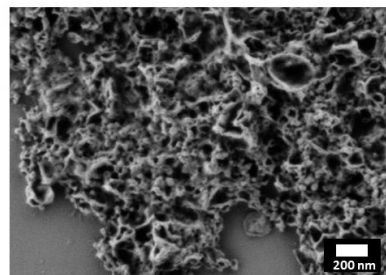**HRP/GOx NCs, high crosslinking**

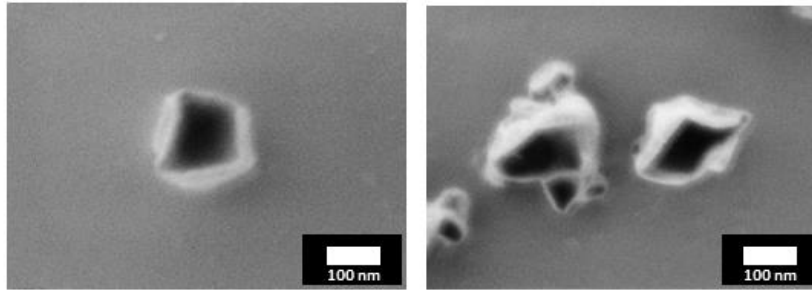Figure 4.1.4: SEM-images of the enzyme-nanoreactors.

Figure 4.1.5: SEM images of HRP-nanoreactors obtained after drying a very diluted suspension of nanoreactors
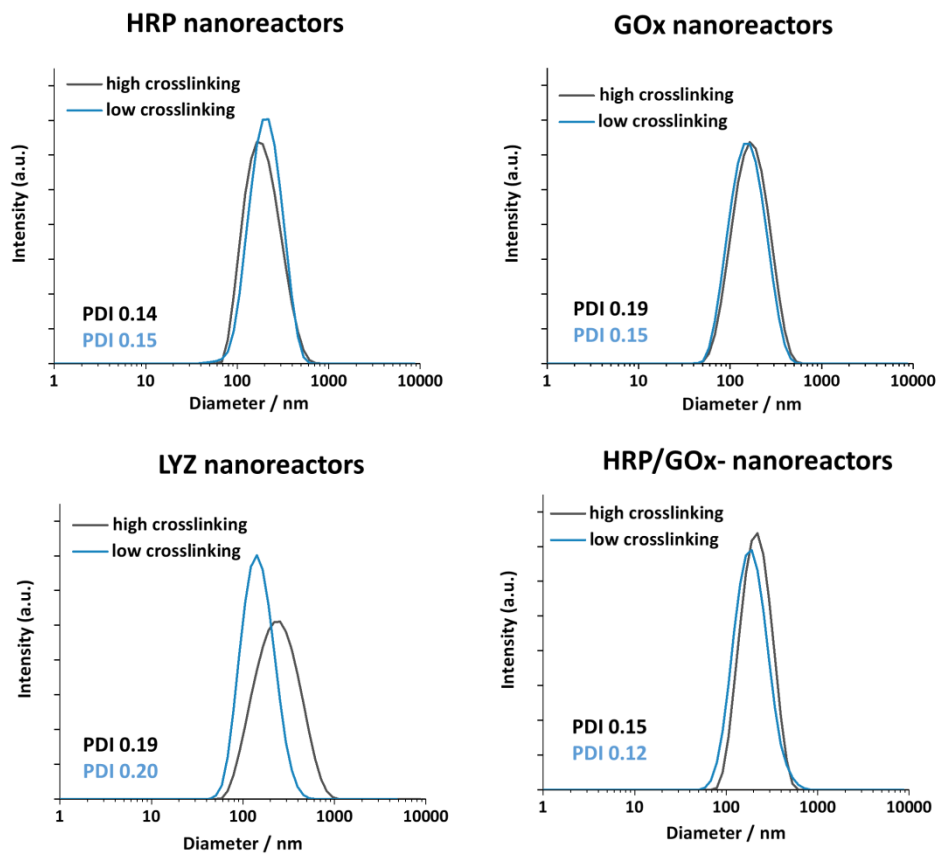

Figure 4.1.6: DLS-measurements of the enzyme-nanoreactors in aqueous suspensions.
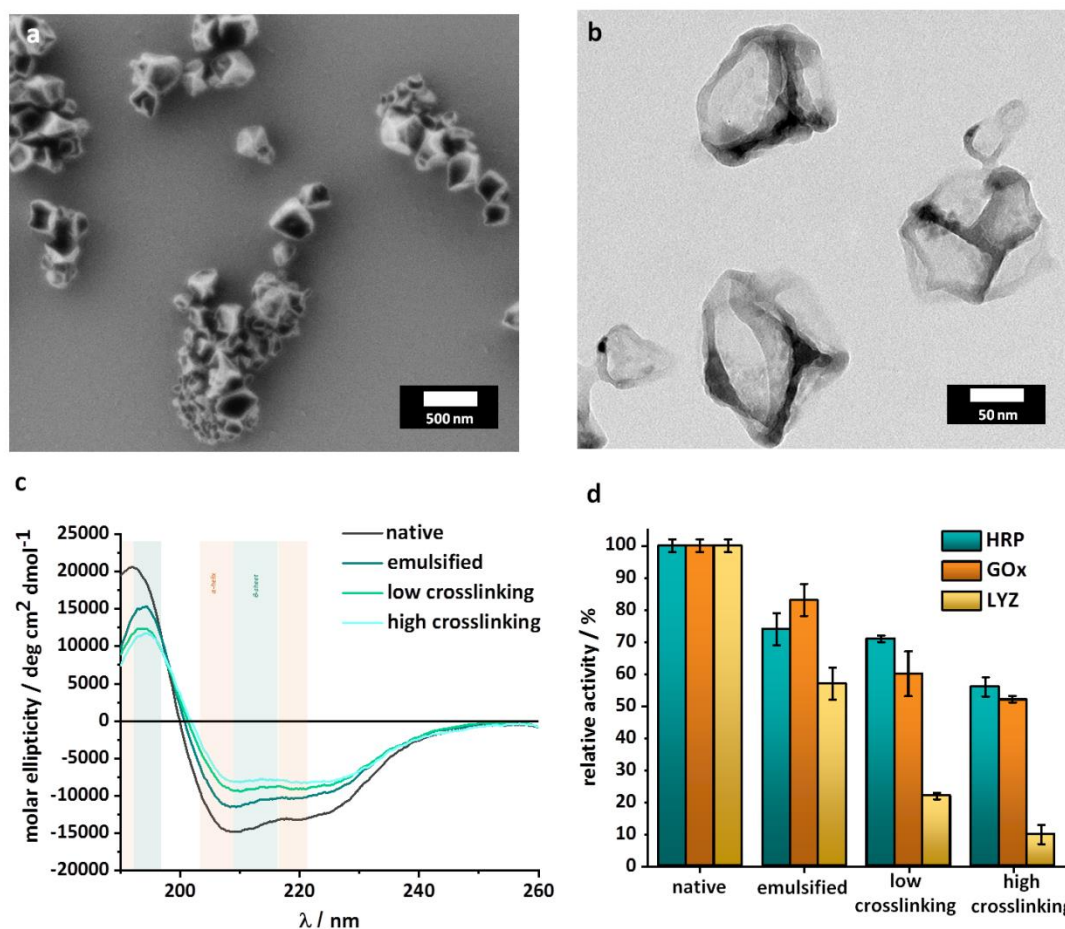
Figure 4.1.7: Characterization of the enzyme-nanoreactors. a) SEM image of the HRP-nanoreactors, b) TEM image of the HRP-nanoreactors, c) CD-spectra of HRP after emulsification and crosslinking, d) relative enzymatic activity of HRP, GOx and LYZ after emulsification and crosslinking.

To demonstrate the versatility of this approach, the nanoreactors were prepared with different enzymes, namely horseradish peroxidase (HRP), glucose oxidase (GOx) and lysozyme (LYZ). Those enzymes were identified as prime candidates because HRP and GOx are robust enzymes, which can be used in clinical diagnostics, organic synthesis and food processing, and LYZ is a more delicate lytic enzyme able to degrade the cell wall of bacteria, making it of interest in medicine, cosmetics and in the food industry. Nanoreactors were formed with all the enzymes with the same control over size and size distribution (Figure 4.1.6). Such crosslinked enzyme or protein nanocapsules typically are biocompatible nanosystems, degradable by biological proteases, even after their crosslinking.[196, 242] The fraction of the enzymatic activity preserved during the synthesis was similar for HRP and GOx, but more limited for LYZ (Figure 4.1.7 d).

One of the critical factors influencing the catalytic activity of an enzyme is its folding and the resulting three-dimensional structure, and chemical reactions can (irreversibly) alter the enzyme folding properties and decrease the catalytic activity. Circular dichroism spectroscopy (CD) was used to evaluate the secondary structure of the enzyme and qualitatively monitor changes in the structure after the different steps of the synthesis. The CD spectra (Figure 4.1.7 c and Figure 4.1.8) show the influence of each step of the nanoreactor formation on the 3D structure of the enzymes. The intensity of the peaks between 200 and 230 nm, typical of a mixture of α-helices and β-sheets, decreased after the emulsification and after the crosslinking of the enzyme. For the HRP nanoreactors, the results indicated that a fraction of the native enzyme structure was either degraded or converted to random coils both after the emulsion and after the interfacial reaction. Similar results were obtained for the GOx and LYZ nanoreactors (Figure 4.1.8).
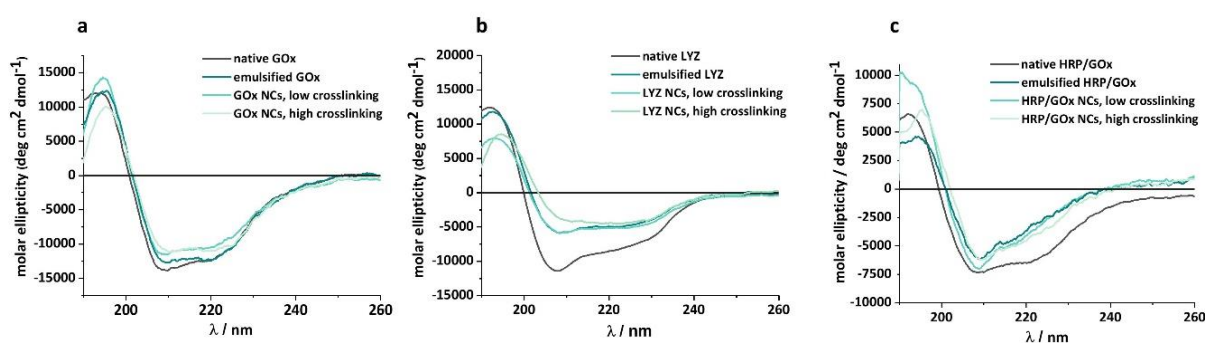

Figure 4.1.8: CD-spectra of a) GOx, b) LYZ, c) GOx/HRP after emulsification and crosslinking.

Enzymatic activity of the nanoreactors

In order to quantify the influence of the degradation observed by CD on the performance of the nanoreactors, enzymatic activity assays were used to measure the remaining biological activity. Figure 2 d shows that, in the case of both HRP and GOx, the most significant deactivation of the enzyme occurred during the emulsification process. In comparison, the reaction between the enzyme and the TDI only marginally influenced the enzymatic activity, in keeping with the loss of the 3D structure observed by CD.

The nanoreactors synthesized with HRP and GOx both retained up to 70 ± 2% of their native activity. While HRP and GOx only showed a limited decrease of the activity during the crosslinking reaction, the synthesis of LYZ-nanoreactors was accompanied by a significant decrease in enzymatic activity. After the synthesis of LYZ nanoreactors, only ca. 22 ± 2% of the native enzymatic activity was maintained in agreement with the steep changes observed in the structure of LYZ observed by CD spectroscopy (Figure 4.1.8 b). In the case of LYZ, the emulsification process also decreased the

enzymatic activity. However, while GOx and HRP were relatively insensitive to the crosslinking reaction, LYZ was negatively impacted by the crosslinking reaction.

The result from the enzymatic activity assay demonstrated that the combination of a mild emulsification process with the covalent, but limited, crosslinking of the enzymes proceeding at room temperature and at physiological pH contributed to the preparation of enzymatically active, uniform, and reproducible full-enzyme-nanoreactors. A significant degree of enzymatic activity was preserved for the different enzymes used, chosen for their distinctive structural stability and sensitivity. Even in the case of LYZ, an enzyme both thermo- and mechano-sensitive, up to 22% of the native activity was preserved. The results provided a favorable assessment of the potential of the technique, where emulsification was followed by interfacial crosslinking, to synthesize similar nanoreactors from a range of different enzymes despite the partial loss of activity observed.

A reduction in the apparent enzymatic activity can be caused by a reduction in the number of available reaction sites where the substrates can bind to the enzyme or by a reduction of the reaction rate. The reaction kinetic of single-substrate enzymes, like those used here, can be described by the Michaelis-Menten model. The kinetic parameters obtained with the native enzyme were compared to those obtained with the emulsified and with the crosslinked enzyme-nanoreactors. The parameters V_{max} (the maximum rate of substrate conversion) and K_m (the Michaelis constant representing the substrate concentration at the half-maximal reaction rate) were used to describe the enzymatic reaction kinetic (Equations 3.1, 3.2). To study the effect of the processing condition on the enzyme, the activity of each enzyme was measured using established protocols.

For the kinetic reaction profile of HRP, the conversion of a substrate (ABTS) was investigated for the native, emulsified and crosslinked enzyme (0.05 µM, based on the total amount of enzyme, both active and inactive) at different concentrations of hydrogen peroxide (between 1.0 and 2.5 mM) (Figure 4.1.9). Both the emulsified and the crosslinked enzyme showed a moderate decrease in the initial rate of substrate conversion in comparison to the native enzyme (Figure 4.1.9 b). This slower initial reaction rate indicated a decrease in the catalytic rate constant. Moreover, the HRP nanoreactors reached a complete conversion of the substrate after a longer time (40 min for 1 mM H_2O_2 and 60 min for 2.5 mM H_2O_2) compared to the native HRP (20 min for 1 mM and 2.5 mM H_2O_2).
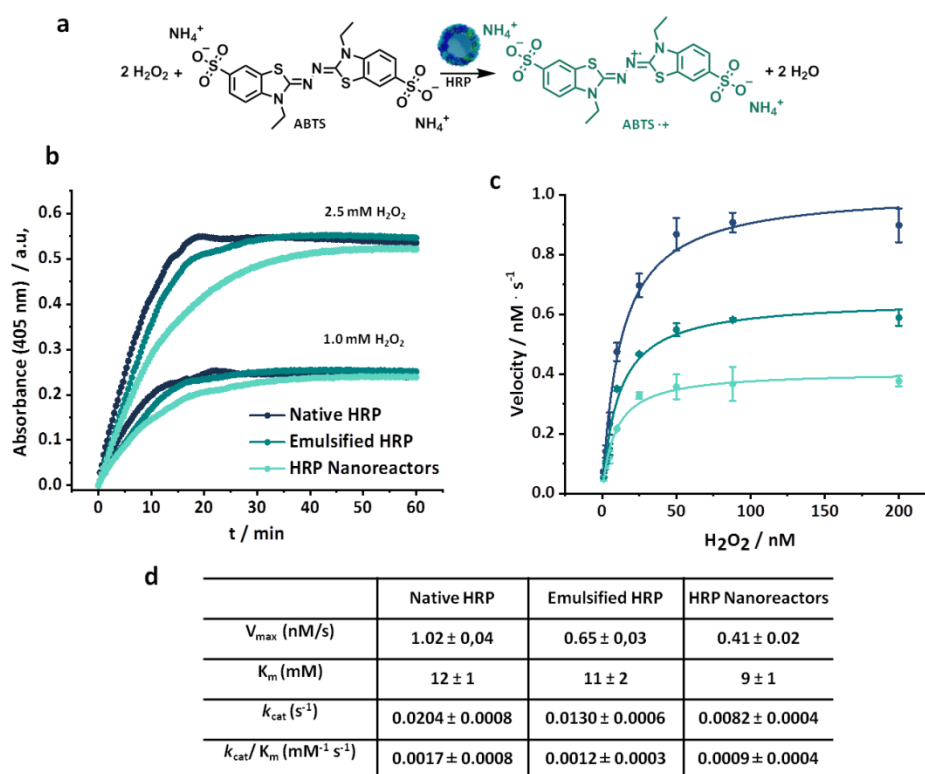
Figure 4.1.9: a) Oxidation of ABTS in presence of hydrogen peroxide and horseradish peroxidase, b) kinetic of the ABTS conversion in presence of native, emulsified and crosslinked HRP, c) Michaelis-Menten plot of HRP-nanoreactors, lines are fits to Equation 3.1., d) Kinetic parameters for native, emulsified and crosslinked HRP.

Figure 4.1.9 c shows the Michaelis-Menten plots for the native, emulsified and crosslinked HRP and displays the relation between the substrate concentration (between 1.0 mM and 200 mM) and the reaction rate observed during the conversion. The resulting K_m value of the HRP-nanoreactors was marginally lower than the K_m of the native HRP (Figure 4.1.9 c and 4.1.10), suggesting that the binding affinity of the substrate for the HRP might increase after the nanoreactor formation. The HRP nanoreactors showed a lower V_{max} in comparison to the native enzyme. The decrease in V_{max} was ascribed either to a reduction of the catalytic rate constant or to a decrease in the effective enzyme concentration. One possible explanation is that upon crosslinking, fewer active centers of the enzyme are accessible by the substrate, and thus, the reaction decelerates. Furthermore, the effective concentration of active enzyme decreases during the formation of the nanoreactors due to the loss of the enzyme structure.
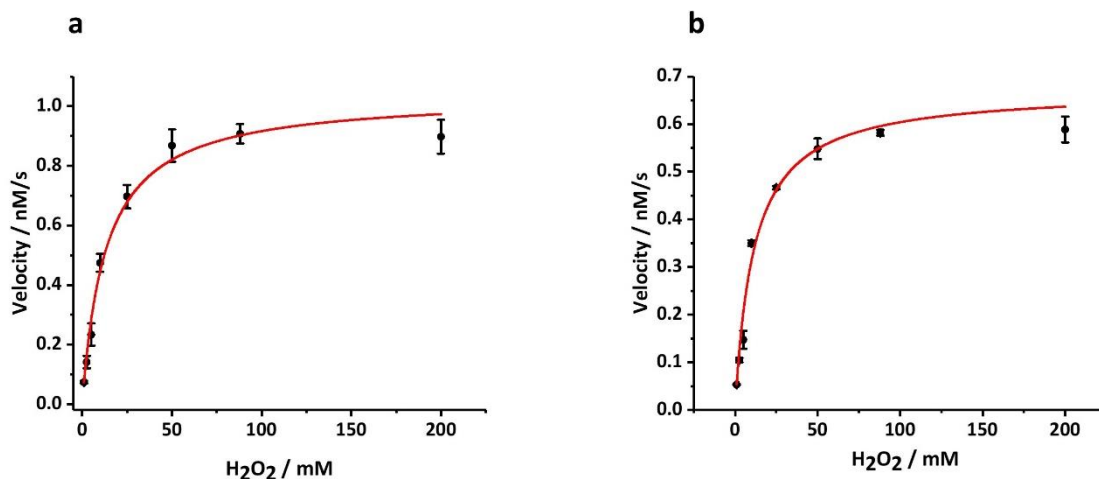
Figure 4.1.10: Michaelis Menten plots for a) native HRP, b) emulsified HRP.

To directly compare the catalytic efficiency of the different systems, the apparent enzymatic activity (k_{cat}/K_m) was calculated based on the total enzyme concentration. Approximately 71% and 53% of k_{cat}/K_m was retained for the emulsified and the crosslinked HRP in comparison to the native HRP. Similar experiments were carried out for glucose oxidase (Figure 4.1.11). The k_{cat}/K_m of the GOx systems was 66% (emulsified) and 29% (crosslinked) compared to native GOx.

a

$$\beta\text{-}D\text{-Glucose} + H_2O + O_2 \xrightarrow{\text{GOx}} D\text{-Glucono-}\delta\text{-lactone} + H_2O_2$$

$$H_2O_2 + \text{o-Dianisidine (reduced)} \xrightarrow{\text{HRP}} \text{o-Dianisidine (oxidized)}$$

b

c

d

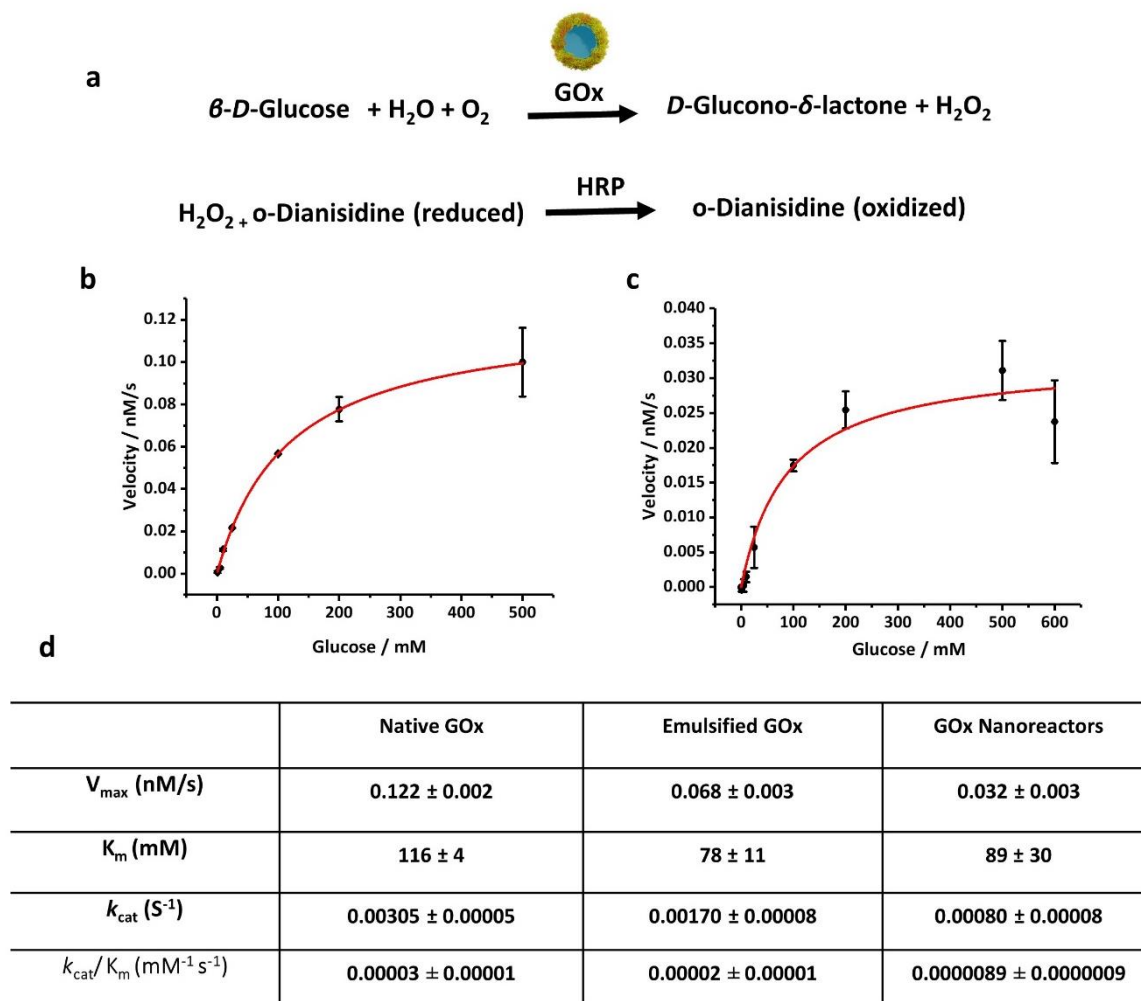|	Native GOx	Emulsified GOx	GOx Nanoreactors
V_{max} (nM/s)	0.122 ± 0.002	0.068 ± 0.003	0.032 ± 0.003
K_m (mM)	116 ± 4	78 ± 11	89 ± 30
k_{cat} (S^{-1})	0.00305 ± 0.00005	0.00170 ± 0.00008	0.00080 ± 0.00008
k_{cat}/K_m (mM^{-1} s^{-1})	0.00003 ± 0.00001	0.00002 ± 0.00001	0.0000089 ± 0.0000009

Figure 4.1.11: a) Oxidation of glucose by glucose oxidase followed by the oxidation of o-Dianisidine by horseradish peroxidase, b) Michaelis Menten plot of native GOx, c) Michaelis Menten plot of GOx- nanoreactors, d) Michaelis Menten parameters for native, emulsified and crosslinked GOx.

Enzymatic activity of the nanoreactors in cells

The novel enzyme-based nanoreactors can be used for the performance of catalytic reactions inside living cells in biological and medical applications. Often, the intracellular activity of native enzymes is hampered by the instability and degradation of native proteins under physiological conditions and their poor cellular uptake.[243] In contrast, the co-incubation of murine macrophages RAW264.7 with the enzyme nanoreactors resulted in the uptake of the particles by the cells (Figure 4.1.13) by an endocytic pathway.[244] To facilitate the observation of the HPR nanoreactors by confocal laser scanning fluorescence microscopy (CLSM), the reactors were labeled with a fluorescent dye, cyanine 5, during the synthesis. Furthermore, the HRP nanoreactors displayed no cytotoxicity towards the RAW264.7 cells (Figure 4.1.12).
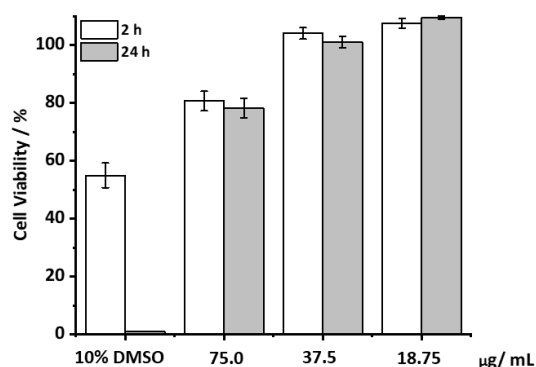
Figure 4.1.12: Cytotoxicity of the HRP nanoreactors. A solution containing the nanoreactors was prepared in cell culture media by successive two-fold dilution and cells were seeded in a 96 wells-plate in cell culture media (200 µL). After 2 or 24 h, 100 µL of CellTiter Glo® solution was added to the wells and the cell viability was determined by luminescence according to the manufacturer protocol.
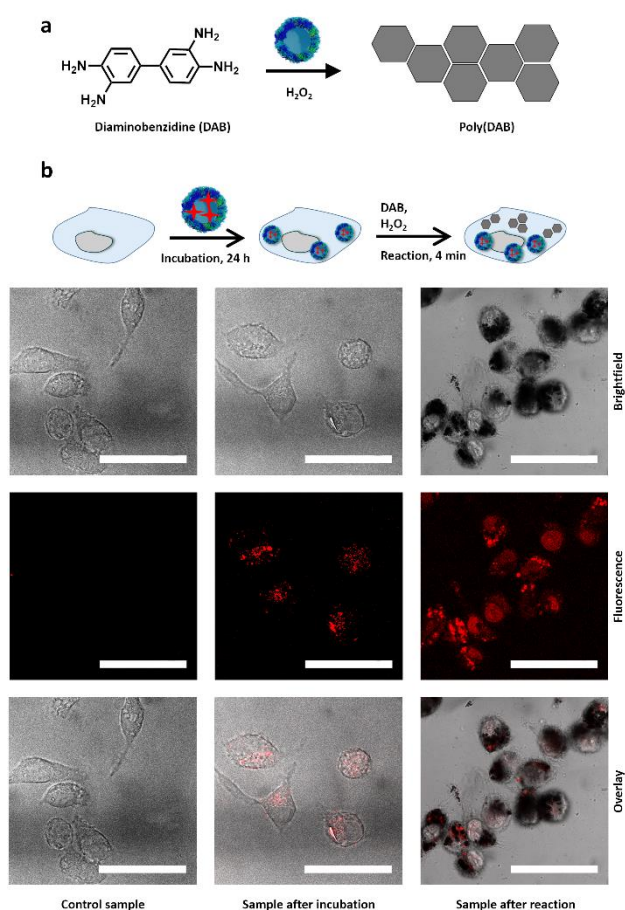

Figure 4.1.13: a) DAB polymerization catalyzed by the HRP nanoreactors, b) confocal fluorescence microscopy images of RAW264.7 cells incubated with HRP nanoreactors (red) for 24 h, before and 4 min after the addition of DAB. In the control experiment, the cells were exposed to DAB but were not co-incubated with the HRP nanoreactors. The scale bars are 50 µm.

The nanoreactors can catalyze the production of new synthetic chemicals within the cellular compartment in order to influence the cell fate or cellular functions such as energy storage or cell differentiation. The production of synthetic material inside the cell is an important challenge, which could provide new possibilities to manipulate, track and control cellular behavior by the *in situ* generation of specific molecules.

One hurdle faced by the production of synthetic chemicals within the cell is the presence of a highly complex intracellular environment able to quench or prevent unconventional reactions.[245] The enzyme nanoreactors overcome this hurdle by preserving their enzymatic activity in cells. Furthermore, they can potentially outperform other systems by acting both as a catalyst for the reaction and as a transport module. Here, as a model reaction to visualize the enzymatic activity of the HRP nanoreactors in cells, the polymerization reaction of 3,3'-diaminobenzidine (DAB) was selected (Figure 4.1.13 a). While monomeric DAB is water-soluble and can freely cross the cellular membrane, polymerized DAB is water-insoluble and precipitated into large insoluble polymer clusters where the HRP activity is localized.[246] After the co-incubation of the cells with the HRP nanoreactors (75 µg mL^{-1}), the cells were washed. Then the cells were fixed with paraformaldehyde (PFA), to increase the permeability of the cell membrane[247] to allow for the fast penetration of the DAB molecules into the cell, and finally exposed to a solution of DAB and hydrogen peroxide for 4 min.

During the reaction time of 4 min, the DAB was converted to poly(DAB) and formed black islands visible by confocal laser scanning fluorescence microscopy (CLSM) (Figure 4.1.13 c). The overlay of the different channels in the CLSM shows the colocalization of the poly(DAB) with the Cy5-loaded HRP-nanoreactors (Figure 4.1.13 b, red dots). When the HRP nanoreactors were not present in the cells, no polymerized DAB islands were observed (Figure 4.1.13 b, control). When the co-incubation period was increased, the amount of poly(DAB) formed during the 4 min of reaction increased as visualized by microscopy recorder after co-incubation periods of 1, 4, and 24 h (Figure 4.1.14). This was the result of the higher cellular uptake observed for longer co-incubation periods. The DAB polymerization within the cellular compartment demonstrated the ability to perform synthetic chemistry inside living cells using those new enzyme-nanoreactors. Here the HRP nanoreactors, which acted as a carrier for a fluorescent probe, efficiently crossed the cell membrane and then performed catalysis inside the cellular compartment. This approach can pave the way for the efficient control over synthetic intracellular chemistry and catalysis.
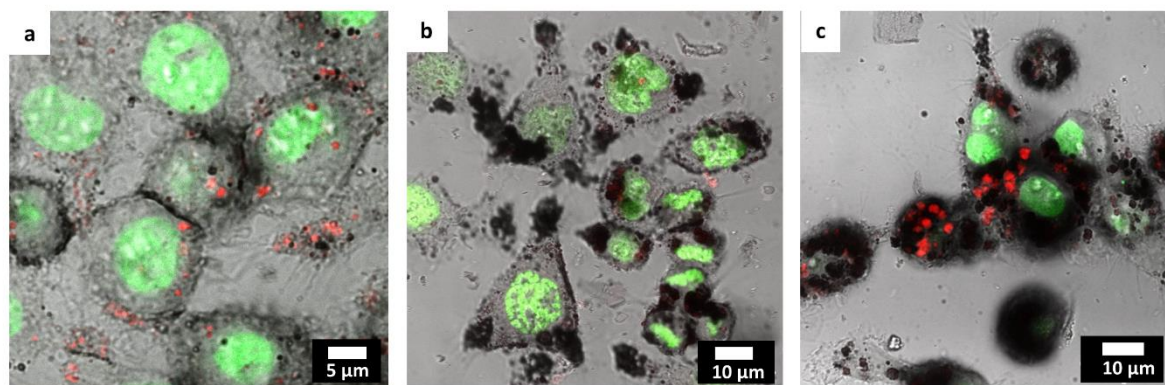
Figure 4.1.14: Confocal laser scanning fluorescence microscopy images of RAW264.7 cells (nucleus stained green) incubated with HRP nanoreactors (red) performing intracellular DAB polymerization (black islands) after a) 1 h , b) 4 h, c) 24 h of incubation.

Enzymatic cascades in binary nanoreactors

A common characteristic of enzymatic reactions in biological systems is that multiple enzymes can be coupled in highly coordinated cascade reactions. Nature can control such cascades with the highest precision and efficiency by organizing the involved enzymes in a confined microenvironment or putting them in the same (cellular) compartments.[248] The enhanced reaction rate of those reactions is thought to arise from the accelerated transport of intermediates between the active sites of the single enzymes in close vicinity.[22] Inspired by the cellular organization of cooperating reaction partners, binary enzyme nanoreactors were designed by combining HRP and GOx in one nanoreactor. A 1:1 ratio of both enzymes was employed and hollow HRP-GOx-nanoreactors were obtained (Figure 4.1.4).

During the formation of the binary nanoreactors, a decrease in the content of α-helix and β-sheet structures in the enzyme mixture was observed by CD spectroscopy in comparison to a native HRP/GOx mixture (Figure 4.1.8). This result was in accordance with the decrease in the relative enzymatic activity of the enzyme mixture in comparison to the native mixture of HRP/GOx measured after the different steps of the HRP/GOx-nanoreactor formation (Figure 4.1.15). Respectively 83 ± 5% and 55 ± 4% of the original enzymatic activity was preserved after the emulsification of the enzyme mixture and after the crosslinking reaction.
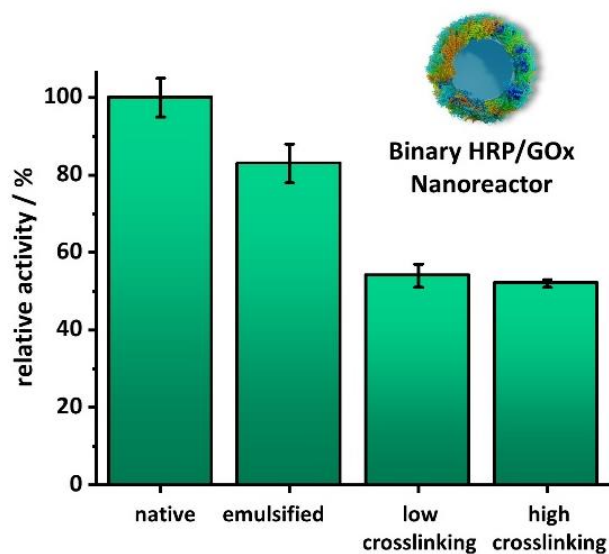
Figure 4.1.15: Relative activity of the HRP/GOx-nanoreactors.

The model cascade reaction for the binary nanoreactors was composed of two conversion steps. First, GOx catalyzed the oxidation of β-D-glucose to D-glucono-δ-lactone and hydrogen peroxide. In the second step, HRP reacted with H_2O_2 to oxidize a substrate dye molecule (Figure 4.1.16 a). The results show that the reaction rate in nanoreactors made with a mixture of HRP and GOx outperformed a mixture of nanoreactors individually made with either HRP or GOx (Figure 4.1.16 b). The binary nanoreactors performed the same cascade reaction at a higher reaction rate than the mixture of nanoreactors. However, after extended reaction time, the total conversion of substrates was identical in both systems (Figure 4.1.18).
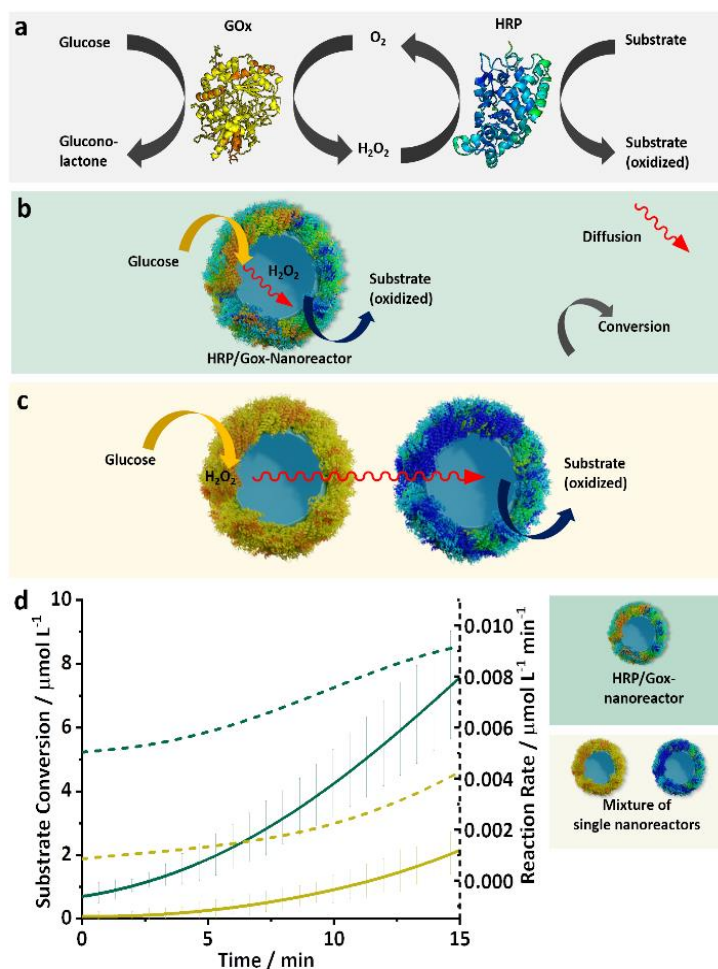
Figure 4.1.16: a) Scheme of the GOX-HRP cascade reaction, b) Cascade reaction in a HRP/GOx nanoreactor, c) Cascade reaction in a mixture of HRP nanoreactors and GOx nanoreactors, d) Substrate conversion and reaction rate of the mixed HRP/GOx nanoreactors and a mixture of single nanoreactors.

To investigate the causes for the acceleration of the reaction in the binary nanoreactors in comparison to the mixture of individual nanoreactors, the oxidation of the substrate by the HRP was triggered by the direct addition of hydrogen peroxide, rather than the cascade of the GOx/glucose. The addition of H_2O_2 resulted in the same reaction kinetic for both the binary nanoreactors and the mixture of the two individual nanoreactors (Figure 4.1.17). This result indicates that the co-immobilization of HRP and GOx in close vicinity accelerated the cascade and suggests that the main reason for the enhanced reaction rate was related to the transport of the hydrogen peroxide between the two enzymatic sites. The faster substrate turnover in the binary nanoreactor was likely influenced by the small interenzyme distances, which facilitate the fast transport of the intermediate (H_2O_2) between the two active sites while preventing the diffusion and dilution of the intermediate into the bulk of the solution. Those results are in good agreement with the reported enhanced cascade kinetics of enzyme reactions in micro/nano- confinements.[217, 249, 250]
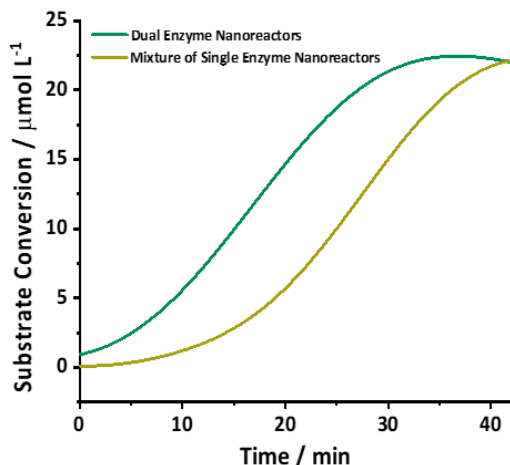
65

Figure 4.1.17: Kinetics of the substrate conversion of the dual HRP/GOx nanoreactors and a mixture of single nanoreactors.
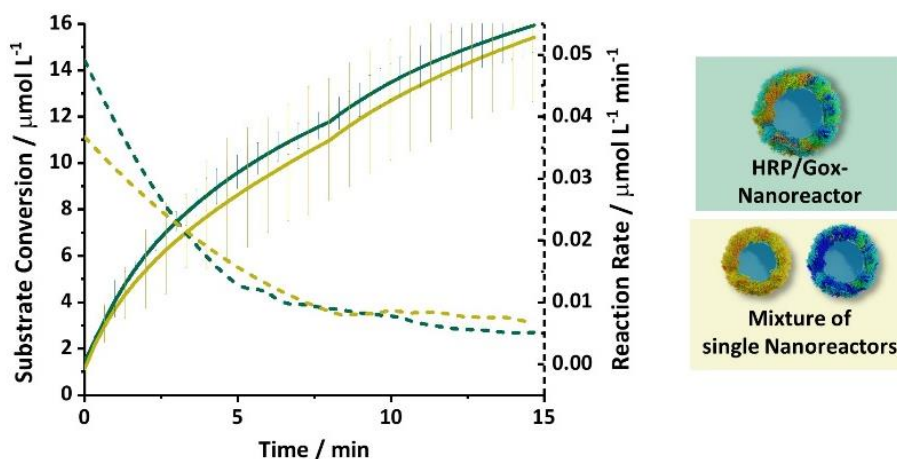

Figure 4.1.18: Kinetic of the substrate oxidation in the presence of either binary HRP/GOx-nanoreactors or a mixture of single-enzyme HRP and GOx nanoreactors during the direct oxidation of the substrate with the addition of peroxide.

Enzymatic conversion of encapsulated payload

Because the shell of the nanoreactors is semi-permeable,[240, 241] small hydrophilic molecules like glucose or peroxide can diffuse through the walls of the nanoreactors, and the catalytic reaction can be performed both on and in the nanoreactors, as observed in the previous cases. However, the method used here to synthesize the enzyme nanoreactors allows for the encapsulation of different reagents inside the hollow aqueous core,[155, 251] and macromolecules can be efficiently trapped inside the nanoreactor without leaking out (Figure 4.1.19).
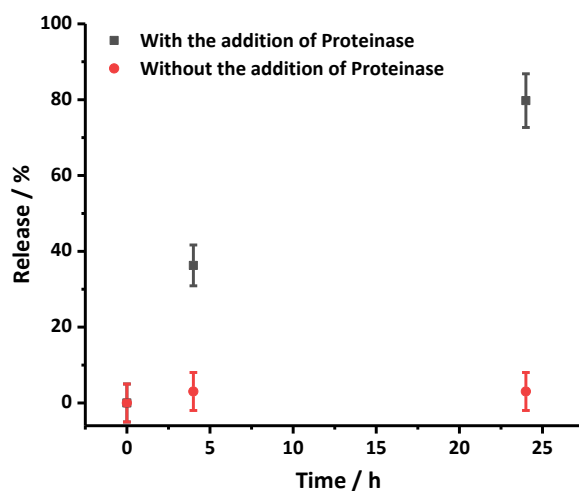
66

Figure 4.1.19: Release of labeled PEG (5 kDa) from crosslinked polypeptide nanocapsules in the presence of Proteinase K (0.1 u mg^{-1} of nanocapsules) and without proteinase K.

Thus, reagents can be encapsulated and carried together with the biocatalyst and can be converted by their carrier on-site. To demonstrate the ability of the system to perform reactions inside the aqueous core of the enzyme nanoreactors, polymer-functionalized luminol, a chemoluminescent reagent, was encapsulated in the HRP/GOx-nanoreactors.

Upon the addition of β-D-glucose to the luminol-containing binary-nanoreactos, the enzymatic cascade reaction was initiated. However, in the present case, the HRP converted the H$_2$O$_2$ to oxidize the luminol resulting in the emission of blue luminescence (Figure 4.1.20). Hence, the nanoreactors actually acted as an on-site nano-light bulb. When the luminol-derivative was encapsulated inside the hollow core, the reaction kinetics of the chemoluminescence was identical to the chemoluminescence generated by the addition of free luminol-derivative (Figure 4.1.20 b) to the external medium. Due to the semi-permeable nature of the shell, in the first case, the reaction could only occur within the confines of the nanoreactors, while in the second case, the reaction could only occur on the surface of the nanoreactor, given that the luminol-derivative cannot diffuse through the shell of the nanoreactor. Since the reaction kinetics was similar both in and on the surface of the nanoreactors, this highlighted the versatility of the nanoreactors, where the reaction rate was not influenced by the locus of the reaction.
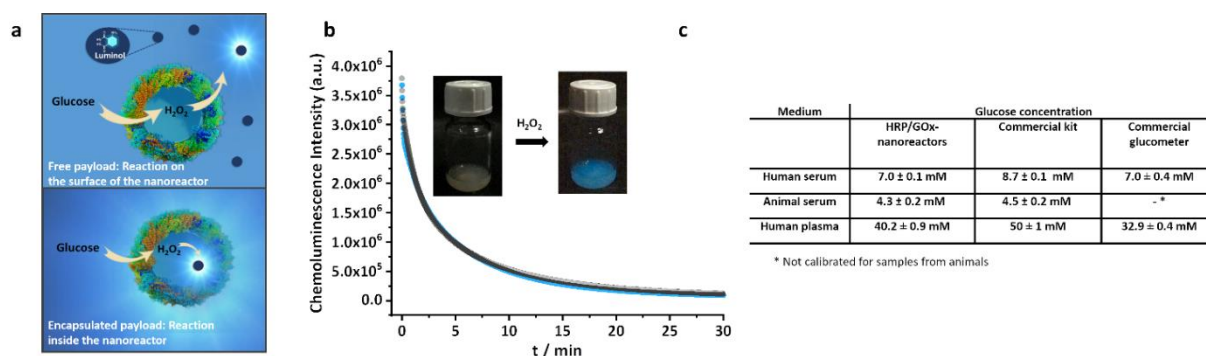
Figure 4.1.20: a) Glucose activated on-site generation of chemoluminescence inside or on the surface of the HRP/GOx-nanoreactors, b) Chemoluminescence of luminol loaded in the HRP/GOx nanoreactors (blue line) and outside of the nanoreactors (black line), inset: photograph of the visible chemoluminescence of HRP/GOx-luminol-nanoreactors upon the addition of H_2O_2, c) Comparison of the quantification of glucose in biological media using the chemoluminescence of luminol in the binary HRP/GOx nanoreactors and by standard methods.

Furthermore, the intensity of the light emitted by the nanoreactor increased with the addition of increasing concentration of glucose (Figure 4.1.21 a). This makes the HRP/GOx nanoreactor containing luminol-derivatives an ideal candidate for glucose sensing in complex biological media. The HRP/GOx nanosensor containing luminol-derivatives showed a high sensitivity with a limit of detection $(10 \cdot \sigma_{blank})$ for glucose of 0.4 µM. However, once the luminol reacted to emit light, it was transformed into aminophthalic acid. Consequently, each luminol molecule can only react once, and the catalysis can only be repeated until the encapsulated molecules were used up.

The glucose-responsive light emission from HRP/GOx-luminol nanoreactors was used to construct a simple, homogeneous and reagentless chemoluminescent glucose sensor and was used to quantify the glucose contained in real biological samples like serum and plasma. Despite the complex matrix of the biological media, it was possible to reliably quantify glucose by measuring the chemoluminescence emitted by the nanoreactors (Figure 4.1.20). For the sensing experiment, to prevent the interference of the sample matrix, standard addition experiments were carried out (Figure 4.1.21c) with samples diluted by 100X (serum) or 1000X (plasma) times with PBS-buffer and five times with 0.1 M NaOH prior to the measurements. The quantification experiments showed glucose levels of 7.0 mM for human serum, 4.3 mM for animal (horse) serum and 40.2 mM for human plasma. The results obtained were in agreement with the glucose level measured by a commercial glucose assay or a commercial glucometer. No significant deviations were observed for the three methods, except for the glucometer, which failed to measure animal samples. The results confirm the potential of the self-sustaining enzyme nanoreactors for their use in detection and sensing.
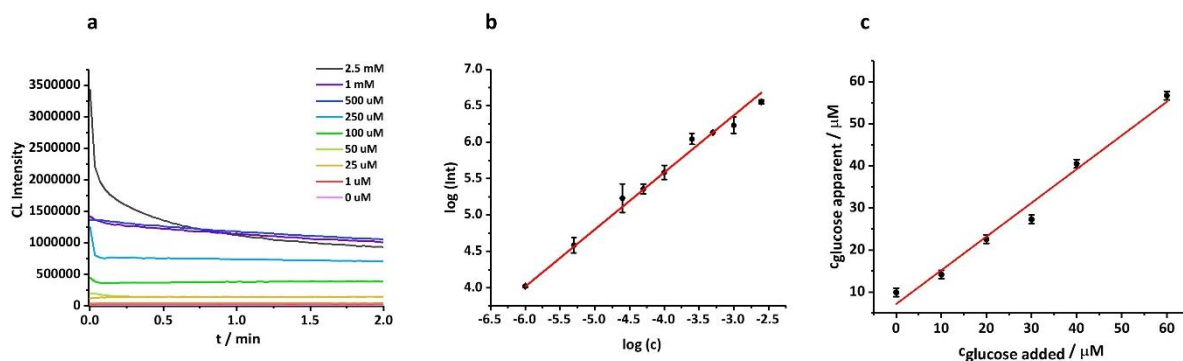
Figure 4.1.21: a) Time-dependent chemoluminescence curves of luminol loaded HRP/GOx-nanoreactors for various glucose concentrations, b) calibration curve for glucose sensing with HRP/GOx-luminol-nanoreactors and c) exemplary standard addition experiment for animal serum.

4.1.3 Conclusions

In this work, self-sustaining nanoreactors carrying the required reagents in their core were designed. The enzymes were crosslinked as hollow nanoreactors without the use of any additional material. Their inner aqueous core was able to act as reservoir for the reactant and the enzymatic shell actively catalyzed the on-site conversion of the payload. We used three different enzymes for the synthesis of the nanoreactors, and preserved a high enzymatic activity after their formation. The nanoreactors were taken up by cells and were still able to perform their enzymatic catalysis within the cells. Furthermore, the combination of both horseradish peroxidase and glucose oxidase yielded nanoreactors performing an enzymatic cascade reaction. The encapsulation of luminol, a chemoluminescent reagent, allowed for the development of a precise sensor for the quantification of glucose in biological media. The results obtained prove the applicability of the system in complex biological environments.

This approach is versatile and can be employed with different enzymes and reactants. Thus, it provides an adaptable platform for more complex biomedical applications, such as the development of *in cellulo* drug nanofactories.

4.2 Controlling the semi-permeability of protein nanocapsules influences the cellular response to macromolecular payload[*]

The previous section showed how proteins with an intrinsic biological function can be formulated as hollow nanocapsules. This allows for both, the design of highly degradable and biocompatible protein nanocarrier, and for the incorporation of biological function into the carrier itself. This approach provides a great platform for the delivery of protein biomacromolecular therapeutic agents. It opens up the possibility to encapsulate and deliver any other biomacromolecular payload in such a carrier.

When biomacromolecular therapeutic agents are encapsulated in protein nanocapsules, the release of this type of payload is more complex due to their restricted diffusion through the nanoshell compared to small molecule cargo. If the nanocarrier designed for this purpose is highly degradable, it enables the controlled release of model encapsulated macromolecules. Here, to gain insight over the release parameters of model macromolecules from protein-based nanocapsules, ovalbumin nanocapsules with a varying semi-permeability of the nanocapsule shell were developed. By changing the crosslinking degree of the protein in the nanocapsule shell, the resulting mesh size of the nanocarrier was adjusted. The crosslinking degree did not influence the degradability of the capsules by natural proteases and a high biodegradability was demonstrated with all formulations. However, the crosslinking significantly affected the release profiles of macromolecular cargo and different release kinetics were observed for the different crosslinking degrees. Further, the insights in the release properties of the protein nanocapsules were transferred to the delivery and effective release of a bioactive macromolecular vaccine adjuvant *in vitro* for the design of a nanovaccine.

---

[*] This chapter is based on the article: "Controlling the Semi-Permeability of Protein Nanocapsules Influences the Cellular Response to Macromolecular Payload" by M. Machtakova, S. Wirsching, S. Gehring, H. Thérien-Aubin, K. Landfester, manuscript in preparation. Contributions: M.M., H.T.-A. designed the experiments. M.M., and S.W. performed the experiments, M.M. prepared and characterized the nanocapsule, S.W. performed cell studies. M.M., S.W. and H.T.-A. analyzed the data. M.M., S.W., S.G. H.T.-A. and K.L. discussed the results and wrote the manuscript.

4.2.1 Introduction

The delivery of macromolecular therapeutics is becoming increasingly important in the development of nanomedicines.[6, 33] [252-254] From biomacromolecular therapeutic agents, such as peptides, proteins, or nucleic acids to high molecular weight polyprodrugs, new therapeutic strategies are emerging for the treatment of various diseases.[6, 255] However, the release of such large payloads from a nanocarrier matrix represents a major challenge, which is attributed to the restricted diffusion and large hydrodynamic radius of those molecules.[256, 257] Understanding the parameters influencing the release of such macromolecular payloads is the key to get insights into their release mechanism and to their successful application. Thus, a system based on degradable protein nanocapsules encapsulating macromolecular payloads was designed to study the parameters, namely size of the payload and mesh size of the shell, influencing the release. The optimized system also provides a unique and practical platform for the delivery and release of bioactive macromolecular payloads in biological systems.

The design of drug delivery systems for macromolecular payloads is more complex than for low molecular weight therapeutic agents. In addition to the typical challenges associated with drug delivery systems such as degradability, biocompatibility, extended circulation time, and targeting, the delivery of macromolecular payloads is also plagued by a complex release from the drug delivery system. The release usually occurs by a combination of degradation of the matrix and the diffusion of the payload through and from the nanocarrier.[258] While the degradation is mainly controlled by the chemical composition of the delivery system, the diffusion process is dependent on the ratio of mesh size of the carrier to the radius of the payload. Consequently, macromolecular payloads with a large hydrodynamic radius display reduced diffusion and release kinetic. Furthermore, the mesh size of the matrix, in turn, is affected by the degree of crosslinking in the nanocarrier and the degradability of the system. Often, the mesh size in smart polymer nanocarriers can be tuned by environmental cues, such as a change in the pH value of the environment or by the presence of a specific level of biomolecules, such as enzymes.[254, 259] These biochemical cues lead to an increase in the mesh size induced by the swelling or the partial degradation of the nanocarriers, promoting the release of the encapsulated payload.[260] This strategy is efficient for the encapsulation and release of small molecules but is not necessarily well-suited for macromolecular payloads because their diffusion is heavily restricted due to their high molecular weight and large hydrodynamic radius.[257] [256] Therefore, the limited increase in the mesh size resulting from the swelling or partial degradation of the nanocarriers might no longer be sufficient to ensure the successful release.

Several nanosystems have shown potential for the encapsulation of (bio)macromolecules. For example, proteins and enzymes were successfully encapsulated in polymer nanosystems for the development of therapeutic or catalytic nanoreactors.[261, 262] Moreover, macromolecular genetic materials, such as DNA or RNA were efficiently encapsulated and delivered *in vivo*, which has led to the development of novel therapies.[263-265] However, the challenge of a controlled release of the macromolecular payload remains. In some nanosystems, no release of such payloads can be observed. Rather, the selectivity of the carrier membrane is altered in order to ensure the influx of small molecule substrates to access the encapsulated (bio)macromolecule, while the target payload remains inside the carrier.[234, 266] In other systems, an uncontrolled release of encapsulated macromolecules can occur due to the limited stability of the nanocarrier system in complex biological environments.[267]

Crosslinked protein nanocapsules can provide a solution to both the controlled delivery with a stable carrier and the sufficient release of macromolecular payload. This class of delivery vehicle provides excellent structural stability and a high degree of biodegradability, which can be exploited to control the release of payload.[196, 268] The hollow nanocapsules are composed of crosslinked biopolymers and have a high loading capacity in their inner aqueous core.[268] They are highly degradable by intracellular proteinases under natural conditions but preserve their structural integrity in biological media during their delivery to the site of action.[201, 242] The crosslinking degree of the proteins in the shell tunes the mesh size of the capsule and hence controls the release kinetic. Proteins from the albumin family, such as human serum albumin or ovalbumin, have been widely used to prepare protein nanosystems, and some of those have already been used in clinical therapy, demonstrating the potential of such nanocarriers.[201, 269, 270] However, the release profile of payloads encapsulated in such nanocarriers is complex and is influenced by the semi-permeability of the nanocapsule shell and consequently affects the final biological response to the molecules vectorized with such nanocarriers.

In this study, the aim is to control the release of model macromolecular payload from crosslinked ovalbumin nanocapsules by tuning the crosslinking degree of the nanocapsule shell. Furthermore, to gain a fundamental understanding of the release mechanism of macromolecular payloads from protein NCs, the tunable biodegradability of the shell was correlated to the release kinetics of model payload of different molecular weights (Figure 4.2.1). Then, this fundamental understanding of the release of macromolecular payloads was applied to tune the biological activity of macromolecular functional payload delivered to dendritic cells. The results show that the appropriate biological response hinges on the adequate control of the release conditions.
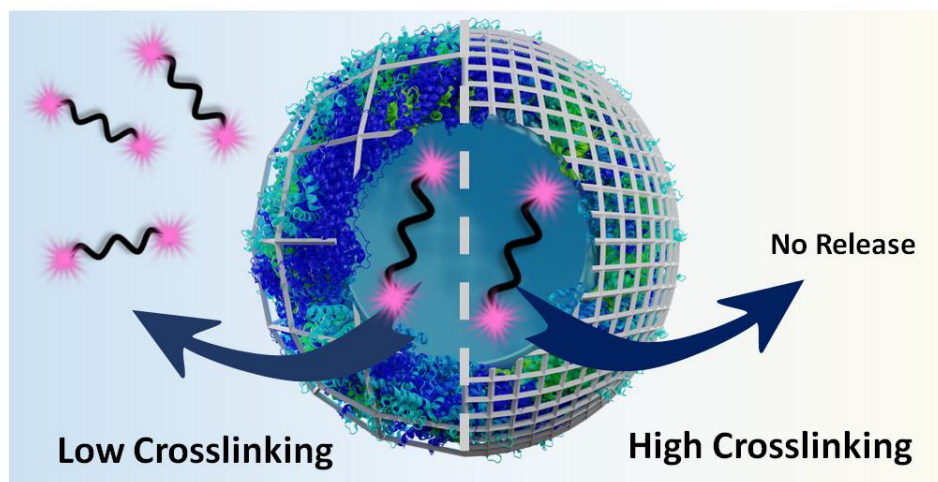
Figure 4.2.1: The crosslinking density of the shell governs the release of high molecular weight payload from protein nanocapsules induced by proteases.

4.2.2 Results

Preparation of the nanocapsules

The density of the nanocapsule shell is of the utmost importance to control the release of encapsulated payload. The crosslinked protein shell hinders the diffusion of the macromolecules and prevents the leakage of the payload from the nanocapsules (NCs). Therefore, tuning the crosslinking density of the protein shell can influence the barrier properties of the NCs and the release of the cargo. Here, protein NCs were designed by crosslinking ovalbumin (OVA) with 2,4-toluene diisocyanate (TDI), resulting in NCs with varying shell densities.[271, 272] The reaction between OVA and TDI occurred at the interface of an inverse miniemulsion composed of aqueous droplets of OVA solution in toluene. Then, TDI was added to the toluene phase and was let to react with the nucleophilic amino groups of OVA. After the reaction, a solid protein shell surrounding an aqueous core was obtained (Figure 4.2.2). Later, the NCs were transferred to water followed by the evaporation of the remaining toluene.

Tuning the molar ratio between the number of nucleophilic lysine residues in the OVA protein and the amount of TDI used allowed to control the crosslinking degree (CL) of the NCs shell. The CL directly affects the mesh size of crosslinked nanosystems, as the number of crosslinking points increases, the distance between two crosslinking points will decrease if the number of polymer chains present in the system remains constant. In the current case, the polymer content was kept the same, and the number of crosslinking points was varied. An equimolar ratio of TDI/lysines resulted in OVA NCs with a medium CL. While increasing the molar ratio to 3:1 led to highly crosslinked NCs, decreasing the ratio to 1:3 results in NCs with a low CL. SEM and TEM (Figure 4.2.2 a and Figure 4.2.3) analysis show the formation of solid protein NCs with a clear core-shell morphology for every CL.

Consequently, considering that the extent of reaction between the TDI and the OVA remained constant with the different amounts of TDI used, the mesh size would decrease linearly with the molar concentration of TDI.

The chemical composition of the NCs shell was studied for purified and dried NCs by FT-IR spectroscopy (Figure 4.2.2 b and c). All samples showed the peaks characteristic for OVA, and the NCs samples also show an additional signal at 1740 cm^{-1} attributed to the vibration of the urea-groups created after the crosslinking reaction between the amino groups of the lysines and the TDI. The increase in the molar fraction of TDI added to the reaction resulted in an increase in the urea peak intensity, confirming the increased CL of the NCs prepared with large amounts of TDI (Figure 4.2.4). Furthermore, circular dichroism spectroscopy (CD) was used to evaluate the secondary structure of the OVA protein and to qualitatively monitor changes in the structure after the crosslinking with various amounts of TDI (Figure 4.2.2 d). The intensity of the peaks between 200 and 230 nm, typical of a mixture of α-helices and β-sheets, decreased accordingly with the increasing amount of TDI used. The loss of the secondary structure observed was in keeping with the loss of structure and function observed during the crosslinking of enzymes under similar conditions.[184]

While the ratio of TDI/lysines significantly influenced the composition and CL of the NCs shell, it had no impact on the size and size distribution of the capsules. The average size of all particles was determined by dynamic light scattering (DLS) (Table 4.2.1 and Figure 4.2.5). The average size of the NCs in toluene was between 235 and 250 nm in toluene, independently of the CL degree. The zeta-potentials of the redispersed NCs in PBS buffer were negative due to the residual amount of anionic surfactant (SDS) used to stabilize the NCs in water.

Table 4.2.1: Physicochemical characterization of the crosslinked OVA NCs.

CL density	Toluene		Water		
	Diameter /nm	PDI	Diameter /nm	PDI	ζ-potential /mV
High	250	0.09	230	0.25	-4.7
Medium	240	0.16	190	0.16	-16.7
Low	240	0.22	160	0.13	-21.8

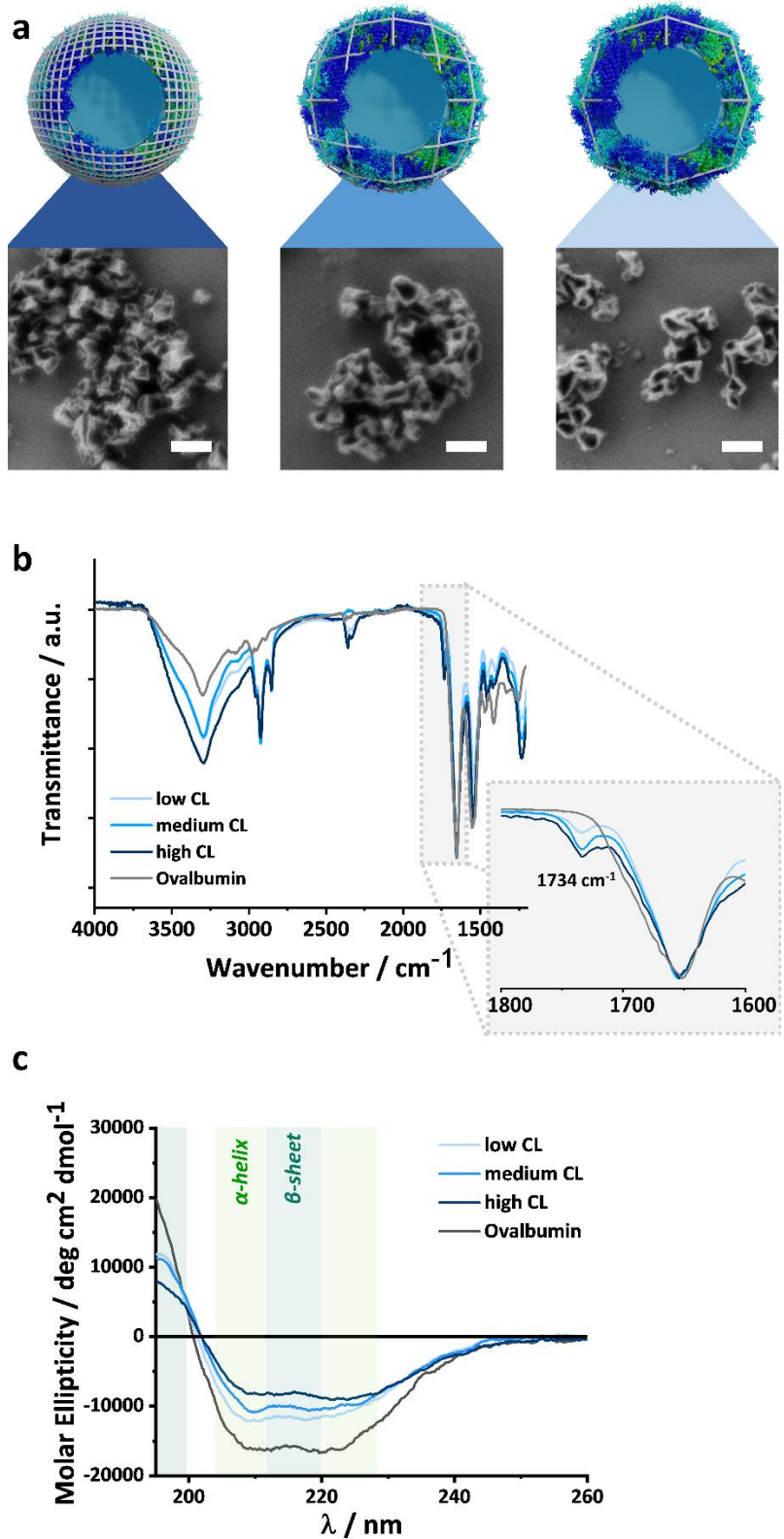Figure 4.2.2: Effect of the CL on the structure and composition of the OVA NCs. a) SEM images of the NCs with different CL, the scale bars are 200 nm, b) FT-IR spectrum of the NCs prepared with different crosslinker/protein ratio, c) Zoom-in FT-IR spectrum of the NCs prepared with different crosslinker/protein ratio from 1600 cm^{-1} to 1800 cm^{-1}, d) CD-spectrum of the NCs with different crosslinker/protein ratio.
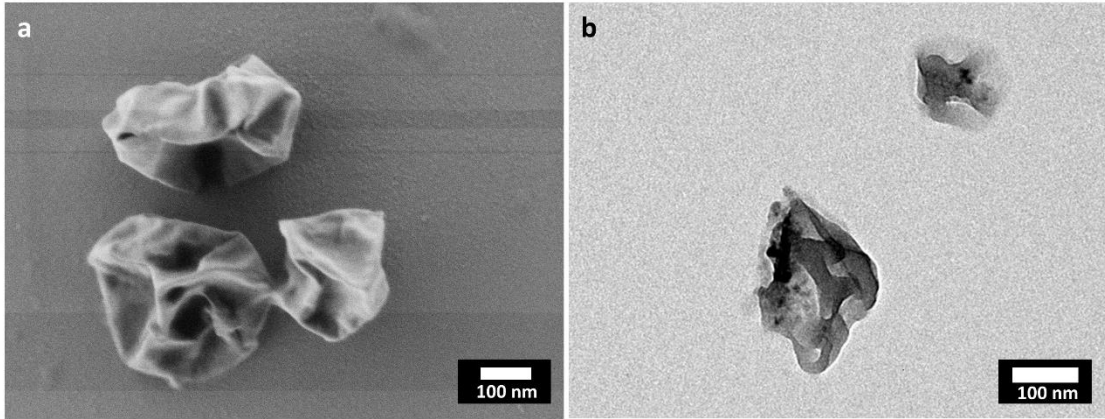
Figure 4.2.3: a) SEM and b) TEM image of single OVA nanocapsules with low CL density.
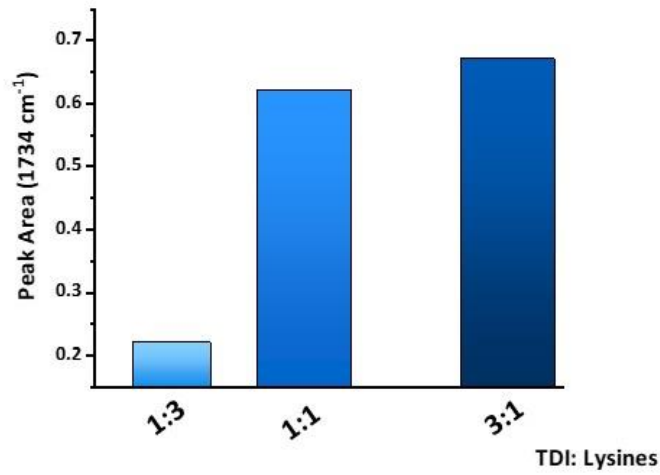
Figure 4.2.4: Increase in the urea linkages present in the OVA NC with the increasing amount of crosslinker (TDI). Peak area of the IR-spectrum at 1734 cm^{-1} for OVA NCs with 3:1, 1:1 and 1:3 ratio of TDI:Lysines.

Figure 4.2.5: Size distribution of the OVA NCs measured by DLS for a) low CL, b) medium CL and c) high CL as prepared in toluene (black) and after transfer to water (blue).

Encapsulation of macromolecular payload

Different macromolecular payloads with molecular weights ranging from 5 000 to 600 000 g mol^{-1} were prepared to study the effect of the payload size on the release.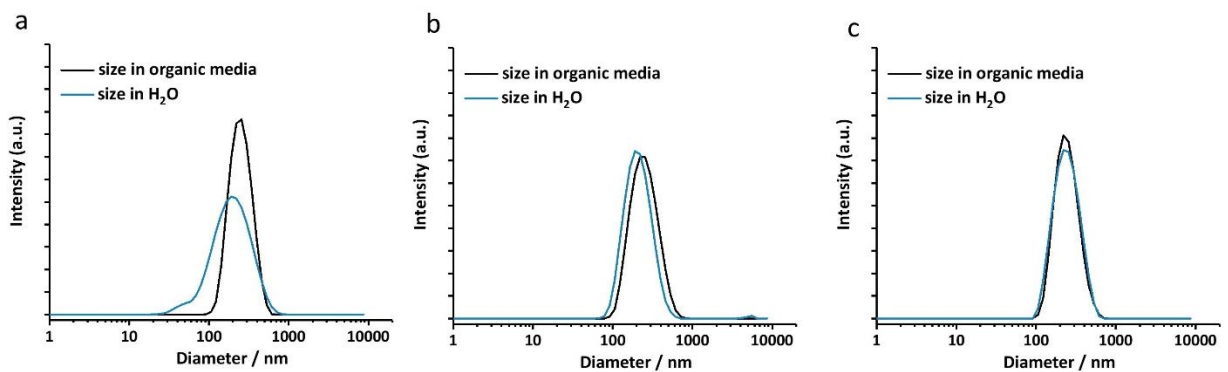 The model payloads were a series of different poly(ethylene glycol)s (PEGs) functionalized with rhodamine. Rhodamine-isothiocyanate was reacted with different PEGs to yield payloads with controlled molecular weight and size, highly water-soluble, and reliably quantifiable by fluorescence spectroscopy. The resulting PEG payloads had a specific hydrodynamic radius, determined by DLS, ranging from 2 to 22 nm for PEG 5 kDa and PEG 600 kDa, respectively (Figure 4.2.6).
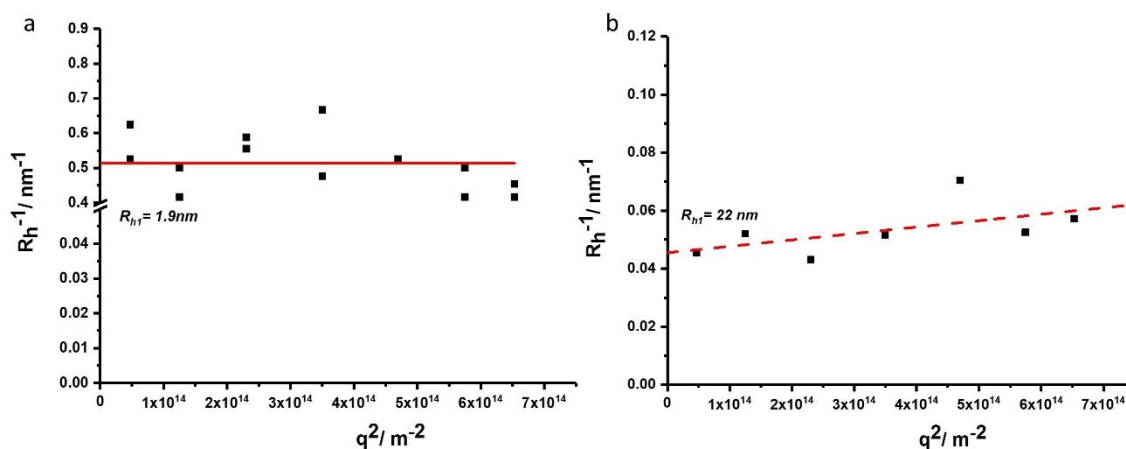

Figure 4.2.6: Hydrodynamic radius of PEG-Rhodamine prepared with a) PEG 5 kDa and b) PEG 600 kDa.

The encapsulation of the different payloads in the nanocarriers was almost quantitative in every case when measured in the organic phase. After the transfer of the nanocapsules from toluene to water, the apparent encapsulation efficiency resulted from the encapsulation of the payload and the initial mass transport of the payload out of the capsule following the water transfer process. Some payload molecules might have been trapped in the shell or at the surface of the nanocapsules during the synthesis and those molecules were quickly released after the transfer of the NCs to water. This process led to a moderate decrease of the encapsulation efficiency from 100% to ca. 70-90%, as measured by UV/Vis spectroscopy (Figure 4.2.8 a). Furthermore, the size of the payload molecules affected their encapsulation efficiency. The largest PEG molecule, PEG 600 kDa, was encapsulated less efficiently than smaller payloads. A constant mass loading of the payloads was used for the different molecular weights; consequently, more molecules were present for smaller payloads, and the number of molecules washed away during the water transfer remained essentially the same for the different payloads. The CL also affected the encapsulation efficiency. This phenomenon was more pronounced

for smaller payloads than large ones. The encapsulation efficiency increased with the CL. At lower CL density, the looser mesh size of the NC shell allowed for the washing off of more molecules entrapped within the shell during the transfer to water. Once the NCs were transferred to water, and the initial washing of the loosely or non-encapsulated molecule occurred, there was no leakage of the encapsulated payload (Figure 4.2.7). The shell of the nanocapsule acting as a semi-permeable membrane which prevented the mass transport of the molecules trapped in the inner core of the nanocapsules.
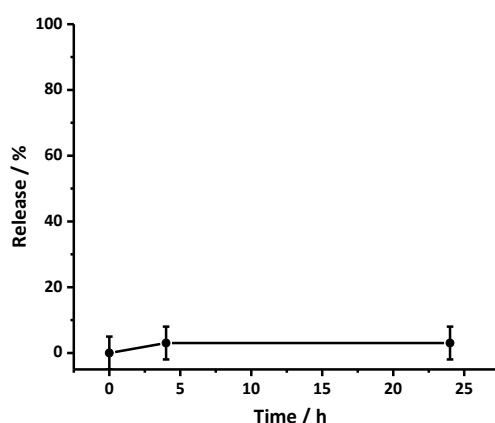

Figure 4.2.7: Release of PEG-Rhodamine (MW 5 kDa) from crosslinked OVA nanocapsules in the absence of enzymatic degradation by proteinase K.

Biodegradability of the NCs

A major advantage of the protein NCs is their high potential to be biodegraded by naturally occurring enzymes. Various types of proteinases are commonly present under *in vivo* conditions and can induce the degradation of the proteins employed as building blocks for the NCs. However, the structural variations induced by the crosslinking of the protein could potentially change their conformation and hence their recognition and digestion by enzymes.[273, 274] Proteinase K is a natural protease with a high ability to cleave peptide bonds in the protein amino acids, more specifically where alanine residues are present.[275] The OVA NCs can be enzymatically degraded by proteinase K leading to the generation of free amino groups on the surface of the nanocapsules, which can be quantified by a fluorescamine assay (Figure 4.2.8 b).[276] The results show that the addition of 1 u of proteinase K mg^{-1} of NCs resulted in an increase of amino group concentration in the sample. Interestingly, the number of amines formed by the degradation of the NCs prepared with different CL followed a similar kinetic. Consequently, the degradability of the capsules was independent of the CL density and the conformational changes observed in the protein structure (Figure 4.2.2 d). However, to monitor the

degradation via the fluorescamine assay, a higher concentration of protease than what is normally found in serum was used.[277] Under typical blood concentrations of proteases and in the presence of protease inhibitors, protein-based nanocarriers were shown to be stable over several days, which is a prerequisite for a successful *in vivo* application of those nanocarriers.[278]
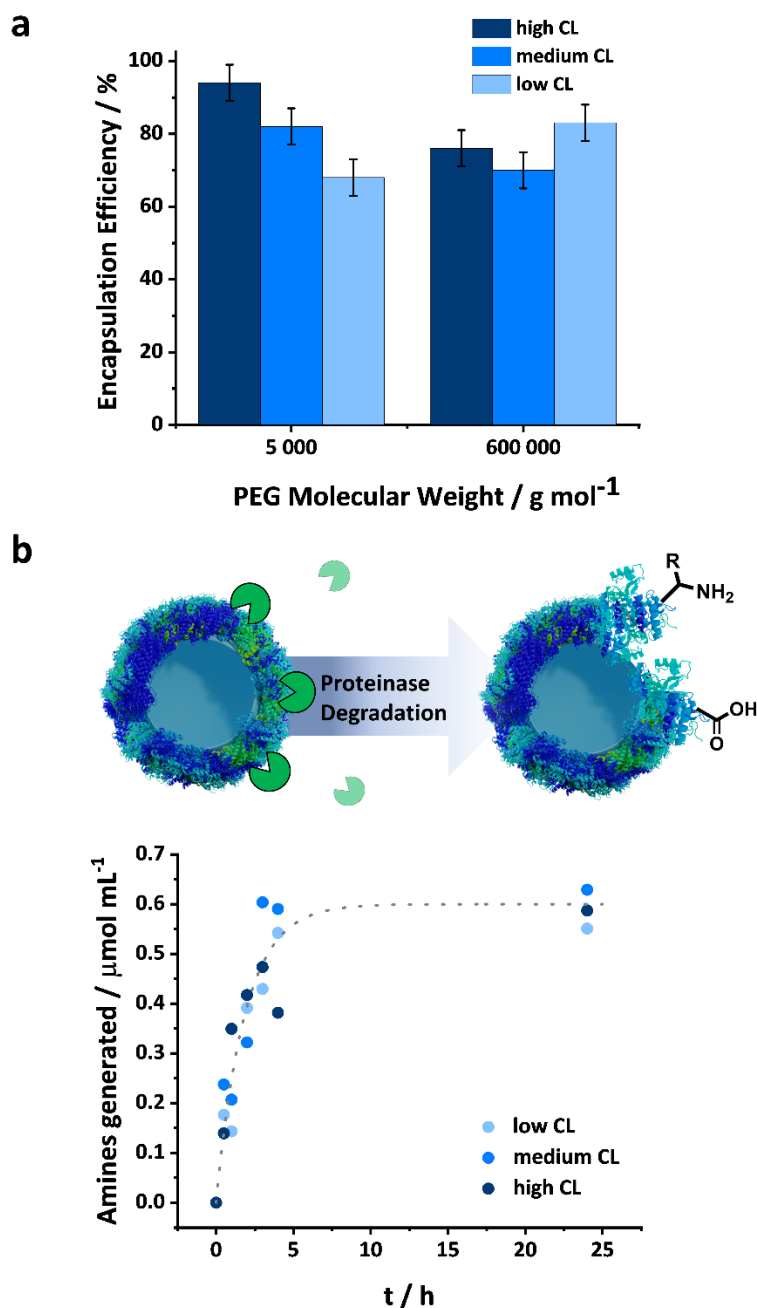

Figure 4.2.8: a) Encapsulation efficiency of macromolecular payloads (rhodamine-labeled PEGs) in the NCs with varying crosslinking degrees, b) generation of amines during the degradation of the OVA NCs by proteinase K (1 u per mg of protein NCs).

Release of macromolecular payload

As the nanocarriers were degraded by proteinase K, the mesh size of the NCs shell increased. The degradation influenced the semi-permeability of the nanocapsule shell, and led to the release of the encapsulated payload over the degradation period (Figure 4.2.9). An obstruction model[279] can be used to describe the release of the payloads from crosslinked NCs. Originally developed to explain the release from crosslinked polymer hydrogels, it can also be applied to describe the release from the protein nanocapsules used here. After the transfer to water, the crosslinked protein chains swell and behave similarly to a poorly swollen hydrogel. Consequently, the release of the payload from the NC is directly proportional to the diffusion of the payload through the crosslinked polymer shell. The effective diffusion coefficient (D) of the payload through the shell is governed by three major parameters, the diffusion coefficient of the payload in water (D_0), the average mesh size of the network ξ, and the radius of the payload (*R*):

$$D = D_0 \exp\left(-\pi \left(\frac{R+r_f}{\xi+2r_f}\right)^2\right)$$

(Equation 4.1)

where r_f =protein chain radius.[279]

In this model, the solute is considered to be a hard sphere not interacting significantly with the network. Furthermore, the network is considered as immobile compared to the mobility of the solute and there is a distribution of mesh sizes in the network resulting from the random distribution of fibers as proposed by Ogston.[280] However, this model remains a suitable tool to qualitatively address the release of macromolecular payload from protein nanocapsules upon degradation.

According to Equation 4.1, the diffusion and the release of macromolecular payloads depend on their size and the mesh size of the protein network, which itself would vary with the initial CL degree and the degradation of that network. The protein nanocapsules with high, medium and low CL density all efficiently encapsulated the macromolecular payloads, and small molecules could even be efficiently encapsulated at a high CL degree. Without the degradation of the protein network, no release occurs for PEG 5 kDa, even from the low CL nanocapsules, showing that the final mesh size of the nanocapsule was smaller than the hydrodynamic radius of the payload (Figure 4.2.7). Given that the mesh size in Equation 4.1 represents the average of a distribution of mesh sizes in the network[280], the value obtained must be smaller than the hydrodynamic radius of the payload (Equation 4.6) to fully prevent its release.

As the OVA NCs were degraded by proteinase K, as evidenced by the generation of amine during the cleavage of the peptidic bonds, the release of the encapsulated payload occurred because the mesh size increased from the initial size ξ_0 to a value superior to a threshold value varying on the hydrodynamic radius of the payload to be released (Equation 4.6 and 4.7). The extend of the payload released was measured by fluorescence following centrifugal ultrafiltration, a mild technique to separate the media and the nanocarriers without subjecting the formulation to high shear forces.[281] Figure 4 a and b show the effect of the crosslinking density, i.e. the mesh size of the nanocapsules, on the release of encapsulated molecules. The release curves show that in the first 4 h, highly crosslinked NCs only released ca. 10% of their payload although degraded by 1 u proteinase K per mg of nanocapsules, while NCs with lower CL degree release 20 and 80% of their payload for medium and low CL at identical conditions, respectively (Figure 4.2.9 a).

While the degradation kinetic of the crosslinked OVA NCs by proteinase was not affected by the crosslinking density (Figure 4.2.8), the release kinetic of the payload encapsulated within those NCs was significantly affected by the CL degree (Figure 4.2.9 a). As the CL degree increased, the initial mesh size decreased. In every case, the proteinase K cleaved the same number of peptidic bonds. Statistically, the average increase in the mesh size generated by the cleavage of a peptidic bond would increase exponentially with the decreasing initial CL degree.

This phenomenon was evidenced by the rapid initiation of the release of macromolecular payload from the low CL NCs. For the release to occur from the low crosslinked nanocapsules, in the case of PEG 600 kDa, the threshold mesh size to observed release was ca. $26\xi_0$ (Equation 4.8) corresponding to the generation of ca. 0.5 µmol mL^{-1} of amine groups produced for a NC suspension of 0.1 wt% (equation 4.11), which is in keeping with the results obtained. When increasing the CL density, the initial mesh size decreased, but not the mesh size needed to observe the release of the payload. Consequently, more peptidic segments need to be cleaved for the release to occur. For the highest CL density used, ca. 6 µmol mL^{-1} of amines should be generated before being able to observe the release of PEG 600 kDa. Hence, no release was observed from the high CL NCs even after 1 day of coincubation with the proteinase when the concentration of amine generated by the degradation process reached 0.8 µmol mL^{-1} (Figure 4.2.9 b). However, in the case of the NCs with the intermediate CL density, only ca. 0.9 µmol mL^{-1} of amine needs to be generated before the release to occur, which roughly corresponds to the degradation observed at the onset of the release (Figure 4.2.9 b). The second parameter influencing the release of the payload is the molecular weight and hydrodynamic radius of the encapsulated cargo. Figure 4.2.9 shows the release of two payloads (PEG 5 kDa and 600 kDa) in the presence of 1 u of proteinase K per mg of NCs. In this case, there were no significant differences in the release kinetics. However, when the protease concentration was decreased to 0.025 u per mg of NCs, the effect of the payload molecular weight on the release kinetics from OVA

NCs can be observed (Figure 4.9.10 and 4.2.9 c). While the larger payload (600 kDa) showed limited release in the early stage of the degradation process, the smaller payload (5 kDa) was released up to 60-80 %. For the release of the PEG 5 kDa to occur, the mesh size of the nanocapsules only needed to increase ca. $1.2\xi_0$, this translates to the generation of ca. 0.18 µmol mL^{-1} of amines, in comparison to the 26-time increase and the generation of 0.54 µmol mL^{-1} of amines needed in the case of PEG 600 kDa. Hence, for the release to occur 3 times more amines have to be generated in samples containing PEG 600 kDa compared to samples containing PEG 5 kDa.
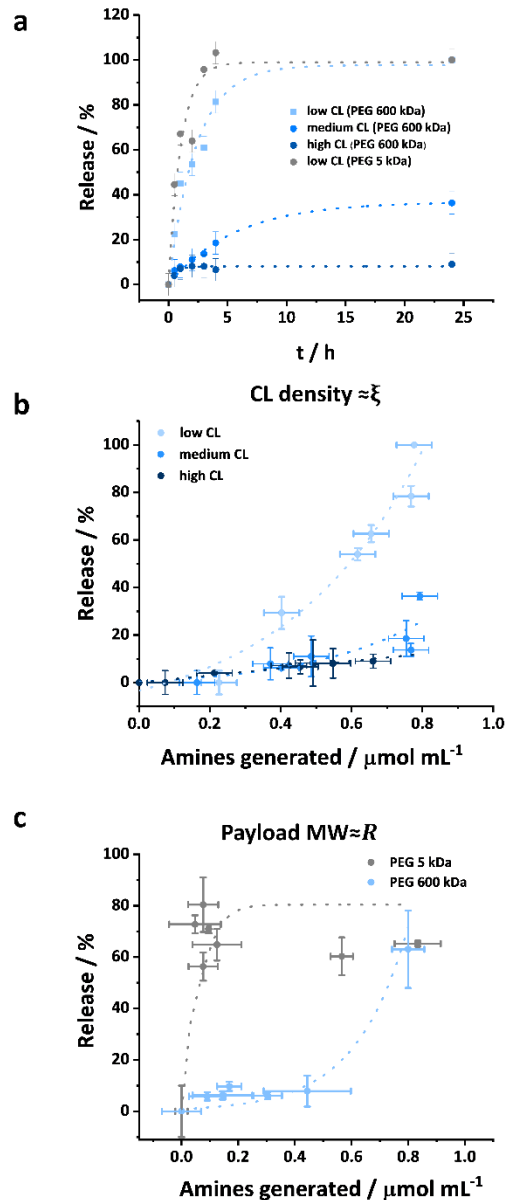
Figure 4.2.9: a) Release kinetics of PEG 600 kDa and PEG 5 kDa from OVA NCs with varying CL density with 1 u of proteinase K mg^{-1} of NCs, b) Release as a function of the degradation of PEG 600 kDa from NCs with different CL density after the addition of 1 u proteinase K mg^{-1} of nanocapsules, c) Release as a function of degradation of PEG of different molecular weight from NCs with a low CL density after the addition of 0.025 u proteinase K mg^{-1} of nanocapsules.

Figure 4.2.10: Release kinetics of PEG of different MW from low CL NCs following incubation of the NCs with proteinase K at a concentration 0.025 u mg^{-1} of NCs.

Additional equations

The obstruction model stipulates that the coefficient of diffusion (D) or a probe of radius (R) in a network composed of fibers of thickness (r_f) creating a mesh of size (ξ) is given by:

$$D = D_0 \exp\left(-\pi \left(\frac{R+r_f}{\xi+2r_f}\right)^2\right)$$

(Equation 4.2)

Thus the average mesh size is:

$$\xi = \frac{R+r_f}{\sqrt{\frac{ln\left(\frac{D}{D_0}\right)}{-\pi}}} - 2r_f$$

(Equation 4.3)

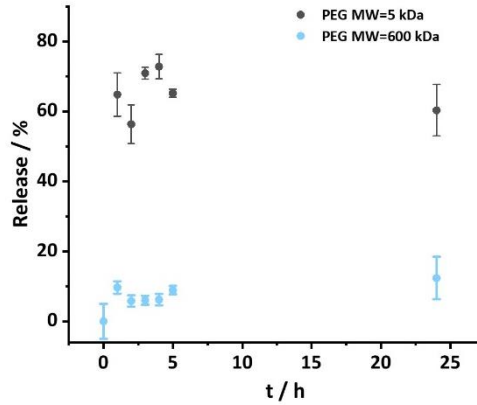Where D_0 is the coefficient of diffusion of the probe in the pure solvent of viscosity η_0, as defined by the Stoke-Einstein relation:

$$D_0 = \frac{k_bT}{6\pi\eta_0 R}$$

(Equation 4.4)

The coefficient of diffusion, using the Einstein–Smoluchowski formalism is defined by a characteristic time (t) and a characteristic distance diffused (r):

$$D = \frac{r^2}{2t}$$

(Equation 4.5)

And, for a molecule to be released, the characteristic distance diffused must be at least the thickness of the nanocapsule shell (ca. 10 nm).

In absence of protease, no diffusion (release) of PEG$_{5K}$ was observed even after 24 h. These value can be used to approximate the maximal D of PEG$_{5K}$ in such system using equation S4 and the unperturbed average mesh size (ξ_0)

$$\xi_0 = \frac{R_{PEG\ 5k} + r_f}{\sqrt{\frac{\ln\left(\frac{D(t)}{D_{0,PEG\ 5k}}\right)}{-\pi}}} - 2r_f = \frac{R_{PEG\ 5k} + r_f}{\sqrt{\frac{\ln\left(\frac{\frac{h^2}{2t_1}}{D_{0,PEG\ 5k}}\right)}{-\pi}}} - 2r_f \qquad \text{(Equation 4.6)}$$

After the addition of protease, the average mesh size increases and this increase in size led to the release of the payload. The diffusing molecules were able to go through the shell of the nanocapsule in less than 30 min.

The release of PEG5k can be observed when the average mesh size is larger than ξ_{PEG5k}:

$$\xi_{PEG_{5K}} = \frac{R_{PEG\ 5k} + r_f}{\sqrt{\frac{\ln\left(\frac{\frac{h^2}{2t_2}}{D_{0,PEG\ 5k}}\right)}{-\pi}}} - 2r_f \approx 1.2\xi_0 \qquad \text{(Equation 4.7)}$$

Similarly, the release of PEG5k can be observed when the average mesh size is larger than $\xi_{PEG600K}$:

$$\xi_{PEG_{600K}} = \frac{R_{PEG\ 600K} + r_f}{\sqrt{\frac{\ln\left(\frac{\frac{h^2}{2t_2}}{D_{0,PEG\ 600K}}\right)}{-\pi}}} - 2r_f \approx 26\xi_0 \qquad \text{(Equation 4.8)}$$

Assuming that the number of "pores" on a nanocapsule of size r_{NC} is:

$$N = \frac{4\pi r_{NC}^2}{\xi^2} \qquad \text{(Equation 4.9)}$$

And, since the number of pores decreases as the nanocapsule is degraded by protease, the average mesh size after a degradation time t can be expressed as:

$$\xi(t) = \sqrt{\frac{4\pi r_{NC}^2}{\frac{4\pi r_{NC}^2}{\xi_0^2} - N_{NH_2}(t)}} \qquad \text{(Equation 4.10)}$$

The number of NH$_2$ per NC produced ($N_{NH2}(t)$) by the degradation after time t will be:

$$N_{NH_2}(t) = \frac{4\pi r_{NC}^2\left(\xi_0^2 - \xi^2(t)\right)}{\xi_0^2\ (i)\cdot\xi^2(t)} \qquad \text{(Equation 4.11)}$$

And the concentration of amine groups produced during degradation (C_{NH2}) in the nanocapsule suspension will be:

$$C_{NH_2}(t) = \frac{N_{NH_2}(t) \times C_{NC}}{N_A} = \frac{4\pi C_{NC} r_{NC}^2\left(\xi_0^2 - \xi^2(t)\right)}{\xi_0^2\ (i)\cdot\xi^2(t)N_A} \qquad \text{(Equation 4.12)}$$

Where N_A is the Avogadro number and CNC is the number concentration of nanocapsules in suspension (C_{NC}).

Intracellular uptake and cytotoxicity

The use of OVA NCs is particularly appealing to target peripheral blood dendritic cells (DCs) because it is a model antigen, which, when co-delivered with immune-stimulating adjuvants, can be used to elicit a robust immune response. The intracellular uptake of the OVA NCs prepared with different CL densities was analyzed *in vitro* in human DCs. For those cellular uptake experiments, OVA labeled with cyanine-5 (Cy-5), a fluorescent molecule, was used in the synthesis of the NCs. First, the DCs were incubated with different concentrations of NCs for 20 h, and the amount of DCs containing the NCs, the Cy-5$^+$ cells, was determined by flow cytometry. Additionally, the fraction of dead cells was quantified by incubating the cells with the live/dead stain 7-AAD. The uptake of NCs moderately increased when increasing the concentration of the NCs in the cell medium from 25 to 100 µg mL^{-1} (Figure 4.2.11).
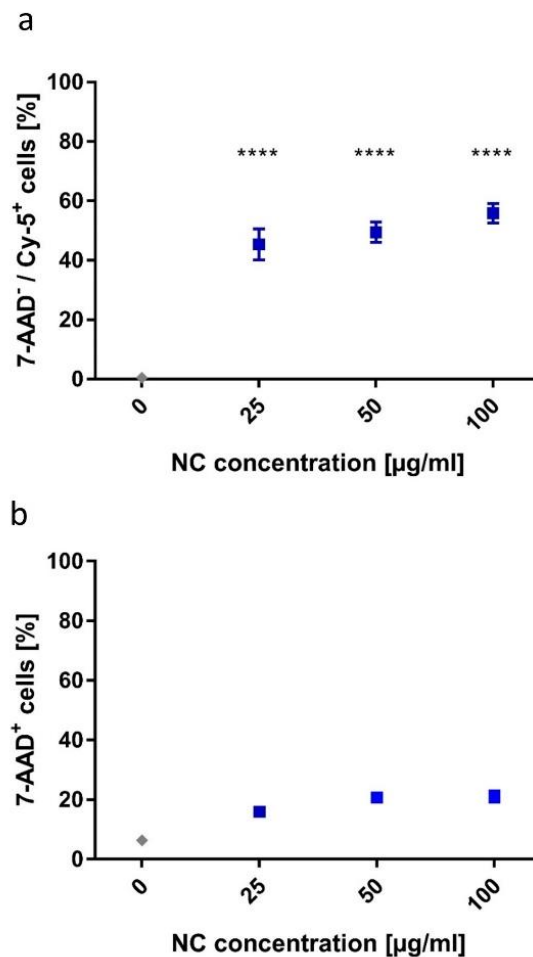

Figure 4.2.11: Uptake (a) and toxicity (b) of increasing concentrations of highly CL OVA-Cy-5 NCs. The DCs were incubated with different concentrations of NCs for 20 h and subsequently analyzed via flow cytometry.

Simultaneously, the toxicity only marginally increased in the same conditions. Furthermore, the CL degree also influenced the cellular uptake and cytotoxicity (Figure 4.2.12). Interestingly, as the CL of the NCs decreased, the fraction of dead cells observed decreased; 15% of the DCs coincubated with the highly CL NCs were 7-AAD positive, whereas only 11 and 10% of the DCs were dead when coincubated with medium and low CL NCs, respectively (Figure 4.2.12 b). The results observed here were similar to those observed for other NCs made from OVA or other proteins albeit the here reported uptake is a bit lower at comparable NC concentrations.[282-284] Of note, however, is that those studies were not performed using primary dendritic cells, but rather monocyte-derived dendritic cells, DC cell lines or macrophages. Another study using primary plasmacytoid DCs (pDC) and targeting different receptors using functionalized PLGA NCs reported cellular uptake ranging from 5 – 45%, depending on the utilized targeting moiety.[285]
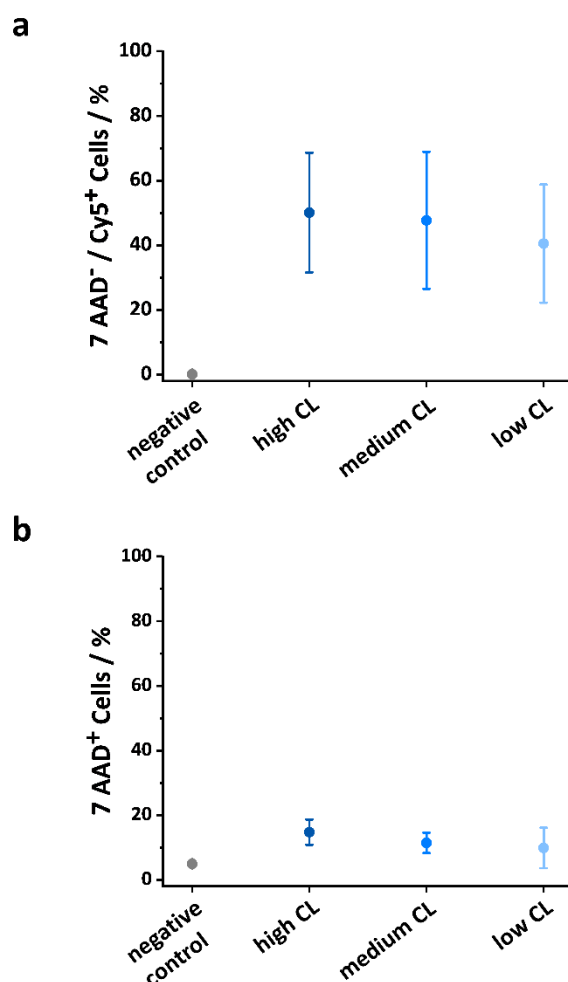

Figure 4.2.12: Comparison of uptake and toxicity of OVA-Cy-5 NCs with different CL degrees. a) Percentage of Cy-5 positive and 7-AAD negative cells, b) percentage of 7-AAD negative cells (dead cells) after the incubation with 50 μg mL^{-1} OVA NCs with different CL degrees for 20 h. Data represents mean ± SD (n = 3).

In Vitro release of a macromolecular adjuvant and cell activation

The design and the resulting properties of the protein NCs are essential for their use as nanodelivery system *in vitro* and potentially *in vivo*. In this regard, the structure-function relationship of the OVA NCs with varying CL degrees was tested with a model macromolecular payload in peripheral blood dendritic cells aiming at the design of a nanovaccine. For the development of nanovaccines, OVA NCs are potent model antigens, which can be used to co-deliver immune-stimulating adjuvants.[201] The immune-stimulant resquimod (R848) served as a relevant model adjuvant cargo due to its potent anti-viral and anti-tumor properties.[286] A successful delivery and release of R848 in the immune system cells, like the dendritic cells, leads to the upregulation of specific surface proteins on the DC.[287] In order to develop this stimulatory effect, the immune-stimulant has to reach specific receptors, which in the case of R848, are localized in the endosomes of the DCs. Hence, the controlled intracellular delivery and release of R848 are essential.

However, R848 is a poorly water-soluble, small molecule, and its use as a vaccine adjuvant is hampered by the rapid diffusion of the small R848 molecule and its rapid dissociation from the antigen upon injection.[288] [289] A possible approach to solve those two pitfalls includes the co-encapsulation of an antigen and R848 in liposomal formulation,[290] or polymer nanoparticles.[285] However, this solution comes with the risk of also generating immunity against the carrier compounds.[199] Here, the strategy proposed to solve both of those issues was to attach the hydrophobic R848 to the water-soluble, non-immunogenic polymer PEG and to encapsulate the macromolecular adjuvant in NCs entirely composed of the antigen protein (OVA).

Hence, the small molecule R848 was modified at the exocyclic -NH$_2$ by attaching it to a PEG (5 kDa) via NHS-Ester chemistry. The PEG was further labeled with rhodamine for its efficient quantification (Figure 4.2.13 a, b). This modification did not alter the therapeutic efficacy of the adjuvant, as shown by comparison of the activation of DCs with R848 and the modified R848 (Figure 4.2.14). The results were in keeping with the preserved activity of R848 on the stimulation of TLR-7 receptors after derivatization at the NH$_2$ with a low molecular weight PEG-linker and RNA.[291]

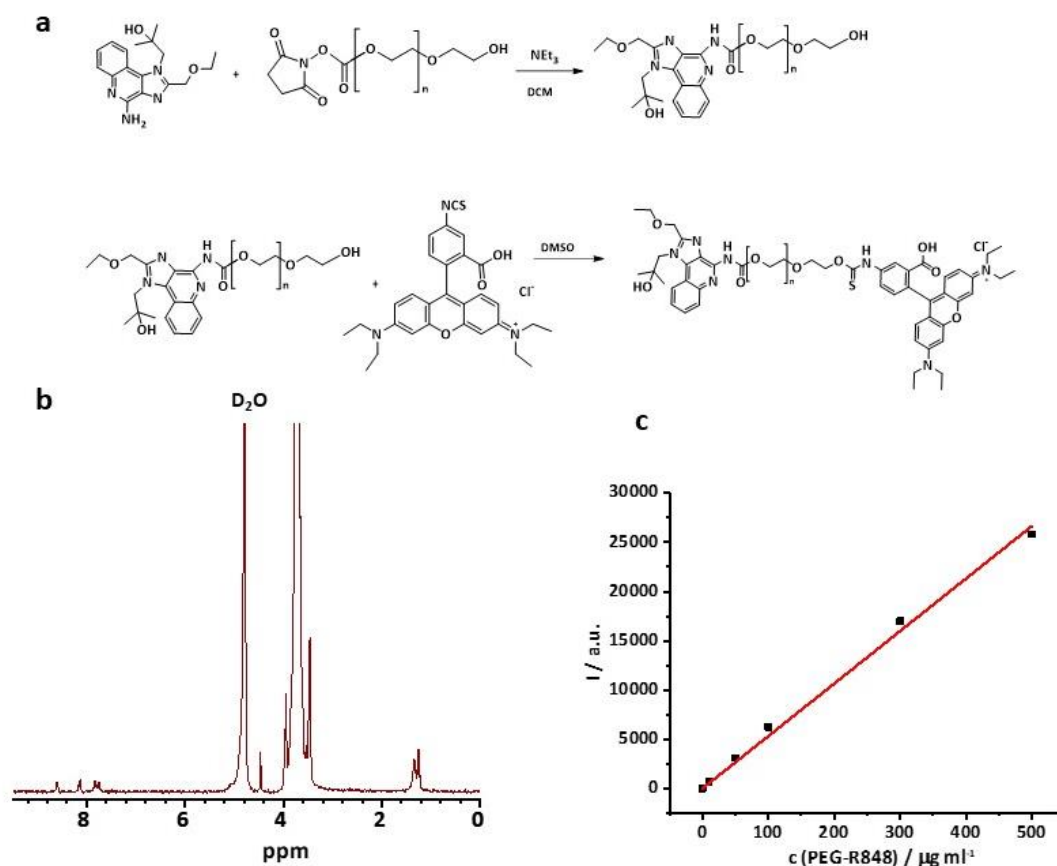Figure 4.2.13: a) Synthesis of PEG-R848, b) ^{1}H-NMR spectrum of PEG-R848, c) Calibration curve of Rhodamine B-PEG-R848.

After the synthesis, the macromolecular stimulant, PEG-R848 was encapsulated in OVA NCs with varying CL, to demonstrate how the delivery and release of macromolecular payloads can be controlled even *in vitro* by the rational design of the NCs.
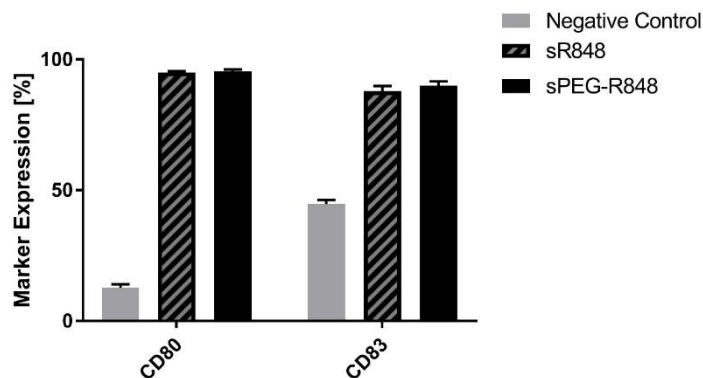
Figure 4.2.14: Activation of DCs after incubation with soluble R848 and PEG-functionalized R848. The activation of cells was assessed by measuring CD80 and CD83 expression levels via flow cytometry.

Due to the high molecular weight of the modified R848, the macromolecular payload was encapsulated with high encapsulation efficiencies (> 80%) in the NCs with different CL densities. Furthermore, the release of the resulting macromolecular adjuvant from the OVA NCs is essential to the upregulation of specific cell markers in the DC cells. To study the release from the NCs, the NCs loaded with the modified R848 were coincubated with DCs at an effective R848 concentration of 500 ng mL^{-1} for 20 h. Afterwards, the cells were harvested, and the expression of the two activation markers, CD80 and CD83, was measured by flow cytometry. Figure 6 shows that only the OVA NCs with low CL density induced a significant upregulation of the cell markers CD80 (~80%) and CD83 (~70%). The activation was comparable to the positive control with soluble PEG-R848 in an equimolar dose. However, the OVA NCs with high and medium CL density showed no cell marker upregulation, illustrating that those two formulations could not successfully release their macromolecular payload *in vitro* (Figure 4.2.15 a, b) in keeping with the release kinetics measured with the model payload (Figure 4.2.9 a).
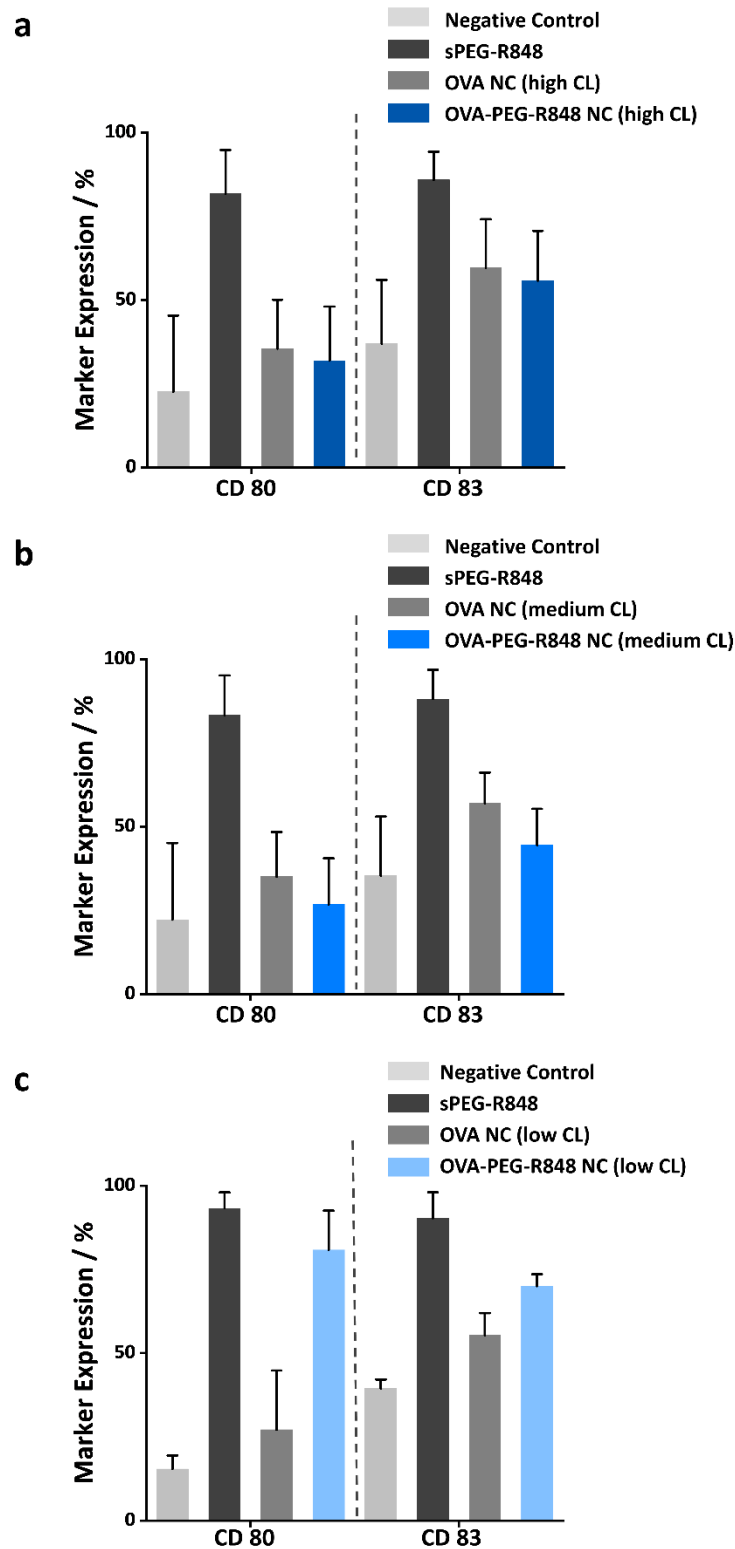
Figure 4.2.15: Activation of DCs after incubation with different OVA-PEG-R848 NC dispersions. The DCs were incubated for 20h with OVA-PEG-R848 NCs with a) high, b) medium or c) low CL densities. Activation of cells was assessed by measuring CD80 and CD83 expression levels via flow cytometry. Data was compared to negative control (no stimulation) and significance was given with p < 0,01 (**), p < 0,0001 (****) (two-way ANOVA). Data represents mean ± SD (n = 3).

4.2.3. Conclusion

Degradable protein nanocapsules with varying crosslinking degrees were synthesized to understand the parameters influencing the release of macromolecular payloads from protein nanocapsules. Protein nanocapsules were prepared by the interfacial crosslinking of nanodroplets containing a solution of proteins and payload. The use of different amounts of crosslinking molecules during the interfacial reaction yielded nanocapsules with different crosslinking density, but with comparable core-shell morphology and encapsulation efficiency. The degradability of the nanocapsules by a natural protease was not affected by the crosslinking density, but the resulting release profiles significantly differed. The initial semi-permeability of the nanocapsule and its response to degradation was influenced by the initial crosslinking density. Submitting the nanocapsules with the highest crosslinking density to enzymatic degradation resulted in no release of the encapsulated payload. However, release occurred from nanocapsules with medium and low crosslinking density. Those nanocapsules were than used to encapsulate an adjuvant (PEG-R848) able to activate specific markers in dendritic cells. The *in vitro* studies showed that the cellular uptake and toxicity of the nanocapsules were only marginally influenced by the crosslinking density, whereas the release of the macromolecular adjuvant only occurred from nanocapsules with the lowest crosslinking density. The results show that such protein nanocapsules can act as an efficient delivery system for macromolecules in a complex biological environment, but only when design with the understanding of the release kinetic. The resulting protein nanocapsules represent a versatile nanocarrier system that can be employed with different small molecule or macromolecular payloads if the initial crosslinking density and mesh size are controlled accordingly. Thus, it provides an adaptable platform for more complex biomedical applications, such as the delivery and release of genetic materials or polyprodrugs.

4.3 De-tolerized aspartyl β-hydroxylase (ASPH) nanocapsules: a novel anti-cancer vaccine[*]

The previous sections showed how protein nanocapsules can be used to transport and release macromolecular payloads while preserving the activity of the biomacromolecules used. This great potential is appealing for the use of catalytic proteins, but also offers novel possibilities for therapeutic proteins, such as antigens. Protein nanocapsules synthesized exclusively from antigen proteins enable the development of novel nanovaccines, since they prevent the possibility of emerging side effects that can occur *in vivo* due to the generation of immunity against body-foreign carrier compounds. Hence, formulating the nanocarrier exclusively out of the specific antigen prevents possible side effects and further increases the dose of antigen delivered. Therefore, the aim of this study was to synthesize nanocapsules out of the antigen protein Aspartyl (asparaginyl)-β-hydroxylase (ASPH), which is often overexpressed in hepatocellular carcinoma (HCC), deliver them to the cells of the immune system and to induce cellular immunity against ASPH.

4.3.1 Introduction

Hepatocelluar carcinoma (HCC) is a hepatic disease and one of the leading causes of cancer death, especially in East Asian countries.[292] Often, it remains undiagnosed in the majority of patients until an advanced stage is reached.[293] However, at that stage, the therapeutic options are limited, and the chance of recovery is small. Hence, novel approaches to treat this disease are urgently needed to improve patient life expectancy.[294] The development of novel immunotherapeutic vaccines for HCC and other types of cancer is highly promising in this respect. It is supported by the observation that patients with tumors that contain tumor specific effector T-cells (T_{eff}) , cells of the adaptive immune system with the function to attack cancer-infected cells, exhibit strong anti-tumor responses.[295] As such, if the anti-tumor immunity can be maximized, the tumor reoccurrence can be diminished and the therapy enhanced.[296]

In order to treat the disease, anti-cancer vaccines have to target the specific antigen protein to the dendritic cells (DC) and induce the DC activation by stimulating a robust T_{eff} cell response.[297]

In this regard, a variety of tumor-specific antigens have been used for the development of vaccines against cancer, but none of those have accomplished significant success in clinical trials.[298] This impedes the evaluation of novel antigens for the development of anti-cancer vaccines.

Aspartyl (asparaginyl)-β-hydroxylase (ASPH) is one promising antigen suitable for this purpose. It is a transmembrane protein, which belongs to the family of prolyl and lysyl hydroxylases[202] and plays a major role in regulating cell growth, such as differentiation and cell migration.[203] It is known to be overexpressed in a majority of tumors affecting the pancreas, breast, prostate, kidney, bladder and liver (in the case of HCC).[299] In the case of HCC, the overexpression of ASPH specially produces a malignant phenotype with increased cell motility and metastases.[203] The fact that ASPH is increasingly expressed on the surface of HCC tumor cells, but not on the cells in the near surrounding, suggests that ASPH could be used as an immunotherapeutic target in anti-cancer vaccines.[204] Indeed, ASPH-loaded dendritic cells injected subcutaneously suppressed the growth of a tumor in a mouse model of HCC.[300]

However, a spontaneous clearance of tumors by endogenous immune responses is rare.[301] An immunosuppressive tumor microenvironment significantly contributes to the escape of tumor cells from immune attacks leading to generally weak immune responses against the administered antigen.[302] Multiple mechanisms are the cause, including exhausted T_{eff} cells with a lost capacity to proliferate and lyse antigen-expressing target cells and subsequent cell-surface expression of multiple inhibitory checkpoint receptors. Furthermore, the accumulation of regulatory T_{reg} cells in the tumor microenvironment leads to the inhibition of T_{eff} cells maturation and to the production of immunosuppressive factors. Those mechanisms significantly affect tumor-specific immunity and decrease the anti-cancer vaccine efficacy.[303]

Hence, the activation of the innate immune system combined with the antigen-delivery is essential to optimize the vaccine efficacy. Immunostimulatory adjuvants are able to activate the adaptive immune system and can be co-delivered with the antigen to enhance the immune cell responses.[304] In this regard, many novel and well-characterized adjuvants have been developed, which opened many new opportunities in vaccine development.[200] For instance, Monophosphoryl Lipid A (MPLA), a Toll-like receptor 4 agonist, which has already been approved by the FDA for the use in hepatitis B virus and human papillomavirus vaccines, promotes immune cell responses.[305] Delivering the anti-cancer antigen to dendritic cells combined with simultaneous maturation by co-delivered adjuvants is thus a promising approach for future anti-cancer treatments.[200]

Nanoparticles, and especially nanocapsules, offer a great possibility for the co-delivery of antigen and adjuvant since they can easily load multiple active agents, protect the antigen from proteolytic degradation and enhance the intracellular uptake of the biomacromolecule. If the nanocapsule itself can be synthesized of the antigen protein, as described in this thesis, the effective

concentration of the antigen is significantly increased and simultaneously potential side effects emerging from the immunization against potential body-foreign carrier material are prevented. In the previous sections, the synthesis of robust and biodegradable protein nanocapsules was described. Those nanocapsules were made of ovalbumin or catalytic enzymes, using the method of miniemulsion droplets as the template for the interfacial crosslinking of proteins. This method is particularly interesting due to its transferability for the polymerization of other proteins serving as antigens in vaccination approaches. Hence, the synthesis of full-ASPH nanocapsules by inverse miniemulsion delivering immunostimulatory adjuvants, is a promising strategy for the development of anti-cancer vaccines.

4.3.2 Results and discussion

Scaling down the nanocapsule synthesis

When aiming at the production of full-antigen nanocapsules, only very low amounts of the protein are usually available. Since the ASPH protein needs to be produced from a *pichia pastoris* cell culture and then purified by a His-tag affinity chromatography, only a limited amount can be used in the preparation of a batch of nanocapsules. The process developed in Section 4.1 to preserve the activity of the biomacromolecular building block typically works with an amount of 10 mg of protein. However, the key limiting factor is the volume of pre-emulsion injected in the interaction chamber, in the case of the microfluidizer used here 1 mL. To make this process compliant with the minute amount of ASPH produced, the formation of the nanocapsule needed to be scaled down. Furthermore, during the downscaling of the synthesis, it must be ensured that the batches show consistent performances and that the resulting nanocapsules are identical in quality and reproducibility to those obtained with traditional batch size.

During microfluidazation, the interaction chamber in injected with a pressurized pre-emulsion (c.a. 1 mL). Typically, this pre-emulsion is composed of 10 wt% of dispersed phase, the rest being the tenuousous organic phase. The usual concentration of protein in the dispersed phase is 10 wt%, which translates to 10 mg of protein in 0.1 mL of dispersed phase. This is incompatible with the production of ASPH. Different strategies can be used to reduce the amount of protein needed to prepare the nanocapsules. The amount of dispersed phase to continuous phase can be decreased or the amount of protein in the dispersed phase can be reduced.

Changing the phase volume ratio

The phase volume ratio is an important parameter of emulsions and is given by the ratio of the volume of the dispersed phase to the volume of the continuous phase. If the ratio is increased, a potential phase inversion of the emulsion may occur. However, if decreasing the ratio, the stability and dispersity of the emulsion are also hampered, since the coverage of the droplets by the surfactant and the concentration of droplets are influenced.

Typically, a ratio of 1/10 is employed in the nanocapsule synthesis by miniemulsion. However, if not enough material is present to provide this ratio, less dirspersed phase could be used while keeping the total volume of the emulsion the same. To test the effect of the ratio of dispersed phase to continuous phase on the quality of the protein nanocapsules, four different miniemulsion samples were prepared by using OVA as the model protein. Table 4.3.1 shows the single parameters that were adjusted. In this test series, the volume of the dispersed phase was decreased stepwise from 0.10 mL to 0.01 mL.

Table 4.3.1: Samples for the down-scaling of protein nanocapsules synthesis.

Phase volume ratio	Total volume of miniemulsion	Volume of continuous phase	Volume of dispersed phase	Mass of protein	Size in Cyclohexane	PDI
1/10	1.10 mL	0.10 mL	1.00 mL	10.0 mg	306 nm	0.25
1/20	1.10 mL	0.05 mL	1.05 mL	5.0 mg	370 nm	0.30
1/50	1.10 mL	0.02 mL	1.08 mL	2.0 mg	304 nm	0.22
1/100	1.10 mL	0.01 mL	1.09 mL	1.0 mg	340 nm	0.42

All samples were processed identically and crosslinked with the appropriate amount of TDI crosslinker. After the purification, they were evaluated according to their size and size distribution by DLS. Figure 4.3.1 shows the DLS curves and the PDI values obtained from the single samples. All samples were similar in size (200-300 nm), but the size distribution was narrower for 1/10 (PDI=0.25). At lower ratios of dispersed phase, the formation of either aggregates or large nanocapsules was observed (Figure 4.3.1 a). When the ratio decreases to 1/100 the PDI value doubles to 0.42 when compared to the sample with the 1/10 ratio. This indicates that the decrease in the volume of dispersed phase used negatively influences the size distribution of the resulting nanocapsules. However, when employing a ratio of 1/50 or even 1/20, the impact is low and still acceptable. Hence, a ratio of 1/50 were chosen as a minimal ratio and the resulting mass of protein as minimal mass needed for the synthesis of one protein nanocapsule batch. The increasing polydispersity coming in hand with the decreasing phase volume ratio can be attributed to the lower collision of droplets in the microfluidizer microchannel. As the number of droplets also decreases in the total emulsion, less collisions occur and lower droplet

disruptions may occur. This leads to an increased droplet polydispersity and resulting broader size distributions of the nanocapsules. Hence, the down scaling of the nanocapsule synthesis by decreasing the phase volume ratio is a critical step and has to be evaluated thoroughly if employed in further studies.
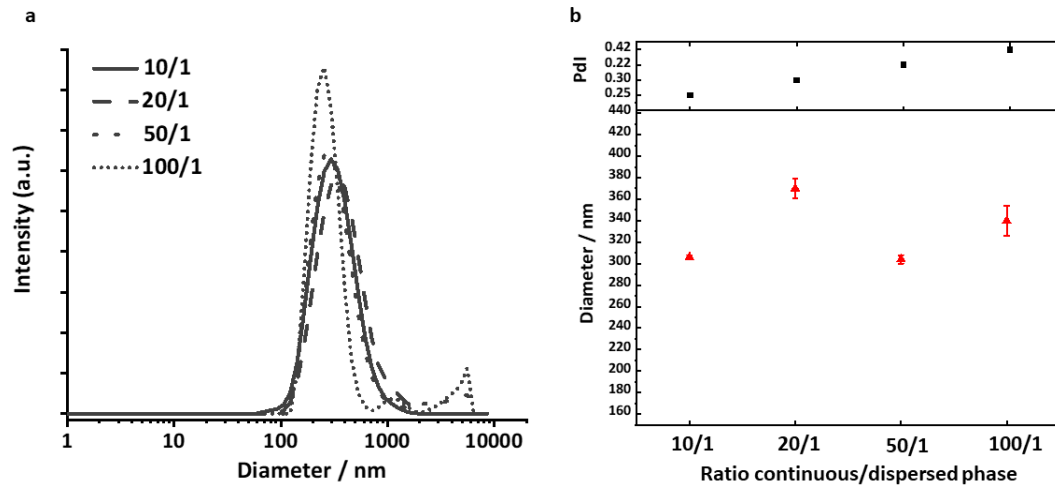
Figure 4.3.1: Characterization of NCs with carrying continuous/dispersed phase ratio. a) DLS curves, b) medium diameter and PDI value.

Changing the concentration of protein in the dispersed phase

Typically, the concentration of protein in the dispersed phase is 10 wt%. If less protein is available, the concentration could be decreased to 5 wt%. Therefore, OVA NCs were prepared with 1.10 mL of total volume and 0.1 mL of dispersed phase. Instead of 10 mg, 5 mg of OVA were used in the dispersed phase. Figure 4.3.2 b shows the TEM image obtained from OVA NCs with a 5 wt% concentration of protein in the dispersed phase. It can be observed, that nanocapsules with a clear core-shell morphology were still obtained. The concentration of protein has an impact on the resulting mesh size of the nanocapsule and hence significantly influences the encapsulation efficiency of the nanocapsules. Thus, decreasing the concentration of protein even more would lead to a loose protein gel without a clear core shell morphology and with unefficient encapsulation properties.
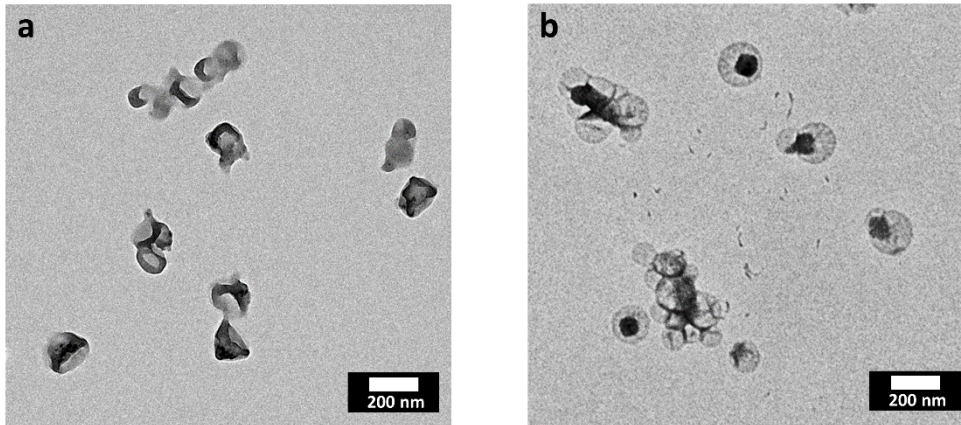
Figure 4.3.2: TEM image of OVA NCs synthesized with a) 10wt% and b) 5wt% of OVA in the dispersed phase.

Synthesis of the ASPH NCs

After the synthesis of the ASPH protein, it was used to formulate hollow nanocarriers entirely composed of the ASPH. The synthesis procedure was scaled down, so that only 5 mg of protein were used per synthesis. The experiments were conducted over a period of several months and small batches of nanocapsules were produced when needed to avoid the aging of the sample. The ASPH NCs were synthesized by crosslinking the protein with 2,4-toluene diisocyanate (TDI), resulting in NCs with a solid ASPH shell. The reaction occurred at the interface of an inverse miniemulsion composed of aqueous droplets of ASPH solution in cyclohexane. Then, TDI was added to the cyclohexane phase and let to react with the nucleophilic amino groups of ASPH.

After the reaction, a solid protein shell surrounding an aqueous core was obtained, as confirmed by scanning electron microscopy (SEM) and transmission electron microscopy (TEM) (Figure 4.3.3 a and b). Later, the NCs were transferred to water followed by the evaporation of the remaining cyclohexane. Dynamic light scattering was used to determine the size of the nanocarriers (Figure 4.3.3 c). The ASPH nanocarriers had an average diameter of 333 nm when dispersed in cyclohexane and 400 nm in aqueous dispersions after purification.

Figure 4.3.3: Characterization of the ASPH NCs: a) transmission electron microscopy (TEM) image of ASPH NCs in the cyclohexane phase, b) scanning electron microscopy image (SEM) of the ASPH NCs in the cyclohexane phase, c) DLS of the ASPH NCs in the cyclohexane phase and after transfer to water.
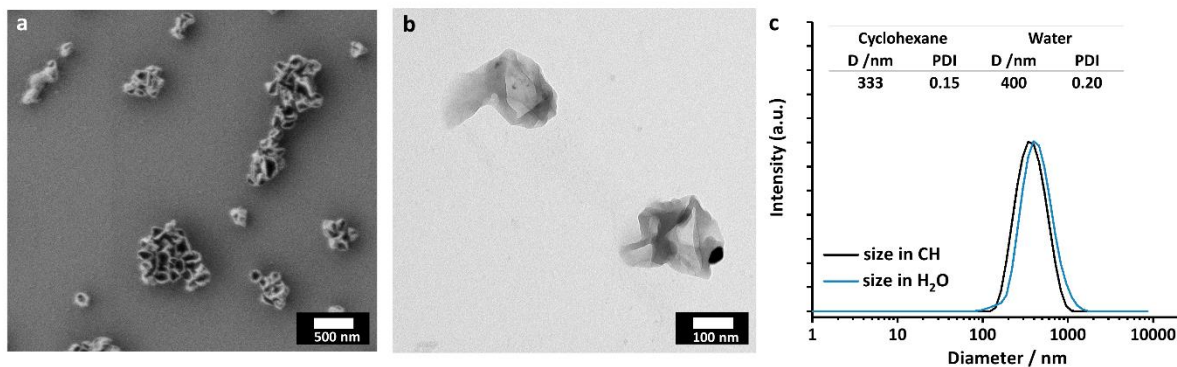
After the transfer of the nanocapsule to water, MPLA, an amphiphilic adjuvant, was adsorbed on the nanocarriers in defined quantities. A loading capacity with MPLA of 5 µg mL^{-1} MPLA for 1 mg mL^{-1} of nanocapsules was measured using a limulus amebocyte lysate assay. This finding is comparable to a loading of up to 0.8 wt% after incorporation of MPLA in PLGA nanoparticles as reported previously.[306]

Intracellular uptake and toxicity of the ASPH NCs

The intracellular uptake of the ASPH NCs was analyzed *in vitro* in human DCs and in dependence of the concentration of the NCs. For the uptake experiments, ASPH labeled with cyanine-5 (Cy-5), a fluorescent molecule, was used in the synthesis of the NCs. The DCs were incubated with different concentrations of the ASPH NCs and with ASPH NCS coated with MPLA for 20 h and the amount of DCs containing the NCs, the Cy-5$^+$ cells, was determined by flow cytometry. Additionally, the number of dead cells was quantified by incubating the cells with the live/dead stain 7-AAD. The uptake of NCs moderately increased with the concentration of the NCs in the cell medium (Figure 4.3.4) and the toxicity marginally increased from the incubation between 10 and 25 µg mL^{-1}. In total, the prepared nanocapsule formulations showed no significant toxicity profile even at the concentration range from 1-25 µg mL^{-1}. Those results verified a sufficient removal of potentially toxic residual substances, such as the crosslinker, needed during synthesis and redispersion process.
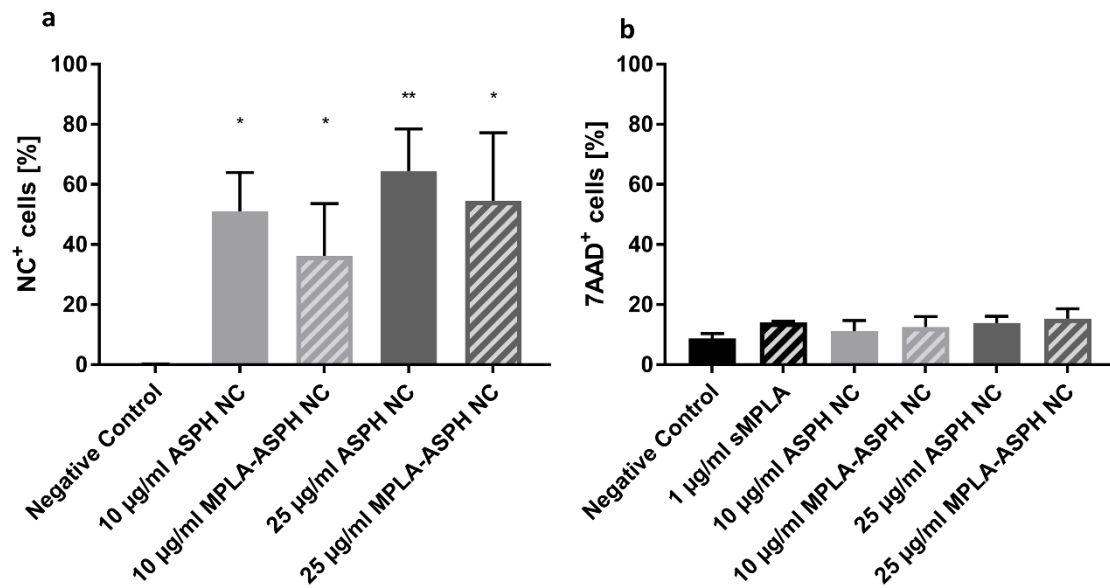
Figure 4.3.4: Comparison of uptake and toxicity of ASPH-Cy-5 NCs with different concentrations. a) Percentage of Cy-5 positive and 7-AAD negative cells, b) percentage of 7-AAD negative cells (dead cells) after the incubation with 10 and 25 µg mL^{-1} OVA NCs with different CL degree for 20 h. Data represents mean ± SD (n = 3).

In vitro cell activation

The coating of the antigen nanocapsules with immune activating adjuvants allows to induce the activation and maturation of dendritic cells with respect to the secretion of cytokines and the expression of surface markers *in vitro*. MPLA-adsorption on the ASPH-NCs induced a significant upregulation of CD40 and CD80 expression by monocyte derived dendritic cells (Figure 4.3.5). The activation was slightly weaker compared to the positive control with soluble MPLA at a concentration of 1 µg mL^{-1}. This effect depended on the applied NC concentration and the incubation with ASPH NCs without MPLA did not induce a significant upregulation of surface marker expression even at high nanocapsule concentrations.
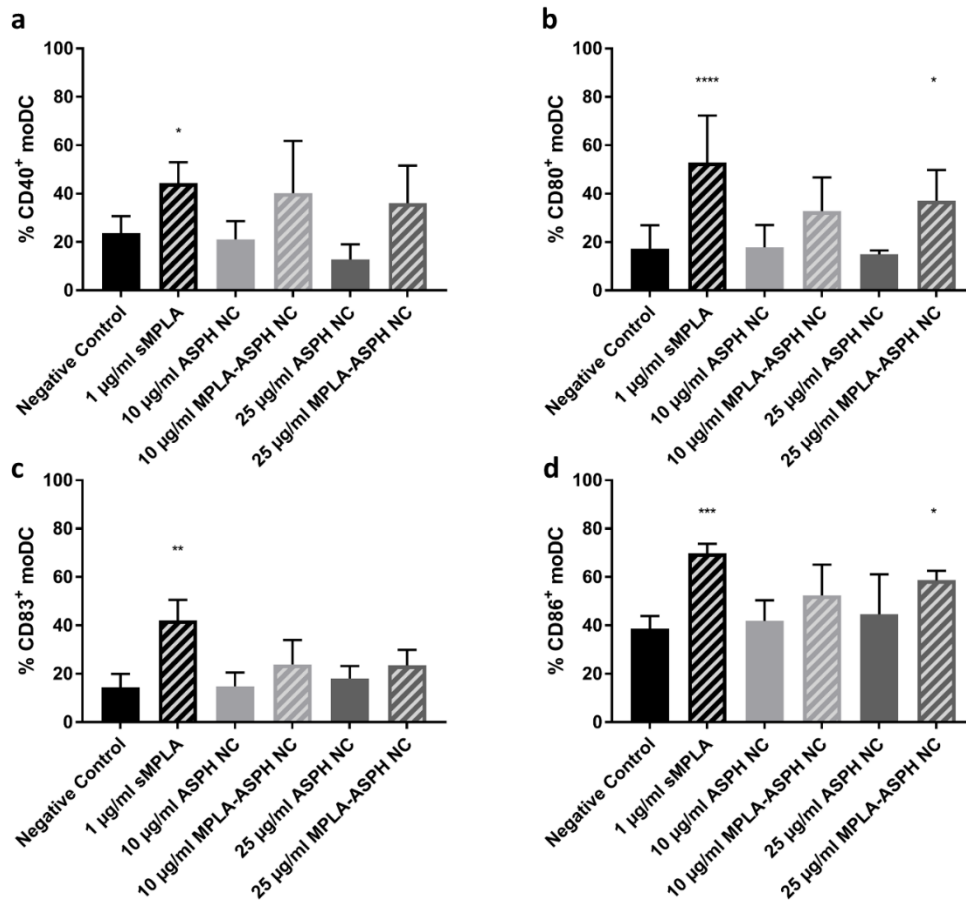
Figure 4.3.5: Activation of DCs after incubation with different ASPH NC dispersions. Activation of cells was assessed by measuring CD80, CD40, CD83 and CD86 expression levels via flow cytometry. Data was compared to negative control (no stimulation) and positive control (soluble MPLA). Data represents mean ± SD (n = 3).

In vitro immunization

In the last set of experiments, the generation of an ASPH-specific immune response was tested. Monocyte derived dendritic cells were incubated with the ASPH native protein and the MPLA-coated ASPH NCs. In the case of an effective digestion of the ASPH by the dendritic cells, they should display the antigen fragments on the cell surface. T_{eff} cells, which include CD4+ and CD8+ T cells, recognize the antigen fragments and become activated to kill infected or malignant cells and the secretion of cytokines, primarily TNF-α and IFN-g, by T_{eff} cells induces anti-tumor and anti-viral microbial effects. Hence, the analysis of the number of cells displaying the characteristic cytokine markers, allows to evaluate the antigen-specific immune response. Figure 4.3.6 shows the evaluation of ASPH-specific T-cells after 7 days of co-culture. Unfortunately, the absence of detectable CD8+ and CD4+ cells in both cases, the native protein and the ASPH NCs, evidences no generation of an ASPH specific immunity.

CD4$^+$ Th1 T cells
(expressing two or more markers among CD154, IFNg and TNFa)

CD8$^+$ CTL T cells
(expressing two or more markers among CD137, IFNg and TNFa)
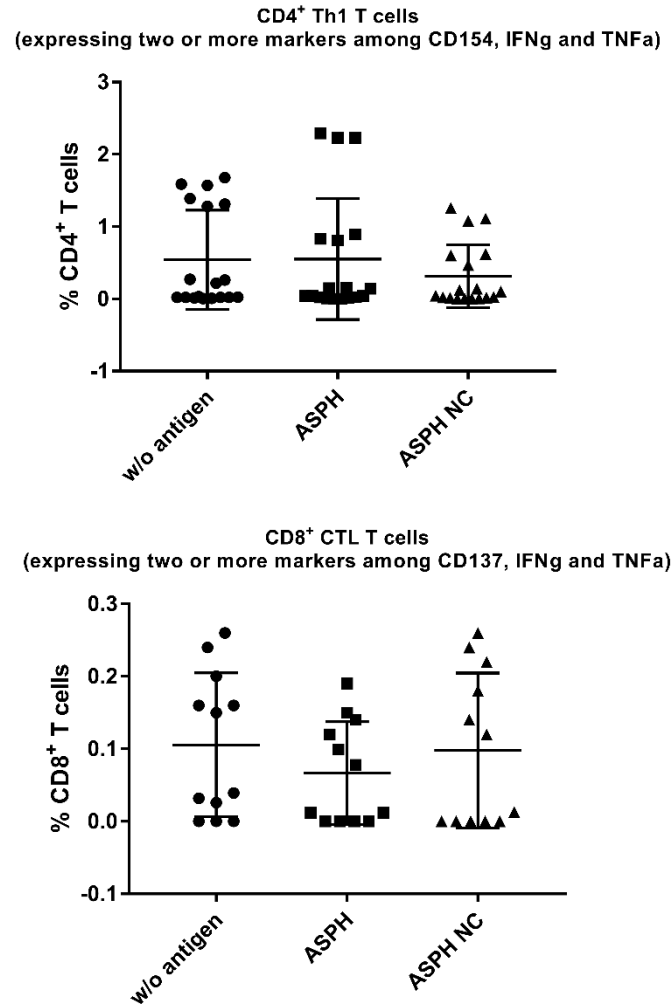
Figure 4.3.6: Co-culture data of native and nanoparticulate ASPH. Shown are only unique T cells that express at least two of three activation markers. N=6.

4.3.3. Conclusion

In this proof-of-concept study, protein nanocapsules exclusively of the HCC-specific antigen ASPH were synthesized and functionalized with the adjuvant MPLA. The down-scaling of the synthesis enabled the preparation of the nanocapsules from only 5 mg of protein. The high cellular uptake and low toxicity of the nanocapsules proved the applicability as nanotherapeutics and the capability to target antigen-presenting cells and their efficient maturation and activation. However, so far, no induction of cellular immunity *in vitro* by the ASPH nanocapsule was observed. Those results are in keeping with what was observed simultaneously with native ASPH protein. More biological work would be required to optimize the design of the ideal ASPH nanodelivery vehicle for potential application as an anti-cancer vaccine.

5. Summary and perspectives

5.1 Summary

This thesis highlights some promising approaches to overcome the challenges in the delivery of biocromolecular therapeutic agents. Protein nanocapsules were developed for this purpose. The resulting nanocapsules were biocompatible and biodegradable carriers, and were able to tackle the challenge to release macromolecular payload with a high degree of control. Furthermore, the processing method of the preparation of protein nanocapsules was optimized to the point that the native biological function of the protein was preserved, allowing for the design of highly functional protein nanocarriers. The solutions found could find application for the design of protein nanocapsules while employing various other proteins and allow for the design of novel and multifunctional materials.

To overcome the challenges faced in the preparation of active protein nanocarier, a processing method for the protein nanocapsules was established, which allowed to preserve the intrinsic function of the protein during the nanocapsule synthesis process (section 4.1). For this purpose, enzymes were used as the nanocarrier building blocks, since they provide intrinsic catalytic functions of great interest for many applications and their native functionality can be easily quantified. The use of microfluidization over ultrasound emulsification was a critical step in the nanocapsule synthesis and allowed for the preservation of a high degree of enzymatic activity after the processing of different enzymes (up to 80% of activity). Followed by the interfacial crosslinking of the enzymes, protein nanocapsules with a hollow aqueous interior were obtained. In this process, even multiple enzymes were crosslinked in one nanocapsule allowing for the performance of enzymatic cascade reactions. Simultaneously, the inner aqueous core of the protein capsules acted as a reservoir for catalytic reactants, and after the encapsulation of the agents, the enzymatic shell actively catalyzed the on-site conversion of the payloads (Figure 5.1). In this regard, the protein nanocapsules acted as both a transporter for a biomacromolecular cargo (polymer-functionalized luminol) and as a catalyst for the conversion of the payload. Those multifunctional nanoreactors were also taken up by cells and were able to perform enzymatic catalysis within the complex cellular environment. These findings showed that a mild nanocapsule synthesis process could produce nanocapsules with intrinsic biological functions, which overcome the exclusive purpose of transportation. Moreover, therapeutic proteins, which have to be delivered to a specific organ or cell, can be the main constituting unit of a nanocapsule, while preserving their biological activity and delivering other additional payload with them. Those results provide an adaptable platform for more complex biomedical applications, such as the development of *in cellulo* drug nanofactories based on protein nanocapsules.
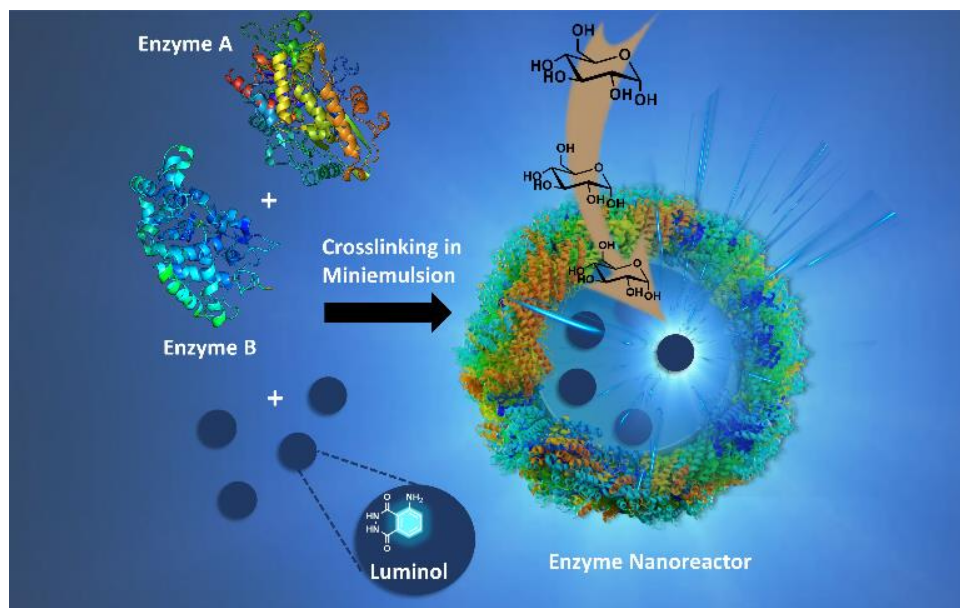
Figure 5.1: Self-sustaining enzyme nanoreactors participate actively in both the transportation and the conversion of the reactants located in their inner core.

Another challenge faced in the delivery of biomacromolecular therapeutic agents is the controlled release of this type of cargo from the delivery carrier. Typically, this process is complex due to the large hydrodynamic radius and high molecular weight of such payload, which leads to a decreased mobility and diffusion. Here, to enable a controlled release of biomacromolecules, highly degradable ovalbumin nanoncapsules were designed as a model delivery system (section 4.2). The control over the permeability of the nanocapsule shell and the release of encapsulated macromolecules was achieved by the tuning of the crosslinking density of the protein shell. The use of different amounts of crosslinking molecules during the interfacial reaction yielded nanocapsules with different crosslinking density, but with comparable core-shell morphology and encapsulation efficiency (> 70%). The degradability of the ovalbumin nanocapules by a protease under artificial conditions was not affected by the crosslinking density, but the resulting release profiles significantly differed. While the nanocapsules with the highest crosslinking density resulted did not show release of the encapsulated macromolecules, the release occurred from nanocapsules with medium and low crosslinking density. After understanding the parameters influencing the release from ovalbumin nanocapsules under artificial conditions, the nanocapsules were successfully used to deliver and effectively release a bioactive macromolecular vaccine adjuvant *in vitro*. Here, after the uptake of ovalbumin nanocapsules with a low crosslinking density, dendritic cells exhibited an elevated activation marker expression attributed to the successful release of the adjuvant and co-localization with the specific receptors localized in the endosomes of the DCs (Figure 5.2).

The developed protein nanocapsules represent a versatile nanocarrier system that can be employed for the controlled release of biomacromolecular therapeutic agents if the initial crosslinking density and mesh size are controlled accordingly. Thus, they provide an adaptable platform for the delivery and release of various materials such as genetic materials or polyprodrugs.
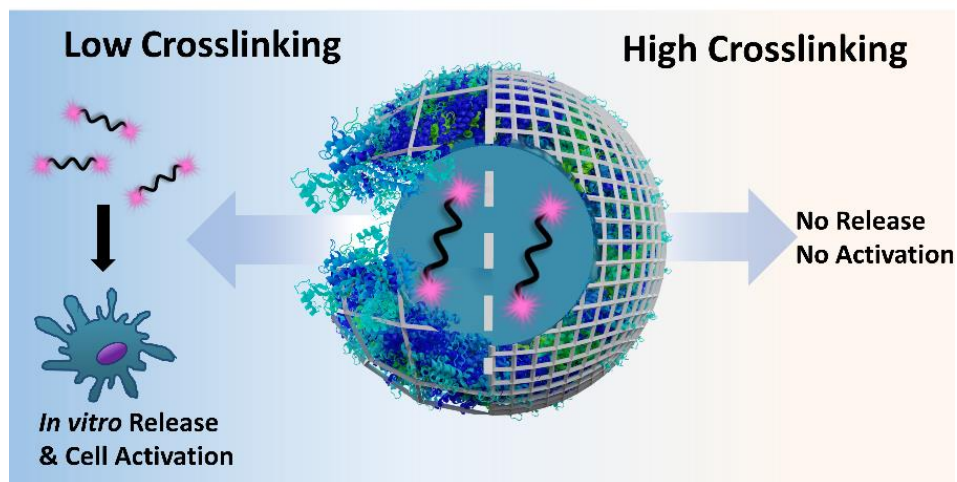
Figure 5.2: The semi-permeability of protein nanocapsules controls the release of and the cellular response to macromolecular payload.

Based on the key findings that protein nanocapsules can both, preserve a high degree of their intrinsic biological function and be highly degradable in the intracellular environment, novel potential applications arise. For the development of anti-cancer vaccines, antigen proteins can thus be formulated as nanocarriers, delivered to the dendritic cells, and there be degraded into antigen fragments for the cross-presentation to T-cells (Figure 5.3). Here, nanocarrier were synthesized from the antigen protein ASPH and the nanocapsule synthesis process was scaled down to the point that only 2-5 mg of antigen were used per batch of capsules (section 4.3). For this purpose, the downscaling experiments were performed with the model antigen ovalbumin and the ratio of continuous phase/dispersed phase in the inverse miniemulsion was varied from 10/1 to 100/1 to reduce the amount of protein needed. The resulting nanocapsules were compared according to their size and size distribution and while increasing the ratio from commonly employed 10/1 to 50/1 resulted in a reasonable PDI value (0.22), a ratio of 100/1 showed a very broad distribution of nanocapsule sizes (PDI 0.42). Further, it was also possible to decrease the solid content in the dispersed phase from 10wt% to 5wt% and still nanocapsules with a clear core-shell morphology were obtained. This reduced the required amount of protein from 10 mg to 2.5 mg. After the optimization of the procedure, full ASPH nanocapsules were synthesized and after the transfer to water, they were functionalized with the immune-stimulating adjuvant MPLA.

The nanocapsules displayed low toxicity and a good uptake by monocyte dendritic cells. Further, they were able to induce the activation of the cells as observed from the elevated expression of activation markers on the cells. The results obtained in this chapter are a great platform for the development of anti-cancer vaccines from antigen nanocapsules, and the procedure can be transferred to further interesting antigens.
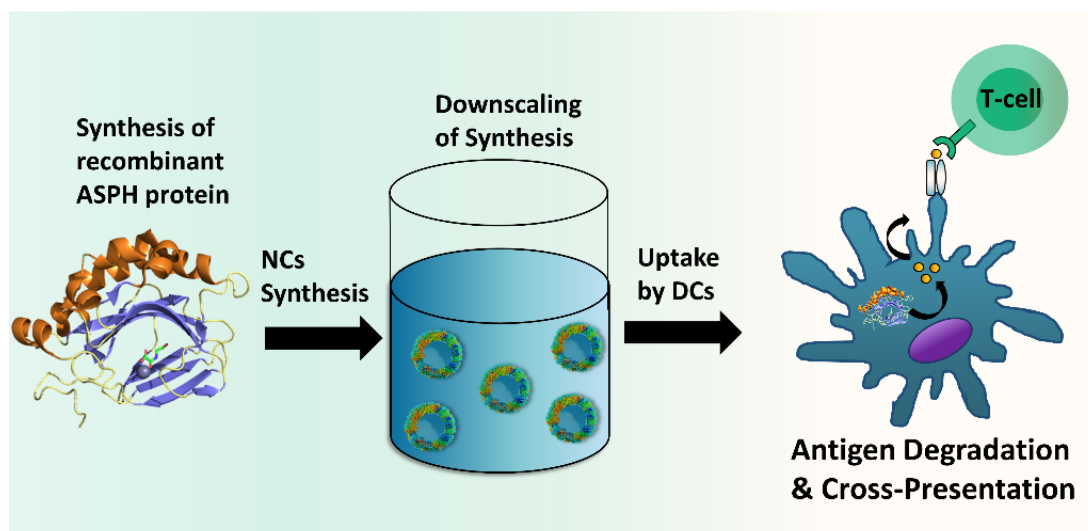
Figure 5.3: The development of nanovaccines from antigen protein nanocapsules requires the downscaling of nanocapsule synthesis, the effective uptake by DCs and the intracellular degradation of nanocapsules to antigen fragments which are presented on the surface of the DCs.

In summary, the results in this thesis show that protein nanocapsules can provide both, a high degree of functionality and a high degree of biodegradability to efficiently act as a carrier, a functional unit and control the release of encapsulated (bio)macromolecules. A biomacromolecular therapeutic agent of interest like a protein, can thus be formulated as a hollow nanocapsule, efficiently taken up by cells and preserving its therapeutic activity. Furthermore, the delivery of other biomacromolecular therapeutic agents can also be realized and controlled using such protein nanocapsules. The nanocapsules prepared displayed excellent biocompatibility and demonstrated ability the control the release of the cargo. Hence, protein nanocapsules have an enormous potential for future biomedical and catalytic applications.

5.2 Perspectives

In the future, the synthesis of the protein nanocapsules with functional proteins should be optimized in regard of the crosslinking reaction. The robust crosslinking between the isocyanate groups of TDI and the nucleophiles of the protein employed here may interfere with the functional groups that are present in the biomacromolecular therapeutic agent. This can harmfully influence the sensitive structure if the biomacromolecules are encapsulated in the inner core of the carrier. In this case, more selective and bio-orthogonal crosslinking reactions should be employed. For example, condensation between hydrazides and aldehydes can be employed if the protein building blocks are modified with one of those functionalities. Furthermore, the copper-free azide alkyne click reaction could be a possible approach. However, in such cases, it would be essential to evaluate the influence of the modification reaction on the structure of the proteins and their activity. This is especially of great relevance for catalytic proteins such as enzymes.

In additions, to gain more control over the release of biomacromolecular therapeutic agents, the incorporation of responsive cleavage points in the protein nanocapsules is a possible method. The protein nanocapsules prepared here were highly responsive to natural enzymes and the enzymatic degradation of the nanocarrier leads to a controlled release of the payload. However, expanding the responsive properties of the nanocapsules to additional environmental triggers, such as changes in the pH value, the redox state, the temperature and the concentration of metabolites would provide a triggered drug release and a more precise control over the effective drug concentration in time and place. The incorporation of such "smart" properties in the protein nanocapsules could be achieved by the use of reversible crosslinking points or the addition of other cleavable functionalities.

Additionally, the simultaneous transport and release of multiple biomacromolecular therapeutic agents should be tested. This approach would allow for a combination therapy and enhance the efficacy of the treatment or overcome multidrug resistance. In this regard, the release of multiple payload from one protein nanocarrier should be studied and correlated to the molecular weight and hydrodynamic radius of the cargo. If the release could be controlled and the release profile adjusted to have the desired pharmacokinetic properties (systemic release of all components vs. sequential release of single components), more efficient treatments can be developed.

Furthermore, it could be favorable to realize a targeted delivery of the nanocarrier to specific organs or cell lines. The introduction of targeting ligands on the surface of the protein nanocapsules could be of high interest for this purpose. Those can include peptides, antibodies or antibody fragments, as well as small molecules such as folic acid. The successful functionalization of the nanocapsules with the targeting moieties would enhance a tumor-specific delivery for the optimized treatment with biomacromolecular therapeutic agents. Simultaneously, the introduction of stealth polymers to the surface would enhance the circulation time of the carrier *in vivo.*

Moreover, more systematic *in vitro* and also *in vivo* studies should be conducted to bring new information about the behavior of the protein nanocapsules in biological media. For example, more insights into the *in cellulo* fate of the nanocarrier are needed to optimize the design in terms of biodegradability and stability. Furthermore, the protein nanocapsules composed of therapeutic proteins should be tested according to their ability to enhance the treatment of diseases *in vivo* and their role in future medical applications.

References

1. L. Milane and M. Amiji, *Drug Delivery and Translational Research*, 2021, DOI: 10.1007/s13346-021-00911-y.
2. F. P. Polack, S. J. Thomas, N. Kitchin, J. Absalon, A. Gurtman, S. Lockhart, J. L. Perez, G. Pérez Marc, E. D. Moreira, C. Zerbini, R. Bailey, K. A. Swanson, S. Roychoudhury, K. Koury, P. Li, W. V. Kalina, D. Cooper, R. W. Frenck, L. L. Hammitt, Ö. Türeci, H. Nell, A. Schaefer, S. Ünal, D. B. Tresnan, S. Mather, P. R. Dormitzer, U. Şahin, K. U. Jansen and W. C. Gruber, *New England Journal of Medicine*, 2020, **383**, 2603-2615.
3. P. S. Kowalski, A. Rudra, L. Miao and D. G. Anderson, *Molecular Therapy*, 2019, **27**, 710-728.
4. J. Houseley and D. Tollervey, *Cell*, 2009, **136**, 763-776.
5. *Nat. Nanotechnol.*, 2020, **15**, 963-963.
6. S. Mitragotri, P. A. Burke and R. Langer, *Nat. Rev. Drug Discov.*, 2014, **13**, 655-672.
7. B. C. Evans, R. B. Fletcher, K. V. Kilchrist, E. A. Dailing, A. J. Mukalel, J. M. Colazo, M. Oliver, J. Cheung-Flynn, C. M. Brophy, J. W. Tierney, J. S. Isenberg, K. D. Hankenson, K. Ghimire, C. Lander, C. A. Gersbach and C. L. Duvall, *Nature Communications*, 2019, **10**, 1-19.
8. M. Schuster, A. Nechansky and R. Kircheis, *Biotechnology Journal*, 2006, **1**, 138-147.
9. S.-M. Jo, F. R. Wurm and K. Landfester, *Nano Lett.*, 2020, **20**, 526-533.
10. J. M. Vose and J. O. Armitage, *Journal of Clinical Oncology*, 1995, **13**, 1023-1035.
11. C. Dohmen, T. Fröhlich, U. Lächelt, I. Röhl, H.-P. Vornlocher, P. Hadwiger and E. Wagner, *Molecular Therapy - Nucleic Acids*, 2012, **1**, e7.
12. H. Farmer, N. McCabe, C. J. Lord, A. N. J. Tutt, D. A. Johnson, T. B. Richardson, M. Santarosa, K. J. Dillon, I. Hickson, C. Knights, N. M. B. Martin, S. P. Jackson, G. C. M. Smith and A. Ashworth, *Nature*, 2005, **434**, 917-921.
13. S. P. Jackson and J. Bartek, *Nature*, 2009, **461**, 1071-1078.
14. D. W. Pack, A. S. Hoffman, S. Pun and P. S. Stayton, *Nat. Rev. Drug Discov.*, 2005, **4**, 581-593.
15. B. Hu, L. Zhong, Y. Weng, L. Peng, Y. Huang, Y. Zhao and X.-J. Liang, *Signal Transduction and Targeted Therapy*, 2020, **5**, 101.
16. G. A. R. Gonçalves and R. d. M. A. Paiva, *Einstein*, 2017, **15**, 369-375.
17. X. M. Anguela and K. A. High, *Annual Review of Medicine*, 2019, **70**, 273-288.
18. N. R. Rabinovich, P. McInnes, D. L. Klein and B. F. Hall, *Science*, 1994, **265**, 1401.
19. A. Wolfram Julie and J. K. Donahue, *Journal of the American Heart Association*, 2013, **2**, 119.
20. N. G. Rainov, *Human Gene Therapy*, 2000, **11**, 2389-2401.
21. W. J. Marks, J. L. Ostrem, L. Verhagen, P. A. Starr, P. S. Larson and R. A. Bakay, *The Lancet Neurology*, 2008, **7**, 400-408.
22. R. T. Bartus, T. L. Baumann, J. Siffert, C. D. Herzog, R. Alterman, N. Boulis, D. A. Turner, M. Stacy, A. E. Lang, A. M. Lozano and C. W. Olanow, *Neurology*, 2013, **80**, 1698.
23. C. Chen, T. Seeger, V. Termglinchan and I. Karakikes, *Continuing Cardiology Education*, 2017, **3**, 163-169.
24. B. Greenberg, J. Butler, G. M. Felker, P. Ponikowski, A. A. Voors, A. S. Desai, D. Barnard, A. Bouchard, B. Jaski, A. R. Lyon, J. M. Pogoda, J. J. Rudy and K. M. Zsebo, *The Lancet*, 2016, **387**, 1178-1186.
25. J. K. Donahue, *The Lancet*, 2016, **387**, 1137-1139.
26. I. P. d. Sousa, C. Gourmel, O. Berkovska, M. Burger and J.-C. Leroux, *Sci. Rep.*, 2020, **10**, 1-11.
27. T. D. Brown, K. A. Whitehead and S. Mitragotri, *Nature Reviews Materials*, 2019, **5**, 127-148.
28. L. Zhao, M. Skwarczynski and I. Toth, *ACS Biomaterials Science & Engineering*, 2019, **5**, 4937-4950.
29. J. Li and D. J. Mooney, *Nature Reviews Materials*, 2016, **1**, 1-17.
30. A. R. Maity and D. Stepensky, *Molecular Pharmaceutics*, 2016, **13**, 1-7.
31. S. S. Andhari, R. D. Wavhale, K. D. Dhobale, B. V. Tawade, G. P. Chate, Y. N. Patil, J. J. Khandare and S. S. Banerjee, *Sci. Rep.*, 2020, **10**, 1-16.

32. M. Björnmalm, K. J. Thurecht, M. Michael, A. M. Scott and F. Caruso, *ACS Nano*, 2017, **11**, 9594-9613.
33. J. Zhou, Z. Shao, J. Liu, Q. Duan, X. Wang, J. Li and H. Yang, *ACS Appl. Bio Mater.*, 2020, **3**, 2686-2701.
34. S. R. Jakka, V. Govindaraj and G. Mugesh, *Angew. Chem. Int. Ed.*, 2019, **58**, 7713-7717.
35. G. Kang, D. W. Carlson, T. H. Kang, S. Lee, S. J. Haward, I. Choi, A. Q. Shen and A. J. Chung, *ACS Nano*, 2020, **14**, 3048-3058.
36. S. E. Park, M. I. Sajid, K. Parang and R. K. Tiwari, *Molecular Pharmaceutics*, 2019, **16**, 3727-3743.
37. F.-S. Du, Y. Wang, R. Zhang and Z.-C. Li, *Soft Matter*, 2010, **6**, 835-848.
38. N. Zhang, C. Li, D. Zhou, C. Ding, Y. Jin, Q. Tian, X. Meng, K. Pu and Y. Zhu, *Acta Biomaterialia*, 2018, **70**, 227-236.
39. J. Nicolas, S. Mura, D. Brambilla, N. Mackiewicz and P. Couvreur, *Chem. Soc. Rev.*, 2013, **42**, 1147-1235.
40. D. A. Richards, A. Maruani and V. Chudasama, *Chemical Science*, 2017, **8**, 63-77.
41. I. Nakase, H. Akita, K. Kogure, A. Gräslund, Ü. Langel, H. Harashima and S. Futaki, *Acc. Chem. Res.*, 2011, **45**, 1132-1139.
42. J. P. Magnusson, A. O. Saeed, F. Fernández-Trillo and C. Alexander, *Polym. Chem.*, 2011, **2**, 48-59.
43. M. W. Tibbitt, J. E. Dahlman and R. Langer, *Journal of the American Chemical Society*, 2016, **138**, 704-717.
44. S. Dreis, F. Rothweiler, M. Michaelis, J. Cinatl, J. Kreuter and K. Langer, *Int. J. Pharm.*, 2007, **341**, 207-214.
45. M. E. Gindy, A. Z. Panagiotopoulos and R. K. Prud'homme, *Langmuir*, 2008, **24**, 83-90.
46. N. Kamaly, Z. Xiao, P. M. Valencia, A. F. Radovic-Moreno and O. C. Farokhzad, *Chem. Soc. Rev.*, 2012, **41**, 2971-3010.
47. M. Tonigold, J. Simon, D. Estupiñán, M. Kokkinopoulou, J. Reinholz, U. Kintzel, A. Kaltbeitzel, P. Renz, M. P. Domogalla, K. Steinbrink, I. Lieberwirth, D. Crespy, K. Landfester and V. Mailänder, *Nat. Nanotechnol.*, 2018, **13**, 862-869.
48. C. Weber, M. Voigt, J. Simon, A.-K. Danner, H. Frey, V. Mailänder, M. Helm, S. Morsbach and K. Landfester, *Biomacromolecules*, 2019, **20**, 2989-2999.
49. J. Simon, T. Wolf, K. Klein, K. Landfester, F. R. Wurm and V. Mailänder, *Angew. Chem. Int. Ed.*, 2018, **57**, 5548-5553.
50. F. Danhier, O. Feron and V. Préat, *J. Controlled Release*, 2010, **148**, 135-146.
51. X. You, Y. Kang, G. Hollett, X. Chen, W. Zhao, Z. Gu and J. Wu, *J. Mater. Chem. B*, 2016, **4**, 7779-7792.
52. J. Fang, H. Nakamura and H. Maeda, *Advanced Drug Delivery Reviews*, 2011, **63**, 136-151.
53. S. Parveen, F. Arjmand and S. Tabassum, *RCS Adv.*, 2019, **9**, 24699-24721.
54. M. Moros, B. Hernáez, E. Garet, J. T. Dias, B. Sáez, V. Grazú, Á. González-Fernández, C. Alonso and J. M. d. l. Fuente, *ACS Nano*, 2012, **6**, 1565-1577.
55. S. Behzadi, V. Serpooshan, W. Tao, M. A. Hamaly, M. Y. Alkawareek, E. C. Dreaden, D. Brown, A. M. Alkilany, O. C. Farokhzad and M. Mahmoudi, *Chem. Soc. Rev.*, 2017, **46**, 4218-4244.
56. M. Marsh and H. T. McMahon, *Science*, 1999, **285**, 215-220.
57. A. Akinc and G. Battaglia, *Cold Spring Harbor Perspectives in Biology*, 2013, **5**.
58. S. E. A. Gratton, P. A. Ropp, P. D. Pohlhaus, J. C. Luft, V. J. Madden, M. E. Napier and J. M. DeSimone, *Proc. Natl. Acad. Sci.*, 2008, **105**, 11613.
59. S. G. Patel, E. J. Sayers, L. He, R. Narayan, T. L. Williams, E. M. Mills, R. K. Allemann, L. Y. P. Luk, A. T. Jones and Y.-H. Tsai, *Sci. Rep.*, 2019, **9**, 1-9.
60. F. Seidi, R. Jenjob and D. Crespy, *Chem. Rev.*, 2018, **118**, 3965-4036.
61. N. Kamaly, B. Yameen, J. Wu and O. C. Farokhzad, *Chem. Rev.*, 2016, **116**, 2602-2663.
62. M. Hamidi, A. Azadi and P. Rafiei, *Advanced Drug Delivery Reviews*, 2008, **60**, 1638-1649.
63. Y. Fu and W. J. Kao, *Expert Opinion on Drug Delivery*, 2010, **7**, 429-444.

64. T. Casalini, F. Rossi, S. Lazzari, G. Perale and M. Masi, *Molecular Pharmaceutics*, 2014, **11**, 4036-4048.
65. Y. Ding, Y. Kang and X. Zhang, *Chem. Commun.*, 2015, **51**, 996-1003.
66. I. R. Fernando, D. P. Ferris, M. Frasconi, D. Malin, E. Strekalova, M. D. Yilmaz, M. W. Ambrogio, M. M. Algaradah, M. P. Hong, X. Chen, M. S. Nassar, Y. Y. Botros, V. L. Cryns and J. F. Stoddart, *Nanoscale*, 2015, **7**, 7178-7183.
67. B. Iyisan, R. Thiramanas, N. Nazarova, Y. Avlasevich, V. Mailänder, S. Baluschev and K. Landfester, *Biomacromolecules*, 2020, DOI: 10.1021/acs.biomac.0c00377.
68. D. Roy, W. L. A. Brooks and B. S. Sumerlin, *Chem. Soc. Rev.*, 2013, **42**, 7214-7243.
69. M. S. Alkanawati, R. da Costa Marques, V. Mailänder, K. Landfester and H. Thérien-Aubin, *Biomacromolecules*, 2020, **21**, 2764-2771.
70. R. Cheng, F. Feng, F. Meng, C. Deng, J. Feijen and Z. Zhong, *J. Controlled Release*, 2011, **152**, 2-12.
71. O. S. Fenton, K. N. Olafson, P. S. Pillai, M. J. Mitchell and R. Langer, *Adv. Mater.*, 2018, **30**, 1705328.
72. S. H. Lee, Y. Y. Kang, H.-E. Jang and H. Mok, *Advanced Drug Delivery Reviews*, 2016, **104**, 78-92.
73. I. Ekladious, Y. L. Colson and M. W. Grinstaff, *Nat. Rev. Drug Discov.*, 2019, **18**, 273-294.
74. M. J. Webber, E. A. Appel, B. Vinciguerra, A. B. Cortinas, L. S. Thapa, S. Jhunjhunwala, L. Isaacs, R. Langer and D. G. Anderson, *Proceeding of the National Academy of Sciences of the United States of America*, 2016, **113**, 14189-14194.
75. X. Pang, Y. Jiang, Q. Xiao, A. W. Leung, H. Hua and C. Xu, *J. Controlled Release*, 2016, **222**, 116-129.
76. Y. Wu, D. Y. W. Ng, S. L. Kuan and T. Weil, *Biomater. Sci.*, 2015, **3**, 214-230.
77. S. Averick, O. Karácsony, J. Mohin, X. Yong, N. M. Moellers, B. F. Woodman, W. Zhu, R. A. Mehl, A. C. Balazs, T. Kowalewski and K. Matyjaszewski, *Angew. Chem. Int. Ed.*, 2014, **53**, 8050-8055.
78. H. Cho, T. Daniel, Y. J. Buechler, D. C. Litzinger, Z. Maio, A.-M. H. Putnam, V. S. Kraynov, B.-C. Sim, S. Bussell, T. Javahishvili, S. Kaphle, G. Viramontes, M. Ong, S. Chu, B. Gc, R. Lieu, N. Knudsen, P. Castiglioni, T. C. Norman, D. W. Axelrod, A. R. Hoffman, P. G. Schultz, R. D. DiMarchi and B. E. Kimmel, *Proc. Natl. Acad. Sci.*, 2011, **108**, 9060.
79. I. Cobo, M. Li, B. S. Sumerlin and S. Perrier, *Nature Materials*, 2015, **14**, 143-159.
80. H. Schlaad, *Bio-synthetic Polymer Conjugates*, Springer-Verlag Berlin Heidelberg, 2013.
81. E. M. Pelegri-O'Day and H. D. Maynard, *Acc. Chem. Res.*, 2016, **49**, 1777-1785.
82. W. Zhao, F. Liu, Y. Chen, J. Bai and W. Gao, *Polymer*, 2015, **66**, 1-10.
83. J. Khandare and T. Minko, *Prog. Polym. Sci.*, 2006, **31**, 359-397.
84. H. Lv, S. Zhang, B. Wang, S. Cui and J. Yan, *J. Controlled Release*, 2006, **114**, 100-109.
85. M. Lucius, R. Falatach, C. McGlone, K. Makaroff, A. Danielson, C. Williams, J. C. Nix, D. Konkolewicz, R. C. Page and J. A. Berberich, *Biomacromolecules*, 2016, **17**, 1123-1134.
86. M. J. Webber, E. A. Appel, B. Vinciguerra, A. B. Cortinas, L. S. Thapa, S. Jhunjhunwala, L. Isaacs, R. Langer and D. G. Anderson, *Proceedings of the National Academy of Sciences of the United States of America*, 2016, **113**.
87. A. Nieto-Orellana, M. Di Antonio, C. Conte, F. H. Falcone, C. Bosquillon, N. Childerhouse, G. Mantovani and S. Stolnik, *Polym. Chem.*, 2017, **8**, 2210-2220.
88. Y. Wang and C. Wu, *Biomacromolecules*, 2018, **19**, 1804-1825.
89. S. L. Turgeon, C. Schmitt and C. Sanchez, *Current Opinion in Colloid & Interface Science*, 2007, **12**, 166-178.
90. C. G. de Kruif, F. Weinbreck and R. de Vries, *Current Opinion in Colloid & Interface Science*, 2004, **9**, 340-349.
91. E. Kizilay, A. B. Kayitmazer and P. L. Dubin, *Adv. Colloid Interface Sci.*, 2011, **167**, 24-37.
92. C. H. Porcel and J. B. Schlenoff, *Biomacromolecules*, 2009, **10**, 2968-2975.
93. Q. Wang and J. B. Schlenoff, *Macromolecules*, 2014, **47**, 3108-3116.

94. R. G. Winkler and A. G. Cherstvy, in *Polyelectrolyte Complexes in the Dispersed and Solid State I: Principles and Theory*, ed. M. Müller, Springer Berlin Heidelberg, Berlin, Heidelberg, 2014, DOI: 10.1007/12_2012_183, pp. 1-56.
95. J. v. d. Gucht, E. Spruijt, M. Lemmers and M. A. Cohen Stuart, *J. Colloid Interface Sci.*, 2011, **361**, 407-422.
96. D. Priftis and M. Tirrell, *Soft Matter*, 2012, **8**, 9396-9405.
97. H. Dautzenberg and J. Kriz, *Langmuir*, 2003, **19**, 5204-5211.
98. F. Weinbreck, R. H. Tromp and C. G. de Kruif, *Biomacromolecules*, 2004, **5**, 1437-1445.
99. E. Lai and J. H. van Zanten, *Biophys. J.*, 2001, **80**, 864-873.
100. A. Dinari, T. T. Moghadam, M. Abdollahi and M. Sadeghizadeh, *Sci. Rep.*, 2018, **8**, 8112.
101. F. Lotfipour, S. Hallaj-Nezhadi, H. Valizadeh, S. Dastmalchi, B. Baradaran, M. B. Jalali and F. Dobakhti, *Journal of Pharmacy & Pharmaceutical Sciences*, 2011, **14**, 181-195.
102. A. K. Blakney, G. Yilmaz, P. F. McKay, C. R. Becer and R. J. Shattock, *Biomacromolecules*, 2018, **19**, 2870-2879.
103. K. Fant, B. Nordén and P. Lincoln, *Biochemistry*, 2011, **50**, 1125-1127.
104. W. R. Gombotz and D. K. Pettit, *Bioconjugate Chem.*, 1995, **6**, 332-351.
105. K. A. Mislick and J. D. Baldeschwieler, *Proceedings of the National Academy of Sciences of the United States of America*, 1996, **93**, 12349-12354.
106. A. Akinc, M. Thomas, A. M. Klibanov and R. Langer, *The Journal of Gene Medicine*, 2005, **7**, 657-663.
107. T. Bus, A. Traeger and U. S. Schubert, *J. Mater. Chem. B*, 2018, **6**, 6904-6918.
108. H. Chang, J. Lv, X. Gao, X. Wang, H. Wang, H. Chen, X. He, L. Li and Y. Cheng, *Nano Lett.*, 2017, **17**, 1678-1684.
109. V. Postupalenko, D. Desplancq, I. Orlov, Y. Arntz, D. Spehner, Y. Mely, B. P. Klaholz, P. Schultz, E. Weiss and G. Zuber, *Angew. Chem. Int. Ed.*, 2015, **54**, 10583-10586.
110. J.-G. Piao, J.-J. Yan, M.-Z. Wang, D.-C. Wu and Y.-Z. You, *Biomater. Sci.*, 2014, **2**, 390-398.
111. H. Debus, M. Beck-Broichsitter and T. Kissel, *Lab on a Chip*, 2012, **12**, 2498-2506.
112. C. L. Grigsby, Y.-P. Ho, C. Lin, J. F. J. Engbersen and K. W. Leong, *Sci. Rep.*, 2013, **3**, 3155.
113. X. Q. Liu and C. Picart, *Adv. Mater.*, 2016, **28**, 1295-1301.
114. P. T. Hammond, *Adv. Mater.*, 2004, **16**, 1271-1293.
115. J. J. Richardson, M. Björnmalm and F. Caruso, *Science*, 2015, **348**.
116. J. J. Richardson, J. Cui, M. Björnmalm, J. A. Braunger, H. Ejima and F. Caruso, *Chem. Rev.*, 2016, **116**, 14828-14867.
117. K. Ariga, E. Ahn, M. Park and B.-S. Kim, *Chemistry – An Asian Journal*, 2019, **14**, 2553-2566.
118. A. C. Santos, P. Pattekari, S. Jesus, F. Veiga, Y. Lvov and A. J. Ribeiro, *ACS Appl. Mater. Interfaces*, 2015, **7**, 11972-11983.
119. S. Correa, N. Boehnke, A. E. Barberio, E. Deiss-Yehiely, A. Shi, B. Oberlton, S. G. Smith, I. Zervantonakis, E. C. Dreaden and P. T. Hammond, *ACS Nano*, 2020, **14**, 2224-2237.
120. Z. J. Deng, S. W. Morton, E. Ben-Akiva, E. C. Dreaden, K. E. Shopsowitz and P. T. Hammond, *ACS Nano*, 2013, **7**, 9571-9584.
121. S. Zhao, F. Caruso, L. Dähne, G. Decher, B. G. D. Geest, J. Fan, N. Feliu, Y. Gogotsi, P. T. Hammond, M. C. Hersam, A. Khademhosseini, N. Kotov, S. Leporatti, Y. Li, F. Lisdat, L. M. Liz-Marzán, S. Moya, P. Mulvaney, A. L. Rogach, S. Roy, D. G. Shchukin, A. G. Skirtach, M. M. Stevens, G. B. Sukhorukov, P. S. Weiss, Z. Yue, D. Zhu and W. J. Parak, *ACS Nano*, 2019, **13**, 6151-6169.
122. F. Caruso and C. Schüler, *Langmuir*, 2000, **16**, 9595-9603.
123. F.-X. Xiao, M. Pagliaro, Y.-J. Xu and B. Liu, *Chem. Soc. Rev.*, 2016, **45**, 3088-3121.
124. A. M. Jhaveri and V. P. Torchilin, *Frontiers in Pharmacology*, 2014, **5**, 77.
125. H. Cabral, Y. Matsumoto, K. Mizuno, Q. Chen, M. Murakami, M. Kimura, Y. Terada, M. R. Kano, K. Miyazono, M. Uesaka, N. Nishiyama and K. Kataoka, *Nat. Nanotechnol.*, 2011, **6**, 815-823.
126. A. Harada and K. Kataoka, *Science*, 1999, **283**, 65.
127. H. Cabral, K. Miyata, K. Osada and K. Kataoka, *Chem. Rev.*, 2018, **118**, 6844-6892.

128. K. Kataoka, A. Harada and Y. Nagasaki, *Advanced Drug Delivery Reviews*, 2001, **47**, 113-131.

129. G. Gaucher, M.-H. Dufresne, V. P. Sant, N. Kang, D. Maysinger and J.-C. Leroux, *J. Controlled Release*, 2005, **109**, 169-188.

130. M.-C. Jones and J.-C. Leroux, *European Journal of Pharmaceutics and Biopharmaceutics*, 1999, **48**, 101-111.

131. K. Knop, R. Hoogenboom, D. Fischer and U. S. Schubert, *Angew. Chem. Int. Ed.*, 2010, **49**, 6288-6308.

132. H. J. Kim, K. Miyata, T. Nomoto, M. Zheng, A. Kim, X. Liu, H. Cabral, R. J. Christie, N. Nishiyama and K. Kataoka, *Biomaterials*, 2014, **35**, 4548-4556.

133. B. S. Kim, H. J. Kim, S. Osawa, K. Hayashi, K. Toh, M. Naito, H. S. Min, Y. Yi, I. C. Kwon, K. Kataoka and K. Miyata, *ACS Biomaterials Science & Engineering*, 2019, **5**, 5770-5780.

134. F.-X. Xiao, M. Pagliaro, Y.-J. Xu and B. Liu, *Chem. Soc. Rev.*, 2016, DOI: 10.1039/C5CS00781J.

135. J. S. Lee and J. Feijen, *J. Controlled Release*, 2012, **161**, 473-483.

136. C. LoPresti, H. Lomas, M. Massignani, T. Smart and G. Battaglia, *J. Mater. Chem.*, 2009, **19**, 3576-3590.

137. T. Trantidou, M. Friddin, Y. Elani, N. J. Brooks, R. V. Law, J. M. Seddon and O. Ces, *ACS Nano*, 2017, **11**, 6549-6565.

138. X. Wang, J. Hu, G. Liu, J. Tian, H. Wang, M. Gong and S. Liu, *Journal of the American Chemical Society*, 2015, **137**, 15262-15275.

139. E. Rideau, R. Dimova, P. Schwille, F. R. Wurm and K. Landfester, *Chem. Soc. Rev.*, 2018, **47**, 8572-8610.

140. L. Luo and A. Eisenberg, *Journal of the American Chemical Society*, 2001, **123**, 1012-1013.

141. F. Meng, C. Hiemstra, G. H. M. Engbers and J. Feijen, *Macromolecules*, 2003, **36**, 3004-3006.

142. Y. Anraku, A. Kishimura, M. Oba, Y. Yamasaki and K. Kataoka, *Journal of the American Chemical Society*, 2010, **132**, 1631-1636.

143. J. Leong, J. Y. Teo, V. K. Aakalu, Y. Y. Yang and H. Kong, *Advanced Healthcare Materials*, 2018, **7**, 1701276.

144. A. Akbarzadeh, R. Rezaei-Sadabady, S. Davaran, S. W. Joo, N. Zarghami, Y. Hanifehpour, M. Samiei, M. Kouhi and K. Nejati-Koshki, *Nanoscale Research Letters*, 2013, **8**, 102.

145. Y.-Y. Won, A. K. Brannan, H. T. Davis and F. S. Bates, *The Journal of Physical Chemistry B*, 2002, **106**, 3354-3364.

146. T. Einfalt, R. Goers, I. A. Dinu, A. Najer, M. Spulber, O. Onaca-Fischer and C. G. Palivan, *Nano Lett.*, 2015, **15**, 7596-7603.

147. L. Messager, J. R. Burns, J. Kim, D. Cecchin, J. Hindley, A. L. B. Pyne, J. Gaitzsch, G. Battaglia and S. Howorka, *Angew. Chem. Int. Ed.*, 2016, **55**, 11106-11109.

148. F. Wang, J. Gao, J. Xiao and J. Du, *Nano Lett.*, 2018, **18**, 5562-5568.

149. P. J. Photos, L. Bacakova, B. Discher, F. S. Bates and D. E. Discher, *J. Controlled Release*, 2003, **90**, 323-334.

150. T. Anajafi and S. Mallik, *Therapeutic Delivery*, 2015, **6**, 521-534.

151. I. Neamtu, A. G. Rusu, A. Diaconu, L. E. Nita and A. P. Chiriac, *Drug Delivery*, 2017, **24**, 539-557.

152. E. Mauri, G. Perale and F. Rossi, *ACS Applied Materials and Interfaces*, 2018, **1**, 6525-6541.

153. H.-Q. Wu and C.-C. Wang, *Langmuir*, 2016, **32**, 6211-6225.

154. T. R. Hoare and D. S. Kohane, *Polymer*, 2008, **49**, 1993-2007.

155. B. Iyisan and K. Landfester, *Macromol. Rapid Commun.*, 2019, **40**, 1800577.

156. Z. Tang, C. He, H. Tian, J. Ding, B. S. Hsiao, B. Chu and X. Chen, *Prog. Polym. Sci.*, 2016, **60**, 86-128.

157. K. Landfester, *Angew. Chem. Int. Ed.*, 2009, **48**, 4488-4507.

158. K. L. P. Dr., *Angew. Chem. Int. Ed.*, 2009, DOI: 10.1002/anie.200900723.

159. L.-P. Lv, Y. Zhao, N. Vilbrandt, M. Gallei, A. Vimalanandan, M. Rohwerder, K. Landfester and D. Crespy, *Journal of the American Chemical Society*, 2013, **135**, 14198-14205.

160. G. Toniolo, E. K. Efthimiadou, G. Kordas and C. Chatgilialoglu, *Sci. Rep.*, 2018, **8**, 1-9.

161. J. Zhou, T. Li, C. Zhang, J. Xiao, D. Cui and Y. Cheng, *Nanoscale*, 2018, **10**, 9707-9719.

162. F. Cavalieri, G. L. Beretta, J. Cui, J. A. Braunger, Y. Yan, J. J. Richardson, S. Tinelli, M. Folini, N. Zaffaroni and F. Caruso, *Biomacromolecules*, 2015, **16**, 2168-2178.

163. J. Fischer, S. J. Beckers, D. Yiamsawas, E. Thines, K. Landfester and F. R. Wurm, *Adv. Sci.*, 2019, **6**, 1802315.

164. M. S. Alkanawati, F. R. Wurm, H. Thérien-Aubin and K. Landfester, *Macromol. Mater. Eng.*, 2018, **303**, 1700505.

165. G. Baier, M. Fichter, A. Kreyes, K. Klein, V. Mailänder, S. Gehring and K. Landfester, *Biomacromolecules*, 2016, **17**, 148-153.

166. G. Baier, S. Winzen, C. Messerschmidt, D. Frank, M. Fichter, S. Gehring, V. Mailänder and K. Landfester, *Macromol. Biosci.*, 2015, **15**, 765-776.

167. K. Maruya-Li, C. Shetty, A. M. Jazani, N. Arezi and J. K. Oh, *ACS Omega*, 2020, **5**, 3734-3742.

168. N. Morimoto, S. Hirano, H. Takahashi, S. Loethen, D. H. Thompson and K. Akiyoshi, *Biomacromolecules*, 2013, **14**, 56-63.

169. K. Kolouchova, O. Sedlacek, D. Jirak, D. Babuka, J. Blahut, J. Kotek, M. Vit, J. Trousil, R. Konefał, O. Janouskova, B. Podhorska, M. Slouf and M. Hruby, *Biomacromolecules*, 2018, **19**, 3515-3524.

170. D. H. N. T. T. H. N. T. N. N. V. L. P. T. P. D. M. H. V. C. K. N. L. G. B. D. H. Nguyen, *Journal of Applied Polmer Science*, 2019, DOI: 10.1002/app.47544.

171. N. Shen, B. Lei, Y. Wang, S. Xu and H. Liu, *New J. Chem.*, 2018, **42**, 9472-9481.

172. A. V. Kabanov and S. V. Vinogradov, *Angew. Chem. Int. Ed.*, 2009, **48**, 5418-5429.

173. A. E. Ekkelenkamp, M. R. Elzes, J. F. J. Engbersen and J. M. J. Paulusse, *J. Mater. Chem. B*, 2018, **6**, 210-235.

174. M. Elsabahy and K. L. Wooley, *Chem. Soc. Rev.*, 2012, **41**, 2545-2561.

175. M. Chan and A. Almutairi, *Materials Horizons*, 2016, **3**, 21-40.

176. K. Landfester and C. K. Weiss, in *Modern Techniques for Nano- and Microreactors/-reactions*, ed. F. Caruso, Springer Berlin Heidelberg, Berlin, Heidelberg, 2010, DOI: 10.1007/12_2009_43, pp. 1-49.

177. Y. Zhao, L.-P. Lv, S. Jiang, K. Landfester and D. Crespy, *Polym. Chem.*, 2015, **6**, 4197-4205.

178. N. Anton, J.-P. Benoit and P. Saulnier, *J. Controlled Release*, 2008, **128**, 185-199.

179. J. K. Oh, R. Drumright, D. J. Siegwart and K. Matyjaszewski, *Prog. Polym. Sci.*, 2008, **33**, 448-477.

180. Q. Fu, J. Xu, K. Ladewig, T. M. A. Henderson and G. G. Qiao, *Polym. Chem.*, 2015, **6**, 35-43.

181. M. Delcea, H. Möhwald and A. G. Skirtach, *Advanced Drug Delivery Reviews*, 2011, **63**, 730-747.

182. T. Tadros, P. Izquierdo, J. Esquena and C. Solans, *Adv. Colloid Interface Sci.*, 2004, **108-109**, 303-318.

183. T. Delmas, H. Piraux, A.-C. Couffin, I. Texier, F. Vinet, P. Poulin, M. E. Cates and J. Bibette, *Langmuir*, 2011, **27**, 1683-1692.

184. M. Machtakova, S. Han, Y. Yangazoglu, I. Lieberwirth, H. Thérien-Aubin and K. Landfester, *Nanoscale*, 2021, **13**, 4051-4059.

185. A. Monroy-Villagrana, L. Alamilla-Beltrán, H. Hernández-Sánchez and G. F. Gutiérrez-López, in *Food Nanoscience and Nanotechnology*, eds. H. Hernández-Sánchez and G. F. Gutiérrez-López, Springer International Publishing, Cham, 2015, DOI: 10.1007/978-3-319-13596-0_9, pp. 163-175.

186. Y. Yang, C. Marshall-Breton, M. E. Leser, A. A. Sher and D. J. McClements, *Food Hydrocoll.*, 2012, **29**, 398-406.

187. A. Durand and E. Marie, *Adv. Colloid Interface Sci.*, 2009, **150**, 90-105.

188. S. Winzen, J. C. Schwabacher, J. Müller, K. Landfester and K. Mohr, *Biomacromolecules*, 2016, **17**, 3845-3851.

189. J. Müller, J. Simon, P. Rohne, C. Koch-Brandt, V. Mailänder, S. Morsbach and K. Landfester, *Biomacromolecules*, 2018, **19**, 2657-2664.

190. K. N. Bauer, J. Simon, V. Mailänder, K. Landfester and F. R. Wurm, *Acta Biomaterialia*, 2020, **116**, 318-328.
191. K. Landfester, N. Bechthold, F. Tiarks and M. Antonietti, *Macromolecules*, 1999, **32**, 5222-5228.
192. K. Landfester, *Macromol. Rapid Commun.*, 2001, **22**, 896-936.
193. Y. Meliana, L. Suprianti, Y. C. Huang, C. T. Lin and C.-S. Chern, *Colloids and Surfaces A: Physicochemical and Engineering Aspects*, 2011, **389**, 76-81.
194. P. Taylor, *Adv. Colloid Interface Sci.*, 1998, **75**, 107-163.
195. K. Landfester, *Adv. Mater.*, 2001, **13**, 765-768.
196. K. Piradashvili, M. Fichter, K. Mohr, S. Gehring, F. R. Wurm and K. Landfester, *Biomacromolecules*, 2015, **16**, 815-821.
197. D. Crespy, M. Stark, C. Hoffmann-Richter, U. Ziener and K. Landfester, *Macromolecules*, 2007, **40**, 3122-3135.
198. K. Piradashvili, E. M. Alexandrino, F. R. Wurm and K. Landfester, *Chem. Rev.*, 2015, **116**, 2141-2169.
199. N. Marasini, M. Skwarczynski and I. Toth, *Expert. Rev. Vaccines*, 2014, **13**, 1361-1376.
200. M. Fichter, K. Piradashvili, A. Pietrzak-Nguyen, L. Pretsch, G. Kuhn, S. Strand, M. Knuf, F. Zepp, F. R. Wurm, V. Mailänder, K. Landfester and S. Gehring, *Biomaterials*, 2016, **108**, 1-12.
201. D. Paßlick, K. Piradashvili, D. Bamberger, M. Li, S. Jiang, D. Strand, P. R. Wich, K. Landfester, M. Bros, S. Grabbe and V. Mailänder, *J. Controlled Release*, 2018, **289**, 23-34.
202. S. Jia, W. J. VanDusen, R. E. Diehl, N. E. Kohl, R. A. Dixon, K. O. Elliston, A. M. Stern and P. A. Friedman, *J. Biol. Chem.*, 1992, **267**, 14322-14327.
203. L. Lavaissiere, S. Jia, M. Nishiyama, S. de la Monte, A. M. Stern, J. R. Wands and P. A. Friedman, *The Journal of Clinical Investigation*, 1996, **98**, 1313-1323.
204. A. Aihara, C.-K. Huang, M. J. Olsen, Q. Lin, W. Chung, Q. Tang, X. Dong and J. R. Wands, *Hepatology*, 2014, **60**, 1302-1313.
205. H. Tian, J. Du, J. Wen, Y. Liu, S. R. Montgomery, T. P. Scott, B. Aghdasi, C. Xiong, A. Suzuki, T. Hayashi, M. Ruangchainikom, K. Phan, G. Weintraub, A. Raed, S. S. Murray, M. D. Daubs, X. Yang, X.-b. Yuan, J. C. Wang and Y. Lu, *ACS Nano*, 2016, **10**, 7362-7369.
206. H. Qi, L. Yang, X. Li, X. Sun, J. Zhao, X. Hou, Z. Li, X. Yuan, Z. Cui and X. Yang, *Biomater. Sci.*, 2019, **7**, 1675-1685.
207. H. Zhang, T. Shibata, T. Krawczyk, T. Kabashima, J. Lu, M. K. Lee and M. Kai, *Talanta*, 2009, **79**, 700-705.
208. K. Renggli, P. Baumann, K. Langowska, O. Onaca, N. Bruns and W. Meier, *Adv. Funct. Mater.*, 2011, **21**, 1241-1259.
209. X. Lian, Y. Huang, Y. Zhu, Y. Fang, R. Zhao, E. Joseph, J. Li, J.-P. Pellois and H.-C. Zhou, *Angew. Chem. Int. Ed.*, 2018, **57**, 5725-5730.
210. J. F. Mukerabigwi, Z. Ge and K. Kataoka, *Chem. Eur. J.*, 2018, **24**, 15706-15724.
211. J. Gaitzsch, X. Huang and B. Voit, *Chem. Rev.*, 2016, **116**, 1053-1093.
212. F. H. Arnold, *Angew. Chem. Int. Ed.*, 2018, **57**, 4143-4148.
213. A. Küchler, M. Yoshimoto, S. Luginbühl, F. Mavelli and P. Walde, *Nat. Nanotechnol.*, 2016, **11**, 409.
214. K. Rina, P.-R. Javier, D. C.-N. Ruben and V.-D. Rafael, *Nanotechnol. Rev.*, 2017, **6**, 405-419.
215. W.-H. Chen, M. Vázquez-González, A. Zoabi, R. Abu-Reziq and I. Willner, *Nat. Catal.*, 2018, **1**, 689-695.
216. S. F. M. van Dongen, M. Nallani, J. J. L. M. Cornelissen, R. J. M. Nolte and J. C. M. van Hest, *Chem. Eur. J.*, 2009, **15**, 1107-1114.
217. S.-M. Jo, F. R. Wurm and K. Landfester, *ACS Appl. Mater. Interfaces*, 2018, **10**, 34230-34237.
218. B. Thingholm, P. Schattling, Y. Zhang and B. Städler, *Small*, 2016, **12**, 1806-1814.
219. M. Marguet, C. Bonduelle and S. Lecommandoux, *Chem. Soc. Rev.*, 2013, **42**, 512-529.
220. J. Liu, C. Cai, Y. Wang, Y. Liu, L. Huang, T. Tian, Y. Yao, J. Wei, R. Chen, K. Zhang, B. Liu and K. Qian, *Adv. Sci.*, 2020, **7**, 1903730.

221. W. Ke, J. Li, F. Mohammed, Y. Wang, K. Tou, X. Liu, P. Wen, H. Kinoh, Y. Anraku, H. Chen, K. Kataoka and Z. Ge, *ACS Nano*, 2019, **13**, 2357-2369.
222. N. Wagner, M. Gutweiler, R. Pabst and K. Dose, *Eur. J. Biochem.*, 1987, **165**, 177-183.
223. S. F. M. van Dongen, W. P. R. Verdurmen, R. J. R. W. Peters, R. J. M. Nolte, R. Brock and J. C. M. van Hest, *Angew. Chem. Int. Ed.*, 2010, **49**, 7213-7216.
224. M. Galliani, M. Santi, A. Del Grosso, A. Cecchettini, F. M. Santorelli, S. L. Hofmann, J.-Y. Lu, L. Angella, M. Cecchini and G. Signore, *Bioconjugate Chem.*, 2018, **29**, 2225-2231.
225. J. Kim and K. T. Kim, *ACS Appl. Mater. Interfaces*, 2020, **12**, 23502-23513.
226. A. K. Johnson, A. M. Zawadzka, L. A. Deobald, R. L. Crawford and A. J. Paszczynski, *J. Nanopart. Res.*, 2008, **10**, 1009-1025.
227. T. Konno, J. Watanabe and K. Ishihara, *Biomacromolecules*, 2004, **5**, 342-347.
228. J. N. Vranish, M. G. Ancona, E. Oh, K. Susumu, G. Lasarte Aragonés, J. C. Breger, S. A. Walper and I. L. Medintz, *ACS Nano*, 2018, **12**, 7911-7926.
229. X. Huang, M. Li and S. Mann, *Chem. Commun.*, 2014, **50**, 6278-6280.
230. S. Dutta, N. Kumari, S. Dubbu, S. W. Jang, A. Kumar, H. Ohtsu, J. Kim, S. H. Cho, M. Kawano and I. S. Lee, *Angew. Chem. Int. Ed.*, 2020, **59**, 3416-3422.
231. S. Varlas, J. C. Foster, P. G. Georgiou, R. Keogh, J. T. Husband, D. S. Williams and R. K. O'Reilly, *Nanoscale*, 2019, **11**, 12643-12654.
232. S. Talekar, A. Joshi, G. Joshi, P. Kamat, R. Haripurkar and S. Kambale, *RCS Adv.*, 2013, **3**, 12485-12511.
233. L. Cao, L. v. Langen and R. A. Sheldon, *Curr. Opin. Biotechnol.*, 2003, **14**, 387-394.
234. L. D. Blackman, S. Varlas, M. C. Arno, A. Fayter, M. I. Gibson and R. K. O'Reilly, *ACS Macro Lett.*, 2017, **6**, 1263-1267.
235. D. Gräfe, J. Gaitzsch, D. Appelhans and B. Voit, *Nanoscale*, 2014, **6**, 10752-10761.
236. D. M. Vriezema, P. M. L. Garcia, N. Sancho Oltra, N. S. Hatzakis, S. M. Kuiper, R. J. M. Nolte, A. E. Rowan and J. C. M. van Hest, *Angew. Chem. Int. Ed.*, 2007, **46**, 7378-7382.
237. G. Han, J.-T. Wang, X. Ji, L. Liu and H. Zhao, *Bioconjugate Chem.*, 2017, **28**, 636-641.
238. C. Tan, M. Arshadi, M. C. Lee, M. Godec, M. Azizi, B. Yan, H. Eskandarloo, T. W. Deisenroth, R. H. Darji, T. V. Pho and A. Abbaspourrad, *ACS Nano*, 2019, **13**, 9016-9027.
239. A. Jafari, H. Sun, B. Sun, M. A. Mohamed, H. Cui and C. Cheng, *Chem. Commun.*, 2019, **55**, 1267-1270.
240. I. Schlegel, P. Renz, J. Simon, I. Lieberwirth, S. Pektor, N. Bausbacher, M. Miederer, V. Mailänder, R. Muñoz-Espí, D. Crespy and K. Landfester, *Macromol. Biosci.*, 2018, **18**, 1700387.
241. S. Behzadi, C. Rosenauer, M. Kappl, K. Mohr, K. Landfester and D. Crespy, *Nanoscale*, 2016, **8**, 12998-13005.
242. K. Piradashvili, J. Simon, D. Paßlick, J. R. Höhner, V. Mailänder, F. R. Wurm and K. Landfester, *Nanoscale Horiz*, 2017, **2**, 297-302.
243. E. A. Prasetyanto, A. Bertucci, D. Septiadi, R. Corradini, P. Castro-Hartmann and L. De Cola, *Angew. Chem. Int. Ed.*, 2016, **55**, 3323-3327.
244. J. Dausend, A. Musyanovych, M. Dass, P. Walther, H. Schrezenmeier, K. Landfester and V. Mailänder, *Macromol. Biosci.*, 2008, **8**, 1135-1143.
245. J. Geng, W. Li, Y. Zhang, N. Thottappillil, J. Clavadetscher, A. Lilienkampf and M. Bradley, *Nature Chemistry*, 2019, **11**, 578-586.
246. G. Guizzunti and J. Seemann, *Proc. Natl. Acad. Sci.*, 2016, **113**, E6590.
247. X. Yuan, N. Rietzschel, H. Kwon, A. B. Walter Nuno, D. A. Hanna, J. D. Phillips, E. L. Raven, A. R. Reddi and I. Hamza, *Proc. Natl. Acad. Sci.*, 2016, **113**, E5144.
248. G. Begum, W. B. Goodwin, B. M. deGlee, K. H. Sandhage and N. Kröger, *J. Mater. Chem. B*, 2015, **3**, 5232-5240.
249. M. J. Männel, L. P. Kreuzer, C. Goldhahn, J. Schubert, M. J. Hartl and M. Chanana, *ACS Catal.*, 2017, **7**, 1664-1672.
250. K. Vogele, J. List, F. C. Simmel and T. Pirzer, *Langmuir*, 2018, **34**, 14780-14786.
251. K. Landfester and C. K. Weiss, *Adv. Polym. Sci.*, 2010, **229**, 1-49.

252. J. Shi, P. W. Kantoff, R. Wooster and O. C. Farokhzad, *Nat. Rev. Cancer*, 2017, **17**, 20-37.
253. R. van der Meel, E. Sulheim, Y. Shi, F. Kiessling, W. J. M. Mulder and T. Lammers, *Nat. Nanotechnol.*, 2019, **14**, 1007-1017.
254. Y. Qiao, J. Wan, L. Zhou, W. Ma, Y. Yang, W. Luo, Z. Yu and H. Wang, *Wiley Interdiscip. Rev. Nanomed. Nanobiotechnol.*, 2019, **11**, e1527.
255. S. Wang, Z. Wang, G. Yu, Z. Zhou, O. Jacobson, Y. Liu, Y. Ma, F. Zhang, Z.-Y. Chen and X. Chen, *Adv. Sci.*, 2019, **6**, 1801986.
256. M. S. Rehmann, K. M. Skeens, P. M. Kharkar, E. M. Ford, E. Maverakis, K. H. Lee and A. M. Kloxin, *Biomacromolecules*, 2017, **18**, 3131-3142.
257. D. Sandrin, D. Wagner, C. E. Sitta, R. Thoma, S. Felekyan, H. E. Hermes, C. Janiak, N. de Sousa Amadeu, R. Kühnemuth, H. Löwen, S. U. Egelhaaf and C. A. M. Seidel, *Phys. Chem. Chem. Phys.*, 2016, **18**, 12860-12876.
258. J. H. Lee and Y. Yeo, *Chem. Eng. Sci.*, 2015, **125**, 75-84.
259. J. Mu, J. Lin, P. Huang and X. Chen, *Chem. Soc. Rev.*, 2018, **47**, 5554-5573.
260. N. Deirram, C. Zhang, S. S. Kermaniyan, A. P. R. Johnston and G. K. Such, *Macromol. Rapid Commun.*, 2019, **40**, 1800917.
261. G. Yang, L. Xu, J. Xu, R. Zhang, G. Song, Y. Chao, L. Feng, F. Han, Z. Dong, B. Li and Z. Liu, *Nano Lett.*, 2018, **18**, 2475-2484.
262. J. Li, Y. Li, Y. Wang, W. Ke, W. Chen, W. Wang and Z. Ge, *Nano Lett.*, 2017, **17**, 6983-6990.
263. S. Grabbe, H. Haas, M. Diken, L. M. Kranz, P. Langguth and U. Sahin, *Nanomedicine*, 2016, **11**, 2723-2734.
264. J. D. Finn, A. R. Smith, M. C. Patel, L. Shaw, M. R. Youniss, J. van Heteren, T. Dirstine, C. Ciullo, R. Lescarbeau, J. Seitzer, R. R. Shah, A. Shah, D. Ling, J. Growe, M. Pink, E. Rohde, K. M. Wood, W. E. Salomon, W. F. Harrington, C. Dombrowski, W. R. Strapps, Y. Chang and D. V. Morrissey, *Cell Rep.*, 2018, **22**, 2227-2235.
265. J. Li, H. Liang, J. Liu and Z. Wang, *Int. J. Pharm.*, 2018, **546**, 215-225.
266. O. Rifaie-Graham, S. Ulrich, N. F. B. Galensowske, S. Balog, M. Chami, D. Rentsch, J. R. Hemmer, J. Read de Alaniz, L. F. Boesel and N. Bruns, *J. Am. Chem. Soc.*, 2018, **140**, 8027-8036.
267. R. Münter, K. Kristensen, D. Pedersbæk, J. B. Larsen, J. B. Simonsen and T. L. Andresen, *Nanoscale*, 2018, **10**, 22720-22724.
268. M.-L. Frey, J. Simon, M. Brückner, V. Mailänder, S. Morsbach and K. Landfester, *Polym. Chem.*, 2020, **11**, 3821-3830.
269. T. Lin, P. Zhao, Y. Jiang, Y. Tang, H. Jin, Z. Pan, H. He, V. C. Yang and Y. Huang, *ACS Nano*, 2016, **10**, 9999-10012.
270. M. R. Green, G. M. Manikhas, S. Orlov, B. Afanasyev, A. M. Makhson, P. Bhar and M. J. Hawkins, *Ann. Oncol.*, 2006, **17**, 1263-1268.
271. G. Baier, A. Cavallaro, K. Vasilev, V. Mailänder, A. Musyanovych and K. Landfester, *Biomacromolecules*, 2013, **14**, 1103-1112.
272. I. Schlegel, R. Muñoz-Espí, P. Renz, I. Lieberwirth, G. Floudas, Y. Suzuki, D. Crespy and K. Landfester, *Macromolecules*, 2017, **50**, 4725-4732.
273. E. Monogioudi, G. Faccio, M. Lille, K. Poutanen, J. Buchert and M.-L. Mattinen, *Food Hydrocoll.*, 2011, **25**, 71-81.
274. E. V. Petrotchenko, J. J. Serpa, D. B. Hardie, M. Berjanskii, B. P. Suriyamongkol, D. S. Wishart and C. H. Borchers, *Mol. Cell. Proteomics*, 2012, **11**, M111.013524-013521-M013111.013524-013513.
275. W. Ebeling, N. Hennrich, M. Klockow, H. Metz, H. D. Orth and H. Lang, *Eur. J. Biochem.*, 1974, **47**, 91-97.
276. S. Udenfriend, S. Stein, P. Böhlen, W. Dairman, W. Leimgruber and M. Weigele, *Science*, 1972, **178**, 871.
277. J. M. Artigas, M. E. Garcia, M. R. Faure and A. M. Gimeno, *Postgrad. Med. J.*, 1981, **57**, 219.
278. A. O. Elzoghby, W. M. Samy and N. A. Elgindy, *J. Controlled Release*, 2012, **161**, 38-49.
279. N. A. Hadjiev and B. G. Amsden, *J. Controlled Release*, 2015, **199**, 10-16.

280. A. G. Ogston, *J. Chem. Soc., Faraday Trans.*, 1958, **54**, 1754-1757.
281. L. Nothnagel and M. G. Wacker, *Eur. J. Pharm. Sci.*, 2018, **120**, 199-211.
282. S. Gou, Q. Chen, Y. Liu, L. Zeng, H. Song, Z. Xu, Y. Kang, C. Li and B. Xiao, *ACS Sustain. Chem. Eng.*, 2018, **6**, 12658-12667.
283. T. Z. Chang, S. S. Stadmiller, E. Staskevicius and J. A. Champion, *Biomater. Sci.*, 2017, **5**, 223-233.
284. A. Pietrzak-Nguyen, K. Piradashvili, M. Fichter, L. Pretsch, F. Zepp, F. R. Wurm, K. Landfester and S. Gehring, *Nanomedicine*, 2016, **12**, 2383-2394.
285. J. Tel, S. P. Sittig, R. A. M. Blom, L. J. Cruz, G. Schreibelt, C. G. Figdor and I. J. M. de Vries, *J. Immunol.*, 2013, **191**, 5005.
286. H. Hemmi, T. Kaisho, O. Takeuchi, S. Sato, H. Sanjo, K. Hoshino, T. Horiuchi, H. Tomizawa, K. Takeda and S. Akira, *Nat. Immunol.*, 2002, **3**, 196-200.
287. M. M. Alam, D. Yang, A. Trivett, T. J. Meyer and J. J. Oppenheim, *Front. Immunol.*, 2018, **9**, 2982.
288. A. K. Andrianov, A. Marin, R. Wang, H. Karauzum, A. Chowdhury, P. Agnihotri, A. S. Yunus, R. A. Mariuzza and T. R. Fuerst, *ACS Appl. Bio Mater.*, 2020, **3**, 3187-3195.
289. N. Van Hoeven, C. B. Fox, B. Granger, T. Evers, S. W. Joshi, G. I. Nana, S. C. Evans, S. Lin, H. Liang, L. Liang, R. Nakajima, P. L. Felgner, R. A. Bowen, N. Marlenee, A. Hartwig, S. L. Baldwin, R. N. Coler, M. Tomai, J. Elvecrog, S. G. Reed and D. Carter, *Sci. Rep.*, 2017, **7**, 46426.
290. K. J. Peine, G. Gupta, D. J. Brackman, T. L. Papenfuss, K. M. Ainslie, A. R. Satoskar and E. M. Bachelder, *J. Antimicrob. Chemother.*, 2014, **69**, 168-175.
291. I. Hellmuth, I. Freund, J. Schlöder, S. Seidu-Larry, K. Thüring, K. Slama, J. Langhanki, S. Kaloyanova, T. Eigenbrod, M. Krumb, S. Röhm, K. Peneva, T. Opatz, H. Jonuleit, A. H. Dalpke and M. Helm, *Front. Immunol.*, 2017, **8**, 312.
292. A. Forner, J. M. Llovet and J. Bruix, *The Lancet*, 2012, **379**, 1245-1255.
293. E. Breous and R. Thimme, *Journal of Hepatology*, 2011, **54**, 830-834.
294. C. N. Baxevanis and S. A. Perez, *Expert. Rev. Vaccines*, 2016, **15**, 677-680.
295. E. Unitt, A. Marshall, W. Gelson, S. M. Rushbrook, S. Davies, S. L. Vowler, L. S. Morris, N. Coleman and G. J. M. Alexander, *Journal of Hepatology*, 2006, **45**, 246-253.
296. K. F. Chu and D. E. Dupuy, *Nat. Rev. Cancer*, 2014, **14**, 199-208.
297. C. J. M. Melief, T. van Hall, R. Arens, F. Ossendorp and S. H. van der Burg, *The Journal of Clinical Investigation*, 2015, **125**, 3401-3412.
298. L. Buonaguro, A. Petrizzo, M. Tagliamonte, M. L. Tornesello and F. M. Buonaguro, *Journal of Hepatology*, 2013, **59**, 897-903.
299. H. Yang, K. Song, T. Xue, X.-P. Xue, T. Huyan, W. Wang and H. Wang, *Oncol Rep*, 2010, **24**, 1257-1264.
300. M. Shimoda, Y. Tomimaru, K. P. Charpentier, H. Safran, R. I. Carlson and J. Wands, *Journal of Hepatology*, 2012, **56**, 1129-1135.
301. Y.-L. Pang, H.-G. Zhang, J.-R. Peng, X.-W. Pang, S. Yu, Q. Xing, X. Yu, L. Gong, Y.-H. Yin, Y. Zhang and W.-F. Chen, *Cancer Immunology, Immunotherapy*, 2009, **58**, 877-886.
302. H. M. Zarour, *Clinical Cancer Research*, 2016, **22**, 1856.
303. A. A. Self, P. T. Losikoff and S. H. Gregory, *Human Vaccines & Immunotherapeutics*, 2013, **9**, 1569-1576.
304. R. L. Coffman, A. Sher and R. A. Seder, *Immunity*, 2010, **33**, 492-503.
305. M. L. Mbow, E. De Gregorio, N. M. Valiante and R. Rappuoli, *Current Opinion in Immunology*, 2010, **22**, 411-416.
306. F. Sarti, G. Perera, F. Hintzen, K. Kotti, V. Karageorgiou, O. Kammona, C. Kiparissides and A. Bernkop-Schnürch, *Biomaterials*, 2011, **32**, 4052-4057.